COLLISIONLESS RIGID BODY LOCOMOTION

MODELS AND PHYSICALLY BASED HOMOTOPY

METHODS FOR FINDING PERIODIC MOTIONS IN

HIGH DEGREE OF FREEDOM MODELS

A Dissertation

Presented to the Faculty of the Graduate School

of Cornell University

in Partial Fulfillment of the Requirements for the Degree of

Doctor of Philosophy

by

Mario Waldorff Gomes

January 2005

COLLISIONLESS RIGID BODY LOCOMOTION MODELS AND PHYSICALLY BASED HOMOTOPY METHODS FOR FINDING PERIODIC MOTIONS IN HIGH DEGREE OF FREEDOM MODELS

Mario Waldorff Gomes, Ph.D.

Cornell University 2005

This thesis presents collisionless gaits for three different locomotion models, ape brachiation, biped walking, and rimless wheel rolling. All of the models exist in environments which allow energy dissipative collisions (which are the only way for these models to lose energy). However, these collisions can be avoided if the incoming foot or hand touches the support just as its velocity drops to zero. These special collisionless gaits are numerically shown to exist for several brachiation and walking models. These gaits allow the models to traverse a level support indefinitely, with no energy loss. Some of the motions found for the brachiation models look remarkable life-like. This resemblance suggests that the models and the special collisionless gaits have captured an essence the coordination strategy used by brachiating apes. The collisionless motions of the walking model are not life-like, but this is the first motion found for a passive device that can indefinitely traverse a perfectly horizontal support. A homotopy method is presented which was used to find periodic motions in a series of brachiation models with increasing numbers of degrees of freedom.

Biographical Sketch

Mario Gomes was born in Washington D.C. in 1973, to Mario and Gerda Gomes. He received his undergraduate education in Mechanical Engineering at Cornell University during 1991-1995. He received his Master's Degree in Dynamics and Control Systems at the Georgia Institute of Technology during 1995-1997. His first job as an engineer was at Atlantic Orient Corporation, Norwich Vermont, from 1997-1998. He then worked as an engineer at O'Brien and Gere Manufacturing in Syracuse, New York, from 1998-1999. He returned to Cornell University as a Ph.D. student in the fall of 1999.

To my parents:

Gerda Elisabeth Waldorff Gomes

and

Mario Nascimento Noro Gomes

Acknowledgements

I am grateful to my parents, whose support, encouragement, and hard work have given me such wonderful opportunites in life.

Marrying Sonja Keil has been one of the best decisions that I've had the opportunity to make. I am grateful for her love and emotional support.

I thank my advisor, Andy Ruina, for helping to convince me to return to graduate school, and for suggesting an interesting research topic. I have learned a lot from him. I thank my committee members, Steven Strogatz, John Hermanson, and Hod Lipson for interesting discussions about dynamics and animal locomotion.

I also thank Mike Coleman for helping to make the transition back to graduate school a bit easier.

Table of Contents

List of Tables

List of Figures

Chapter 1

Motivation

Our understanding of the coordinated movements of animals is limited. For example, it is not known if general principles exist which explain why animals, humans included, choose certain coordination patterns over others when moving about. There are many ways that one can study movement, the most often used methods are direct observation and modeling (either physical or mathematical). Regardless of what approach one chooses to use, it is often fruitful to study movement extremes. Examples of extreme movements in the human world occur frequently in competitive athletics. Athletes spend large amounts of time, money, effort, training, and sweat in pursuit of the fastest time, highest jump, most beautiful execution, *etc.* In working to achieve those goals, athletes obtain not only stronger muscles and cardiovascular systems but also spend large amounts of time and effort improving their skill level. It is well known that "technique" (skill) is as important as strength and endurance in competitive sport. A current textbook on exercise physiology [68] gives a reason as to why improvements in technique are useful.

> "As you become more skillful at performing an exercise your energy demands during that exercise are reduced. You become more efficient."
> -Wilmore and Costill [68].

An example of the effects of different technique is given in Wilmore and Costill [68] and summarized below. The study examines the performance of two marathons runners who have similar aerobic fitness (as measured by $\dot{V}_{O_2max}$, 64 and 65 ml $\cdot$ kg^{-1} $\cdot$ min^{-1}). Although the two runners were both similarly fit, tests revealed that one runner used significantly less oxygen than the other when both are running at the same speed above 200 m/min. This difference in efficiency gave a large competitive advantage to one of the runners, allowing him to finish marathons about 13 minutes before the other. The study concluded that the difference in energy efficiency was due to a difference in *skill* between the two runners. This example emphasizes one of the main goals of athletes in endurance sports, namely, "How can I improve my coordination strategy to become more energy efficient?".

Almost every coach and athlete has their own theories as to how one improves efficiency in their sport. These theories may be true or have aspects which are valid and helpful, but they have not been proven and are definitely not well-understood. One of the conclusions of the marathon runner study given above was that "Unfortunately, we have no explanation for the underlying causes of these efficiency differences." [68]

The research presented in this thesis will focus on determining the plausibility of using the mass and inertia of one's limbs to reduce one's energetic cost while locomoting. Specifically, we will search for coordination strategies that achieve the theoretical minimum energy expenditure required for locomoting across level ground, zero energy cost. First, other approaches to these questions must be addressed as well as some of the assumptions that we and others must make when trying to answer these questions.

1.1 Experimental approach/ Energy measurements

Experiments are the most direct way to investigate questions of energetic cost in coordinated movements of animals. Several methods for measuring energy use have been developed over the course of many years. Some definitions and background are needed before we discuss these methods, their advantages and disadvantages. What do we mean by energy in the context of biological organisms? What do animals spend metabolic energy on? How is energy consumption measured? What are ways to model energy consumption in mathematical models? The next few sections will discuss these questions as well as some of the answer's inherent assumptions.

1.1.1 Energy in biomechanics

On what do animals spend this metabolic energy? Some of that energy is used to maintain body temperature (assuming that the organism's body temperature is not close to the environment's, *poikilotherms*). Animals' whose body temperature is maintained to be fairly constant are *homeotherms* and are usually endotherms, "whose principal source of body heat depends on high rates of metabolism" [38]). Of course, the animal kingdom cannot be so easily pigeon-holed and many animals fall somewhere in between, either becoming inactive, torpid, or going into hibernation or maintaining body temperature by external methods such as sunning themselves. Cell maintenance also requires energy, the breaking down and conversion of food, the transport of nutrients, waste and oxygen, fighting of infection and disease by the immune system, *etc.* All of these energy expenditures are lumped together into the expression *basal rate of metabolism.* This expression is usually applied to mammals and is defined as, "the minimal rate of a thermoregulating endotherm during rest when it is not digesting a meal and is not exposed to temperatures that require an increase in metabolism." [38]. Energy measurements based on the differences between resting and active subtract out the basal

metabolic rate. Most laboratory measurements made of animal locomotion are done at thermoneutral temperatures and may or may not subtract out the basal metabolic rate.

Aside from growing, maintaining body temperature (if appropriate), and reproducing, locomotion is a major way for animals to expend energy. Depending on the animal, locomotion could mean crawling, slithering, flapping, swimming, undulating, burrowing, walking, hopping, galloping, or running. All forms of locomotion require large repetitive muscle contractions, removal of waste products such as lactic acid and carbon dioxide, conversion of energy stores, and the removal of heat. For many modes of locomotion, metabolism is the main energy source. However, like thermoregulation, where behavior (basking or seeking shade) as well as metabolism can used to achieve a constant body temperature; locomotion can also utilize the environment to help achieve the task of moving the organism from place to place. For example, besides the well-known example of birds using thermal updrafts, they have also been found to utilize wind shears and building wakes to reduce their energetic costs while flying. This naturally leads one to examine other mechanisms that animals may use to reduce their energy consumption when moving about. But first, we examine the various ways in which energy consumption can be measured.

1.2   Ways to measure energy expenditure

The first law of thermodynamics (that energy is conserved for a closed system) leads to one of the widest used, simplest, and least intrusive methods for measuring energy consumption. The energy content of the food that a subject eats can be measured and recorded over a period of several days. Assuming that the subject at steady state and is not changing their body composition during the testing (*i.e.* metabolizing their stores of fat and glycogen without replacement), then the energy content of the food they eat will be well correlated to the amount of energy that they expend in a day of normal activity [1]. This method is most appropriate for use in measuring the energy expenditure during normal daily activities and would be impossible to use for measuring energy consumption during short bursts of activity.

Fluctuations in body mass have also been used to estimate the rate of metabolism in animals. Many animals fast for extended periods of time and changes in the body mass during that time can be recorded and correlated to energy use. However, in animals as in people, the body's response to starvation changes depending on the length of the fast. Differing amounts of fats, glycogen, and proteins are used to provide energy during prolonged fasting [46]. Other animals may have different methods for coping with relatively short fasting periods, such as petrels who

---

[1] Note however, that this is not quite a closed system since, among other things like heat loss and water vapor loss, this method disregards the energy lost in nitrogen-rich urine and in the feces as undigested food.[7]

metabolize oil stored in their stomachs [38]. The dependency on knowing what substance is being metabolized makes it difficult to use this method to provide accurate estimations of metabolic rate.

The rest of the methods listed below are all more indirect measurements of energy expenditure. In order to understand them we need to briefly review the process of metabolism. The following is a simplified summary of information given by Wilmore and Costill [68]. Ingested food is converted to simple starches, fats, and proteins in the intestines. These are later broken down further and used to produce adenosine triphosphate (ATP) in the mitochondria of cells. The two main fuel sources which are used to produce ATP are fats and carbohydrates. Fats contain more energy per mass than carbohydrates. Larger amount of muscular effort will cause more carbohydrates (as opposed to fats) to be used in the generation of ATP. ATP can be produced with processes that use oxygen (aerobic) or ones that do not (anaerobic). Aerobic ATP production is the primary method of producing energy for endurance activities since it is much more efficient than anaerobic ATP production. Aerobic ATP production requires oxygen and produces carbon dioxide. The ratio of O_2 required and CO_2 produced differs depending on the type of fuel used (carbohydrate or fat). The process of converting glucose and fats to ATP is only about 40% efficient. The rest of the energy derived from the food (60%) is transformed into heat. This short summary of the energy transformation within the body gives some clues as to how indirect measurements can be used to estimate the energy expenditure by the body during sustained activity.

1.2.1   Indirect Methods of Energy Measurement

One of the major byproducts of muscle use is heat. When exercising or locomoting an animal must get rid of this heat to maintain non-lethal body temperatures. Humans get rid of this heat by conduction and convection if the ambient temperature is lower than the surface temperature of the skin.[2] Humans also get rid of excess body heat by sweating as the water absorbs heat from the surface of the skin when evaporating. On the other hand, animals such as birds primarily get rid of excess body heat by panting, expelling hot moisture-rich air and replacing it with cooler ambient air [46].

The amount of heat produced by the body during activity can be directly measured using calorimetry. This method requires placing the test subject into an insulated room with a way to absorb and measure the heat produced by the subject. The time constants for this type of procedure are quite large and thus cannot be used for measuring short periods of intense exercise. This method is not primarily used for human studies in part due to the expense of constructing and maintaining such a large calorimeter.

In human studies, the most widely used method for measuring energy expendi-

---

[2]Due to the relatively small temperature difference between the body and surroundings, radiation plays a very small role in the dissipation of body heat.

ture is by the measuring the amount of O_2 and CO_2 exchanged in the lungs. The ratios of the two gasses exchanged differ depending on the ratio of fat and carbohydrates being metabolized. The ratio of the two types of fuel and the amount of fuel metabolized can be estimated using the two quantities being measured. This method depends on the assumption that the gas exchange in the lungs is the same as at the cellular level.

Doubly labeled water can be used to measure CO_2 production in animals [30]. An animal is injected with heavy water (deuterium) and an isotope of oxygen ^{18}O. The oxygen gets eliminated in two main ways, as water and as CO_2. The heavy hydrogen loss is used to figure out how much water was excreted so that the amount of CO_2 produced can be calculated. This procedure involves taking two blood samples (before and after the time of interest) and is mostly used for measuring energy use in the wild or for other situations where they cannot be confined to a calorimeter.

Another method for measuring energy consumption is to measure the amount of mechanical work done by the animal. Fundamentally, this is a measure of power based purely on mechanics. At any point in time each muscle of an animal could be consuming metabolic energy while doing mechanical work. One could look at each actuator and calculate the power that it is producing by measuring its stress and strain rate at all the points in the muscle tissue. The product of stress and strain rate integrated over the muscles spatial dimensions will result in a value for the mechanical power produced by the animal at that moment. The power for all of the muscles can be integrated in time to obtain a measure of the work done by the muscles of the animal during the desired time period. Note that negative and positive work are often treated separately in the space integration when determining the total amount of work done. This differing treatment of negative a positive work is due to the fact that muscle tissue acts differently when producing work or absorbing work. Muscles and tendons can not absorb large amounts of mechanical work, store it, and release it later at no loss. Often, some energy is expended to absorb the work being done on the muscle. Thus, it is a mistake to allow work that is done on a muscle to cancel work that it does on the environment. Therefore, mechanical work is usually defined by modifying the integral of muscle power by changing the sign of negative work (work done on the body by the environment) and scaling it by a factor less than one (sometimes $1/3$ or $1/4$) [74].

$$\text{Work} = \int_0^T \left(\int_V (\sigma \dot{\epsilon})_{pos} + \frac{1}{4} |(\sigma \dot{\epsilon})_{neg}| \, dV \right) dt$$

It is impossible to carry out power measurements to determine the stress and strain rate values at many points in an individual muscle. Often, the muscle is reduced to a one-dimensional telescoping member. With this assumption one can simplify the power calculation by measuring a scalar force magnitude and linear displacement rate ($P = -T\dot{\ell}$) for each muscle. Again, how one treats negative and

positive mechanical power when performing a time integration to determine total energy cost needs to be detailed in the definition of mechanical work.

For a locomoting organism or even for a moving limb, there are too many muscles to instrument[3]. Sometimes only a few of the major muscles are of concern and the rest are ignored in the analysis. Often, a further simplification is made where the torques that the muscles exert around the joints in the body are measured and the relative angular velocity of the joint are used to calculate a joint power. Many times these torques are calculated from kinematics (and often force plate data to reduce errors) using inverse dynamics[4]. At this level of simplification, the muscles with their specific insertion and attachment points have been abstracted away. Note that the level of torque about a joint does not directly correspond to a specific muscle force due to overactuation and/or the presence of multi-joint muscles (muscles which span more than a single joint). Usually, this definition of mechanical work considers only a few joints and the rest are ignored.

Since the rigid-body models examined in this thesis will not have actuators, they cannot produce or absorb work[5]. The general lack of actuators simplifies the power calculation since the non-existent actuators do not apply forces to any points on the limbs, or in other words, the torques about each unactuated joint is zero. If one were to use any of the above definitions for mechanical work on such a system for a given task, one would find that in each case the amount of mechanical work done to complete the task would be zero.

1.3 Modeling

Each of the methods and definitions outlined above have their advantages and limitations. One can clearly see that even in direct observation of animals, accurately determining the amount of energy used to achieve the given locomotor task can be a difficult problem, fraught with assumptions and inaccuracies. However, determining the effects of different factors is difficult, or even impossible, when the systems that one is observing are as complex as a biological organism. In order to discover the dominant features involved in an activity, a simpler system with less factors is required. Some simplification can be done in carrying out observations and measurements, such as not conducting metabolic cost studies of burrowing gophers with pregnant animals in freezing temperatures. However, there is a limit to the types of simplifications that one can make in biological studies. This brings us to another very important and useful way to study locomotion, namely modeling.

---

[3]Determining the force at the end of tendon using instrumentation is an extremely invasive procedure

[4]Inverse dynamics requires a model of the animal, often a rigid body model in addition to joint kinematics and a set of mass and geometry parameters.

[5]Note that actually the walking model in section 5 uses springs which one might interpret physically as muscles which can absorb and release energy with no loss.

Modeling allows one to strip a complex system of the less important processes which impede the clear understanding of a given behavior. This results in a reduced system, or model, which hopefully contains only the essential features which affect the activity of interest. Biomechanical models generally fall into one of two categories, physical models or mathematical models [2]. Physical models are usually physical mock-ups of the biological systems such as Dickenson's larger-than-life oil-submerged fruitfly wing model [17] or using photoelastic models of bones to explore stress patterns under loading. These models allow one to carry out experiments and measurements that would not be possible with the actual animal. Physical models can also be used to verify the results of mathematical models, such as McGeer's passive dynamic walkers. These physical models can be helpful and insightful without being detailed imitations of the actual organism.

Mathematical models of locomotion often consist of sets of ordinary or partial differential equations. These equations are derived, in part, by applying the known laws of nature. Simplifying assumptions are an integral part of model construction and these simplifications are at the root of the power and problems of mathematical modeling. The essential question becomes, "What is the level of detailed required in the model to capture the important aspects of the system to gain insight into the research question?" If one is studying the chemical weathering of granite, then a chemical or molecular model of the rock might be appropriate. However, if one is interested in where a piece of rock will be two seconds after it is thrown up into the air, then a molecular model is inappropriate and needlessly complex. Overly complicated models, are not only unwieldy, but also impede the attempt to gain insight into which features of the model dominate its behavior. As the biomechanist R. McNeil Alexander states, "Very simple models are often the best for establishing general principles ..." [2]. This research is in the same spirit. The locomotion models that have been constructed are simple in that they model only the rudimentary structure of the animal. The model of metabolic cost is also extremely simple. Although these assumptions are inaccurate by definition, the uncomplicated nature of the models allow us to make definite statements about the system's behavior and to hopefully establish some general principles of locomotion.

1.4   Muscle models

Since animals use muscles to move about, a model for how muscles work needs to be incorporated into our animal model. Since we are interested in the energetic costs of coordinated movement, our muscle model must incorporate some model of metabolism or metabolic cost for performing muscular contractions. Several people have created models of muscle tissue. Some of the models that one can use to model muscle tissue are Hill's model [25], Huxley's model [27], Zajac's model [72], Zahalic's model [71], and Cheng-Brown-Loeb's model [13]. The accuracy of these models in varying situations are not well known, and many of the models (usually the Hill type models) do not include energy use. The research presented

here side-steps the complications involved in including a biochemical measure of metabolic cost. We approximate metabolic cost with a measure of the work being done by the body on the environment. Since our models use no actuators or muscles, there can not be any work done by the actuators on the system. Thus, by our measure of metabolic cost, no metabolic energy can be expended by our models.

1.5   Other modeling assumptions

This research uses mathematical models to study animal locomotion. In order to construct a model we need to simplify the biological organism. Our models are not able to reproduce or grow. They need no nourishment or oxygen to survive. They have no cardiovascular or nervous systems. Most of the models have no brains and the others only very simple controllers. We have removed all of the muscles from our models so that they have no actuation. We will assume that the large limbs of the animals are perfectly rigid bodies, not capable of deforming or bending. This allows us to characterize their location in space using six numbers for position and orientation. We will further constrain the motion of these limbs to two-dimensions. This means that now only three numbers are needed to describe the position and orientation of each body. We model the animal's joints, such as elbows and knees, as simple pin joints. These constraints allow an even smaller set of numbers to be used to define the state of the system at any point in time. These simplifications result in a set of non-linear, coupled, ordinary differential equations. We formulate the equations in such a manner as to incorporate the constraints so that we do not end up with a set of differential algebraic equations which is common in biomechanical models of the type we study here. This allows us to side-step the numerical difficulties involved when generating numerically approximate solutions to those equations. Most of the mathematical models that are studied in this thesis, although highly simplified models of the biological systems, are too complicated for analytical solutions. Therefore, numerical solutions are used instead.

1.6   Numerical Integration

Numerical solutions are approximations. They do not give the the true mathematical solution to a set of differential equations. However, the approximate answer can be arbitrarily close. Note that not all numeric approximations are mathematically non-rigorous. Interval arithmetic (which puts strict error bounds on a solution, as opposed to traditional error *estimates*) has been used by Warwick Tucker to prove the existence of periodic motions or to prove that the strange attractor in the Lorentz equations is not a quasiperiodic motion [65]. We do not use interval arithmetic but instead use floating point numbers and standard numerical integration, root-finding routines, and convergence-test estimates of error.

1.7   Previous similar models

The models closest in spirit to the models that we will study in this thesis are the passive dynamic walking models of Tad McGeer. They were, in part, created to determine the minimum amount of active control necessary to produce smoothly forward progressing bipedal walking [34]. These models are capable of gaits that look remarkably like human walking, require no control, are energy efficient[6], and sometimes are asymptotically stable. The fact that the motions look life-like suggests that some property is shared between the model and humans. This shared property could be the lack of significant control. Although this conclusion answers the original question concerning the minimal amount of control necessary for walking which motivated the creation of the model, it may not be the primary cause of the similarity between the passive and actual gaits. Humans do not require a stable passive gait to walk, since we have numerous actuators (muscles) which can, in principle, stabilize unstable periodic gaits with minute energy expenditure. Another characteristic of the passive gait is that it is energy efficient. There are no torques at any of the joints in the model which would have to be created by muscles doing work. Instead, the passive devices use the small amounts of work done by gravity to power their gaits as they walk down shallow ramps. This energy efficiency suggests that the reason for *the similarity between the passive and actual gaits is due to a desire of the animal to reduce its energy expenditure.* This is the central idea that is explored in chapter 2 using various models of ape brachiation.

1.8   How efficient are passive locomotion gaits?

In principle, moving an object across a level support requires no energy input. Energy is not required to move a weight across a frictionless horizontal surface. This lower bound was not achieved, previous to this work, for a walking model.

Although there are no torques applied at the joints, in previous passive dynamic walking models, the device still requires a source of energy to replace the energy lost in collisions between the feet and the floor. In a knee-jointed walker, there are also energy dissipative collisions at the knee joint due to a knee-stop which prevents hyper-extension of the knee. Since the device is moving at a constant average speed, the magnitude of the work done by gravity on the system is equal the magnitude of the energy lost in the collisions that occur during a complete cycle. As the steepness of the ramp is decreased, Garcia *et al.* found that passive dynamic gaits use less and less gravitational potential energy per unit distance to walk [22]. As the ramp slope tends to zero, the amount of energy per unit distance they use tends to zero, and the step length of the gait also tends to zero [22]. The collisions that occur in the model above are the only avenue for energy

---

[6]Energy efficient means that they use a relatively small amount of energy per unit mass per unit distance. This raises the questions of: "How small is small?" and "What is the smallest amount of energy required?"

dissipation. In addition, actuated models can lose energy from work being done on the actuators by the system (eccentric muscle contractions). If all energy losses could be avoided using a specific gait, then a model could traverse a perfectly horizontal support without power (a perfectly efficient gait).

The most efficient gait, given our measure of energy consumption, would be one that moves forward without dissipating any energy and thus requiring no net work to sustain movement. McGeer's walking models were unable to achieve this. However McGeer's passive running model, with a massless sprung foot [33], was able to run across level ground with no energy input (using a symmetric gait).

How can one eliminate energy losses in a collision? Perfectly elastic collisions conserve energy but, plastic collisions, in general, do not. The collisions which occur in these passive locomotion models are modeled as plastic collisions, since they two objects do not immediately separate after the collision. However, if the contacting points on either object collide with zero relative velocity, then no energy is lost in that plastic collision. This research aims to obtain a better understanding of this type of gait. Is it possible to determine if a model is capable of a collision-less gait without doing a detailed search of the model's possible motions? Do these collision-less motions resemble the motion of the animal it is modeling? How can one find these motions in a given model? This work examines these questions using several locomotion models.

1.9   Outline of Remainder of this Thesis

This section gives a brief summary of the remaining chapters of this thesis.

Chapter 2 examines a series of models of ape locomotion. Apes locomote by *brachiating*, where they use their hands to grasp the overhead supports. Unlike walking, where the legs are the supporting limbs, the arms are the supporting limbs in brachiation. There are two distinct gaits used in brachiation, a *continuous-contact* gait where a hand is on a handhold on all times, and a *ricochetal* gait which has a ballistic flight phase. We present a series of models that increase in complexity. For each of the models that we examine, we look for collision-less periodic motions. Section 2.4 gives some of the results of the point-mass-model of brachiation by Bertram *et al.*[5] and also presents a class of ricochetal gaits which were not addressed in [5]. Section 2.5 presents a rigid body extension of the point-mass model, and collisionless periodic motions are found for both continuous contact and ricochetal brachiation. A two link model of an ape is used in Section 2.6. This is the first completely passive model of a brachiator studied, since the massless arm used in the point-mass and single-rigid-body model requires a controller to position the massless arm when grasping a new handhold. The three link and five link models presented in sections 2.7 and 2.8 respectively, are built upon the two link model. Collisionless periodic ricochetal motions are found for both of these models.

Chapter 3 discusses the parameter sets which were used in the brachiation

models. Mass and geometry parameters that are given by Preushoft and Demes[47] and Swartz[60] are shown to be almost identical when applied to the two-link model introduced in section 2.6. We also show that those parameters do not give life-like collisionless periodic motions. We summarize the data collected by Schultz, Erikson, and Napier on gibbon limb measurements and develop a new set of mass and geometry parameters for a gibbon.

Chapter 4 examines an extension to the rimless-wheel, a very simplified model of bipedal working introduced by McGeer [34] and studied in depth by Coleman [14]. Again we look for collisionless periodic motions in our extended rimless-wheel model. This model, although not an accurate representation of people, has some very interesting dynamic behavior and serves as a connecting model between the Chatterjee *et al.* [10] collisionless hopping block model and the collisionless walking model presented in chapter 5.

Chapter 5 examines a more anthropomorphic model of walking with two legs and a torso. Although the motion found is not life-like, it is the first perfectly efficient walking gait with non-vanishing step length.

Chapter 6 outlines several different forms of continuation methods used for finding periodic motions. Two of these methods were used to help find reasonable collisionless periodic motions in the brachiation models as they increased in complexity.

The appendix contains an outline of the numerical procedure used to formulate the equations of motion.

Chapter 2

Brachiation

This chapter has been submitted as a paper for the Journal of Theoretical Biology as a joint effort with Andy L. Ruina. This chapter contains more detail than in the paper.

2.1 Introduction

Brachiation is the hand over hand locomotion used by various primates, especially long armed apes, to move about using their arms as their supporting limbs. In a *continuous contact* brachiating gait, somewhat analogous to upside down walking, the ape has at least one hand on a handhold at all times. In a *ricochetal* brachiating gait there is a flight phase between successive handholds, something like upside down running.

One approach to understanding such motions is through kinematics: one can note how the body parts' positions, velocities, and accelerations vary in time. Due to the nature and large number of the kinematic variables used to define an instantaneous body pose and velocity, it is difficult to use time histories of those variables to understand how they produce a particular movement. It is an arduous or impossible task to determine the relationship between changes in various curves and changes in the overall movement. Trying to construct a movement by creating curves of joint angles versus time is extremely difficult and non-intuitive. There is no simple formula explaining how to control the joints so as to make the whole body move in an appropriate manner. Because this control problem can be difficult in itself, it is easy to miss more basic principles that could be operating. In this paper we pursue the hypothesis that apes coordinate their motion in a manner that minimizes their energy expenditure (Alexander [3]), without explicitly attempting to match natural kinematics *a priori*.

The approach taken here is most closely linked to the passive-dynamic models of human walking pioneered by McGeer [34]. He and his successors [14] [69] [15] have built stable, energy efficient robotic walkers which consist basically of sticks connected by hinges, with no control. These walking devices have surprisingly life-like motions, and use only small amounts of gravitational energy, per unit distance,

to walk downhill. These models certainly suggest that a large part of the human walking control strategy is governed by the natural dynamic motions of the body. However, these passive-dynamic walkers can only walk at non-zero speeds by using gravitational energy to replace the energy lost in the collisions between the foot and the ground. Passive motions which use *no* energy input to locomote at non-zero speeds are sought in all of the brachiation models presented in this chapter.

2.2 Previous Brachiation Work

The comparison between ape brachiation and the swing of a pendulum goes back at least to Tuttle's work in 1968 [66]. Fleagle, in 1974, made the same comparison in more detail, but he studied the kinematics of siamangs using film footage of brachiation [19]. He was the first to use mechanics to aid in understanding continuous contact brachiation and he postulated that siamangs might pump energy into their motion by lifting their legs at the bottom of the motion (much like a child on a swing). Since then others have compared continuous contact brachiation to rigid body pendulums with inertia, most notably Preuschoft and Demes [47] and Swartz [60]. Preuschoft and Demes found that the comparison between a gibbon and a pendulum is good for long armed-apes using a slow brachiation gait (what we call a continuous contact gait). They mentioned the ricochetal gait for a point mass model and described it roughly using mechanics language but they did not do a detailed dynamical examination of that gait. Swartz evaluated the mass and geometry parameters used in the Preuschoft and Demes paper and proposes what she believes are more realistic parameters for a continuous contact rigid body pendulum model. She then uses this model to predict swing period and forward speed. She also predicts realistic ape sizes based on the forces and moments that the model must resist when moving.

Bertram *et al.* [5] throughly studied a point-mass model of a gibbon, looking at the ricochetal gait as well and comparing the model results to data. They propose that the avoidance of collisions is the determining factor for the coordination of brachiation by gibbons. The work presented in this chapter begins with the point-mass model of Bertram *et al.* [5]. Usherwood and Bertram [67] have also studied the effect of overshooting a handhold in the point mass model of brachiation and have concluded that gibbons do tend to overshoot the ideal collisionless path since the consequence of undershooting the next handhold are prohibitively negative. Usherwood and Bertram also propose, but did not investigate, a model identical to the "rigid body with massless arm model", to help qualitatively explain why a gibbon's body is not in line with it's supporting arm for the whole swing phase of a ricochetal gait. Yamazaki [70] studied and simulated a five-link 2-dimensional passive brachiation model in much the same spirit as the work we present here. His model includes a torsional spring and damper at the hip joint and the knee joint, but it is unclear if he includes realistic collisions in his model. Since his model includes no actuators and has dissipative dampers he cannot find periodic

motions. Thus, he minimizes the errors between the starting and ending states, and compares the resulting simulated motion with actual gibbon locomotion via a set of indicies. Looking solely at continuous contact brachiation he concludes that the the body proportions of gibbons are special in that, as a group, they give more efficient brachiation motions than if they were significantly modified.

Some research on the control of under-actuated systems (*i.e.* systems with fewer actuators than degrees of freedom) have used brachiation as an intriguing test-bed to study the efficacy of various control algorithms. Fukuda *et al.* [20] have designed and built a capable two degree-of-freedom brachiating robot with a single actuator between the two links. The robot's adaptive controller allows it to swing up from the static stable equilibrium position and then brachiate on a horizontal ladder with irregularly spaced handholds. Spong [58] developed a controller for "Acrobot" (a theoretically identical two link, two degree-of-freedom system with a single actuator in between the links) so that it could swing up from the stable equilibrium position to an inverted position and balance there.

Nishimura and Funaki [43, 44] designed, simulated, and built a serial three-link under-actuated brachiating robot with two motors, capable of brachiating under a horizontal support. Odagaki *et al.* [45] developed two nonlinear controllers for an identical serial three-link model. Saito *et al.* [51] has designed and built a "realistic" three dimensional robot based closely on the body proportions of a siamang with 12 degrees of freedom and 14 actuators. This robot can swing up and brachiate continuously around and underneath a circular horizontal ladder of handholds. Kajima *et al.* [28] have designed and built "Gorilla Robot II" a 19 link robot with 20 actuators that has successfully brachiated using two distinct continuous contact gaits (over-hand and side-hand).

Most of the work in robotic brachiation is exclusively concerned with the continuous contact gait. However, Nakanishi and Fukuda have developed a control algorithm for their two-link brachiator allowing their simulation to execute a "leaping maneuver" or a single step of ricochetal brachiation [41]. A device capable of executing a single, or series of, "leaping maneuver(s)" has yet to be built.

This work was originally motivated by an informal wager between Andy Ruina and Fukuda *et al.* (private communication at ICRA 97), that their 2-link robot could have energy-free motions. The approach used here is similar in spirit to Bertram *et al.* 's work [5] but with more degrees of freedom.

2.3   Modeling Approach

We approach the minimum-muscle-work hypothesis by looking for solutions with exactly zero energy cost; the solutions we seek do not demand any joint torque at any time. Because all known candidate muscle-use cost estimates are minimized by zero muscle use, we need not concern ourselves with the form of the objective (cost, energy-use) functional that we minimize. Note again that the solution search here is more stringent than that for downhill passive dynamic walking; the motions

we seek not only do not use muscular work but also do not decrease the system's gravitational potential energy either.

All of the models here use one or more perfectly rigid bodies, motion restricted to two dimensions, frictionless hinges, no air resistance, handholds available everywhere on the "ceiling", plastic collisions between hand and handhold, and workless grasp and release of handholds. Most of these modeling assumptions have been used either implicitly or explicitly in earlier analyses of brachiation.

The plastic collision assumption requires some clarification. When the ape's hand comes into contact with a handhold, it grabs on, and the interaction is modeled as a *perfectly plastic* collision. Linear and angular momentum conservation generally demand that mechanical energy be lost in plastic collisions (Where the energy goes depends on detailed non-rigid-body mechanics that do not effect the post-collisional rigid-body motions [9]). However, if the colliding points on two objects have the same velocity when they make contact, then no energy is lost in that "collision" even though it is a plastic or sticking collision. Two objects can still make contact with zero instantaneous relative velocity. The relative velocity just has to be zero at the moment of contact, though it will not be zero before contact is made (see Figure 2.32).

The assumption about workless grasp and release of handholds also needs more detailed discussion. It obviously takes muscular effort to dangle underneath a chin-up bar. Most of one's body weight is supported by bones and ligaments, but it takes active muscular effort to hold on to the overhead bar. The hands of apes are specifically well adapted to grasping [53, 18], and thus we assume that simply supporting their body weight requires negligible energy expenditure. Since the wrists of gibbons have an extremely large range of motion, we assume that a reasonable model of the sustained grasping of the handhold is a pin joint with no joint friction. Initiating the grasp and release of the handhold requires very little muscular work, and our model can enforce and release the constraint without any work being done. The collision that results from suddenly imposing the constraint can absorb work, but enforcing the constraint is workless.

Because our models have no joint or air friction and no muscles to absorb energy, plastic collisions are the only possible way for the model to lose energy. Thus, the solutions we seek don't even have that loss. We also require that the solutions be periodic so that one swing of the motion can be repeated forever, allowing the model to locomote indefinitely.

2.4   Point-Mass Model

The point-mass model of Bertram *et al.* [5] depicted in Figure 2.1 is capable of collisionless continuous-contact and collisionless ricochetal gaits. These solutions can be found by pasting together an arc from the simple pendulum and a parabolic free flight as shown in [5], and depicted here in Figure 2.2. This model has many energy-cost-free motions, but in a control sense, they are not strictly passive as the
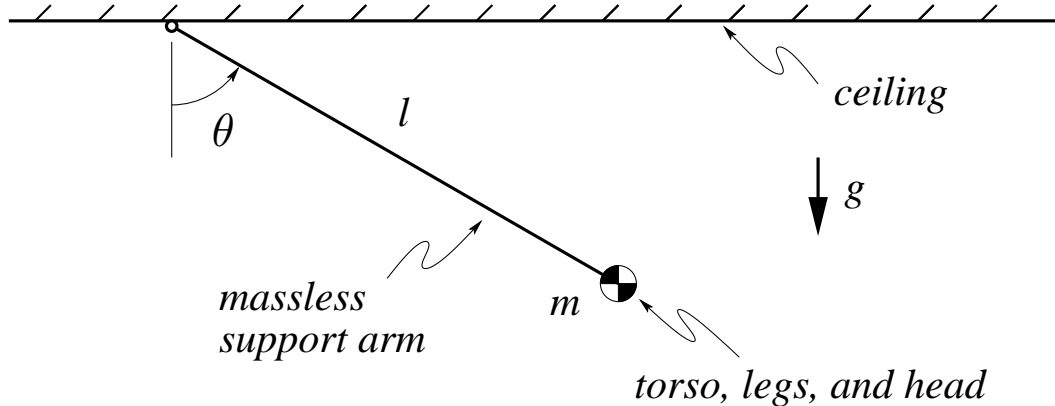
Figure 2.1: Point-Mass Model reproduced from Bertram *et al.* [5]. This model is capable of collisionless continuous-contact and ricochetal motions. The torso, legs, and head of the gibbon are all concentrated to a single point mass. The arms, being a low proportion of the overall body weight, are treated as massless.

massless arm is assumed to be controlled to the appropriate position for grasping each new handhold.

Since, for given initial conditions, the solutions to the differential equations are unique, one way of parameterizing the solutions is in terms of the initial conditions. We define the starting configuration to be the straight down vertical position, $\theta = 0$. Thus, there is only one initial condition to specify, $\dot{\theta}$.

First consider continuous contact gaits. For any initial $\dot{\theta}_0 < 2\sqrt{g/l}$ the pendulum motion will come to a stop at some height at which point a new pendulum arc with a new handhold can be started. This new arc will obtain the same $\dot{\theta}_0$ at the bottom ($\theta = 0$) of the next arc thus making up one segment of a continuous contact gait.

For ricochetal motions, there is a family of solutions for each $\dot{\theta}_0$ that can be parameterized by the release angle, θ_{rel}, anywhere in the interval $0 < \theta_{rel} < \cos^{-1}(1 - l\dot{\theta}_0^2/2g)$.

If one allows the point mass model to grab the ceiling at any point, then any initial angular velocity in the ranges specified above, will result in a collisionless motion.

In the more complex models below, we will similarly parameterize solutions, or possible solutions, by the state of the system in a symmetry position and, for ricochetal motions, also by a hand-release angle.

We found an additional class of motions, depicted in Figure 2.2(c) and 2.3 which gibbons might use to their advantage when brachiating with closely spaced handholds. The gait of the actual gibbon from the previous definitions in section 2.1 would be considered a continuous contact gait (with at least one hand on a handhold at all times). However this same gait in the point-mass model would

circular arcs

ceiling

parabolic arcs

ceiling

(a)

(b)

(c)
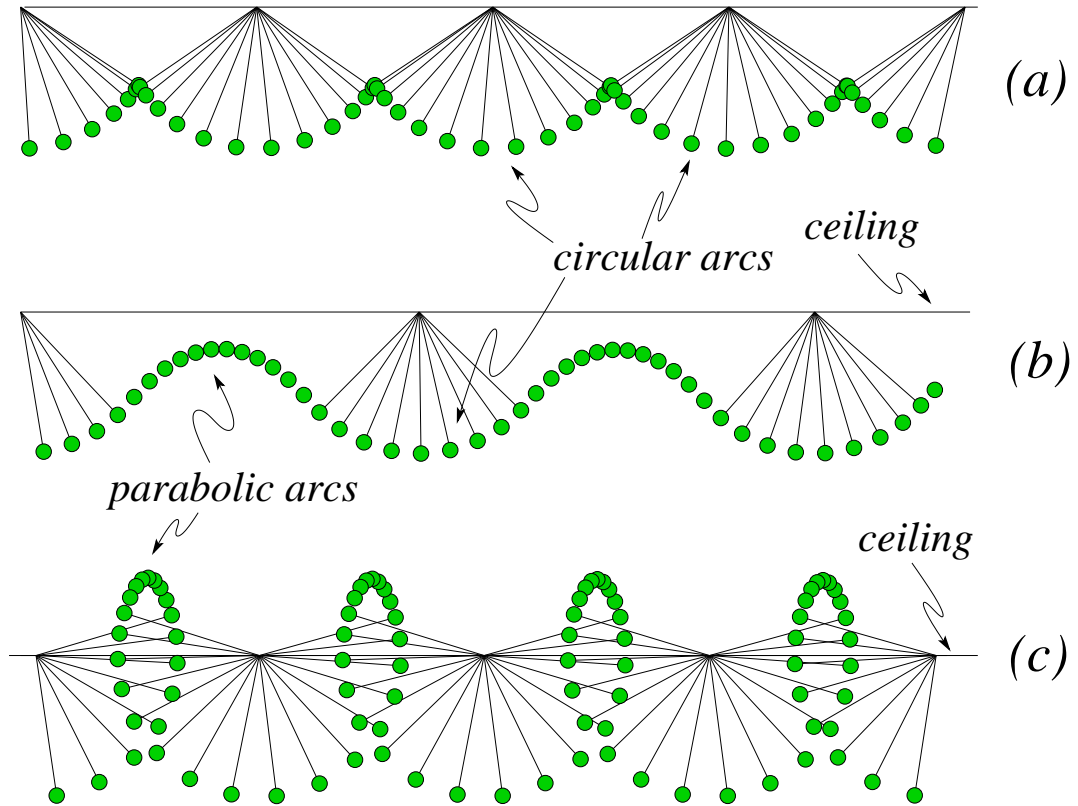
Figure 2.2: Pasting circular arc and parabolic free-flight solutions together to obtain collisionless motions. Figures (a) and (b) are from from Bertram *et al.* [5]. Figure (c) shows a ricochetal solution for this model which does not appear in [5] and is descriptive of some motions seen in gibbon brachiation. Note that $\theta > \pi/2$ when release occurs to obtain a motion with a backwards flight phase as shown in Figure (c).
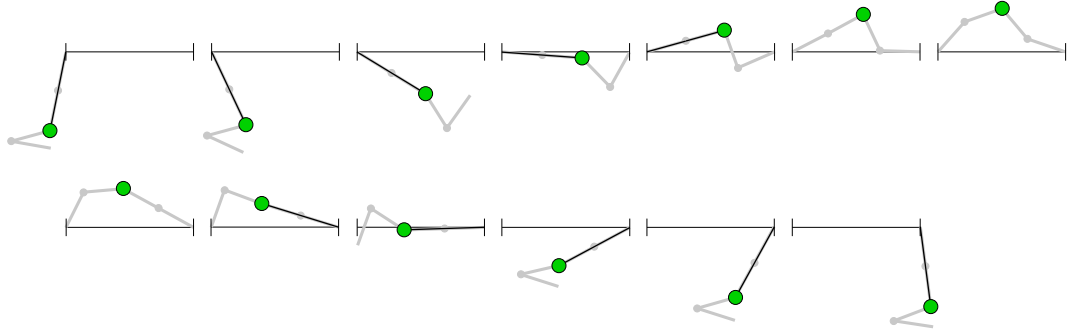
Figure 2.3: A cartoon sketch of the arms of a gibbon overlayed on top of the motion shown in Figure 2.2(c). The class of motions shown in Figure 2.2(c) consists of those ricochetal gaits of the point mass model with a backwards moving flight phase. Note that the arm positions are an interpretation of the results are not included in the point-mass model itself. The cartoon shows that these motions, unlike all other classes of motions discussed here, allow for a finite amount of time with both hands on handholds while transitioning.

be considered a ricochetal gait. Figure 2.2(c) depicts such a motion in the model. The actual gibbon using this gait would have both hands on consecutive handholds during the backwards flight portion of the ricochetal gait.

Usherwood and Bertram [67] have observed this "loop-the-loop" motion when studying gibbon brachiation. They observe "active flexion of the trailing arm" in a gibbon executing continuous contact brachiation. They conjecture that this motion may reduce the energetic losses due to collisions.

There is a practical advantage for this backwards free-flight motion. There is a very high cost associated with missing a handhold in the real world [67]. The motion depicted above allows a gibbon a large window of opportunity to grasp the next handhold. The motion shown in Figure 2.2(c) is a completely passive continuous contact motion where the center of mass of the "gibbon" moves backwards to avoid collision losses when putting tension on the next handhold.

2.5   Rigid Body Model

We now extend the point mass model by replacing the point mass with a rigid body. We still use a massless controlled arm so this model is also not strictly passive, in a control sense. This massless arm is connected to a single rigid body which represents a lumping together of a gibbon's torso, legs, and swing arm. This rigid body, unlike the point-mass body, has a non-zero value for its moment of inertia about its center of mass. The mass and geometry parameters used for this model are listed in the caption for Figure 2.4 and are taken from Preushoft and
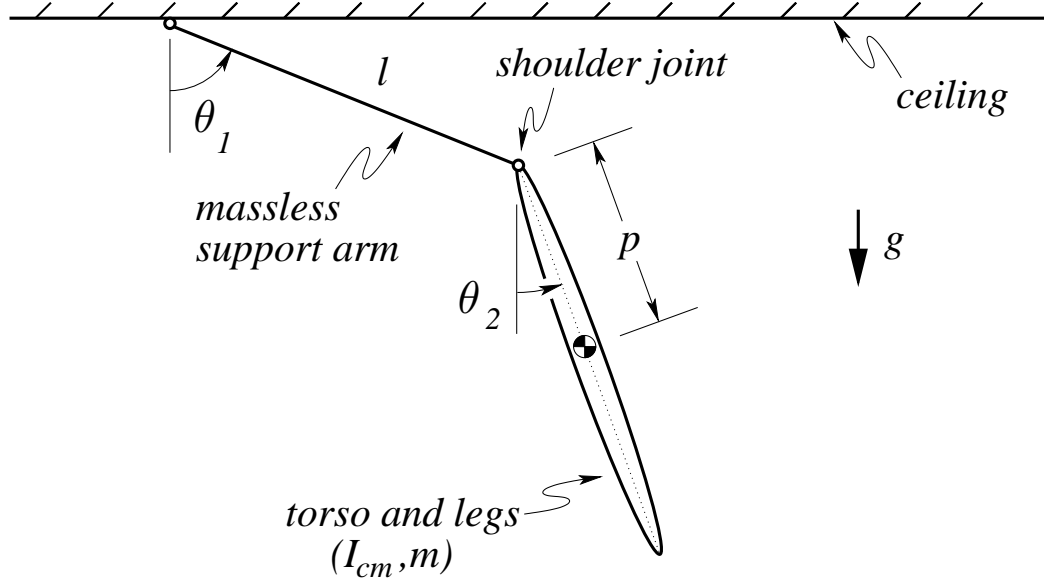
Figure 2.4: The single rigid-body model extension of the point-mass model. The rigid body is modeled as a right circular cylinder representing the gibbon's torso and legs. The cylinder is 0.60 meters long (l_{bod}) with a diameter of 0.25 meters ($2r_{bod}$) and is attached to the arm with a frictionless hinge on the top circular plate of the cylinder. The cylinder's parameters, along with the fact that for a cylinder $I_{cm} = \frac{1}{12}m(3r_{bod}^2 + l_{bod}^2)$, result in the following dimensional parameters: $l = 0.55$m, $m = 5.07$kg, $p = 0.30$m, $I_{cm} \approx 0.172$kg $\cdot$ m^2, $g = 9.81$m/s^2. These parameters are for the cylindrical torso-with-swing-arm of a gibbon given by Preushoft and Demes[47]. We don't use Preushoft and Demes [47] support arm parameters. Instead, since a gibbon's arms are a small percentage of their total body weight, we assume that the supporting arm is massless.

Demes [47]. In the swing phase a frictionless hinge at one end of the rigid body (the shoulder), connects to the massless rigid arm. The hand end of the arm grabs the ceiling when it makes contact and lets go when one or another grab/release criteria is met.

For continuous contact motions, the massless arm provides a constraint at all times; one circular shoulder arc connects to the next. For ricochetal motions, the arm constraint is released at $\theta_1(t) = \theta_{rel}$ at the start of flight and reinstated when the distance from the shoulder to the ceiling (in the direction normal to the shoulder velocity) is again equal to the arm length.

We only seek motions which are symmetric about the mid-swing configuration for the following reason. We are guaranteed (by time reversibility and uniqueness of solutions to ODEs) that if we can find a symmetric motion, it will be collisionless. Note that for non-passive systems (unlike all of the models we present), symmetric motions or even collisionless motions will most likely not conserve energy (since energy can be absorbed in the actuators- eccentric muscle contractions). Thus we define $\theta_1 = 0$ to be $t = 0$ at which time we assume that all links are hanging straight down (or up, see appendix). Solutions are then parameterized by the values of $\dot{\theta}_1(0)$ and $\dot{\theta}_2(0)$.

Unlike the situation for the point-mass model, finding collisionless periodic solutions for the rigid-body model can be a slight challenge. The existence of these special solutions is first examined using a counting argument. For the counting argument, we assume that the mass and geometry properties are given and fixed.

The initial conditions which parameterize our solution space for continuous contact gaits are $\dot{\theta}_1(0)$ and $\dot{\theta}_2(0)$. We pause our numerical integration when $\dot{\theta}_1 = 0$ and calculate the state of our system. $\dot{\theta}_1 = 0$ is special because at that moment the massless arm can release and grab the next hand hold with no collision loss. If our system is again in a symmetric configuration at that moment (t_f), with $\theta_2(t_f) = 0$, then the initial conditions starting this motion are the ones we seek. These initial conditions give a symmetric periodic collisionless motion. All motions which have this symmetry are periodic because the equations of motion are time-reversible, so extending the solution forward in time necessarily leads to a state identical to the state at $t = 0$ and the motion can be continued *ad infinitum*.

Now that we have defined the conditions that we want to meet, we can discuss the likelihood of meeting those conditions via a simple counting argument. To find zero-cost periodic continuous-contact solutions we have two parameters to vary and only one condition to meet, so we expect to find (and do find) a one parameter family of solutions. That is, for each $\dot{\theta}_1(0)$ that is not too large we can find a $\dot{\theta}_2(0)$ so that $\theta_2 = 0$ when $\dot{\theta}_1$ reaches zero. We find these solutions by numerical root-finding on $\theta_2(t_f)$. Numerical integration of the governing differential equations with the state evaluated when $\dot{\theta}_1(t_f) = 0$ gives us the function whose roots we seek (*i.e.* we solve θ_2(when $\dot{\theta}_1 = 0) = F(\dot{\theta}_1(0), \dot{\theta}_2(0)) = 0$ where F is evaluated using numerical integration). The appendix describes more details of the numerical integration, event detection, and the root finding.

Actually there are several (an infinite number) of branches of solutions. They
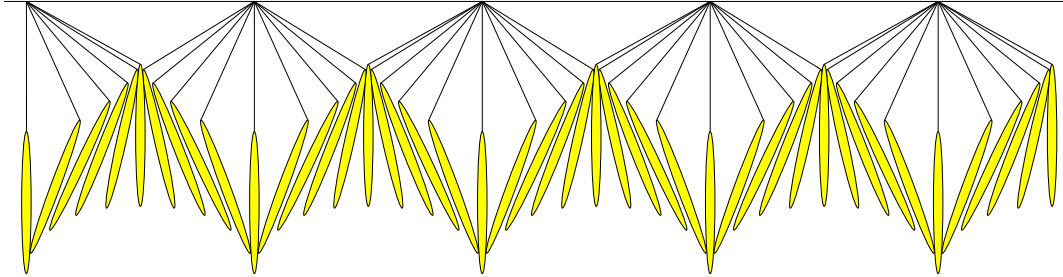
Figure 2.5: A continuous contact motion of the rigid body model. The initial conditions which result in this motion are: $\theta_1 = 0$ rads, $\theta_2 = 0$ rads, $\dot{\theta}_1 = 9$ rads/sec, $\dot{\theta}_2 = $ -8.94693865402 rads/sec. These images are equally spaced in time.

can be grouped by how many times $\dot{\theta}_1$ has passed through zero before we take $\dot{\theta}_1 = 0$ as the start of a new handhold. A simple continuous-contact solution which meets the above requirements is shown in Figure 2.5.

The conditions for determining a collisionless ricochetal brachiation gait are related to, but different from, the conditions given above for a continuous-contact gait. For our ricochetal solutions, we consider the release angle θ_{rel} to be fixed in our solution search. Again parameterizing solutions by $\dot{\theta}_1(0)$ and $\dot{\theta}_2(0)$ (and starting with $\theta_1(0) = \theta_2(0) = 0$) we integrate forward in time, first using the double-pendulum equations of motion and then, following release, the free-flight equations. When the shoulder reaches a relative maximum in height (t_f determined by our Poincaré section: $\dot{y}(t_f) = 0$) we then seek a symmetric solution (with $\theta_2(t_f) = 0$). Again we are trying to meet one condition as a function of two parameters so expect to find a one-parameter family of solutions. And again, it turns out that there are many branches of solutions, some of which are incredibly complex. If we also consider θ_{rel} to be a free parameter we have a two parameter family of collisionless ricochetal motions, two of which are shown in Figure 2.6 and Figure 2.7. Of the infinite number of collision-free motions the simpler ones (fewer back and forth swings between handholds, no over-the-top swings, no mid-flight flips) appear to be more gibbon-like when animated. Both of the models examined which have massless arms require the massless arm to be controlled so that it is in the correct position to grab onto the next handhold. In order to remove this control requirement in the next brachiation model (the two-link model), we replace the massless arm with arms that have mass and inertia.

2.6   Two-Link Model

The two-link-model consists of two rigid bodies hinged together with a pin joint, a crude approximation of the two arms of a gibbon. The torso, head, and legs are modeled as a heavy point mass located at the hinge between the two arms. Adding
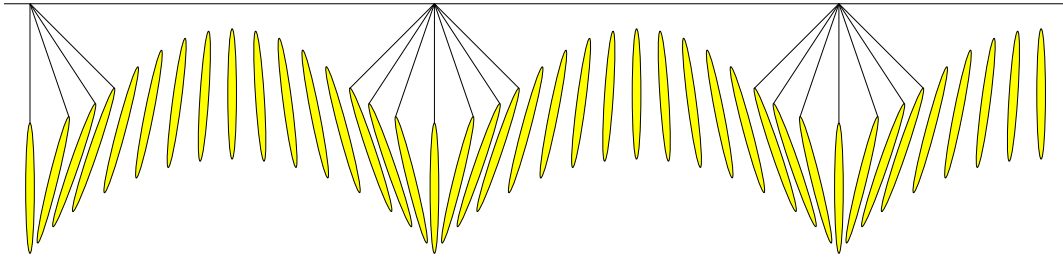
Figure 2.6: A ricochetal motion of the single rigid body model with a massless arm. This motion releases it's hold on the ceiling when $\theta_1 = 45°$. The initial conditions for this motion are: $\theta_1 = 0$ rads, $\theta_2 = 0$ rads, $\dot\theta_1 = 12$ rads/sec, $\dot\theta_2 = $ -9.993972628 rads/sec. N.B. These images are not quite equally spaced in time. We chose to emphasize the symmetry of the motion by using equally spaced time images to exactly capture the end and mid points of the contact motion and a slightly different time step for the free flight motion to capture its symmetry point.
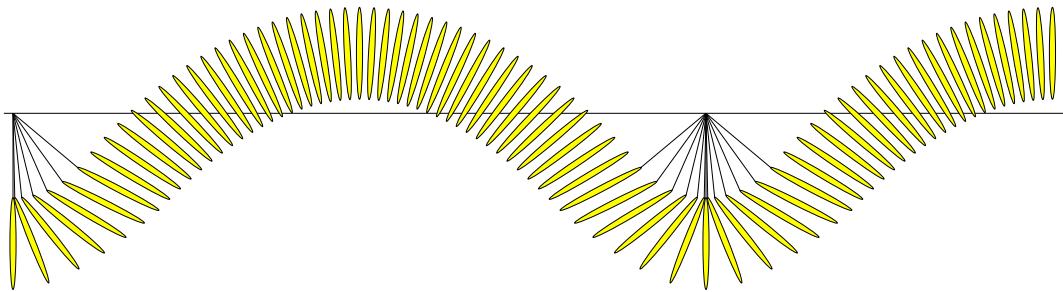
Figure 2.7: Another ricochetal motion of the single rigid body model. This motion releases the ceiling when $\theta_1 = 50°$. The initial conditions are: $\theta_1 = 0$ rads, $\theta_2 = 0$ rads, $\dot\theta_1 = 1/10$ rads/sec, $\dot\theta_2 = 17.45530093$ rads/sec. N.B. These images are *not* equally spaced in time for the same reason given in the caption of Figure 2.6.
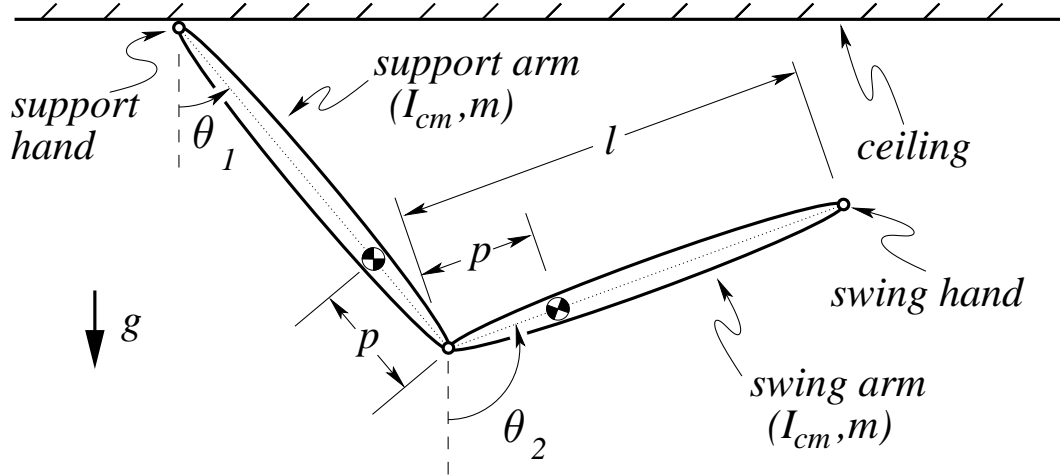
Figure 2.8: This is a depiction of the two-link model of a brachiator. Note that the two links have identical parameters as measured from the central hinge at the "shoulder". The parameters for this model are: $l = 0.61$m, $m \approx 3.083$kg, $p \approx 0.0638$m, $I_{cm} \approx 0.0539$kg $\cdot$ m^2, $g = 9.81$m/s^2. Note that the two links have identical parameters as measured from the central hinge at the "shoulder". The torso has been shrunk to a point mass, placed at the central hinge between the two arms, and divided evenly between the two arms for the purpose of calculating the arm's parameters. See chapter 3 for more detail on how these particular parameter values were chosen.

a point mass at the hinge is dynamically identical to a modification of the mass distributions of the two links. This model is equivalent to the two-link robotic brachiator of Fukuda et al. [20] after the removal of all their motor torques at the central hinge.

For this model we will only examine the continuous contact motions, but we will look at them more thoroughly than the other models.

A continuous-contact gait counting argument now predicts only isolated initial conditions leading to periodic zero-collision solutions for a given set of physical parameters. Our numerical searches find many such isolated solutions with varying complexity. We think there are an infinite number of such solutions because of the chaotic nature of a double pendulum.

Most of the collisionless periodic motions that is model is able to achieve do not resemble gibbon-like brachiation (Figures 2.12-2.15). However, the model is capable of two gibbon-like continuous-contact motions, shown in Figure 2.9 and 2.12.

The single motion described by Figures 2.9, 2.10, and 2.11 begins with both hands on the ceiling and the whole system motionless. One hand releases its grasp and the links begin to move under the pull of gravity. Halfway through the motion
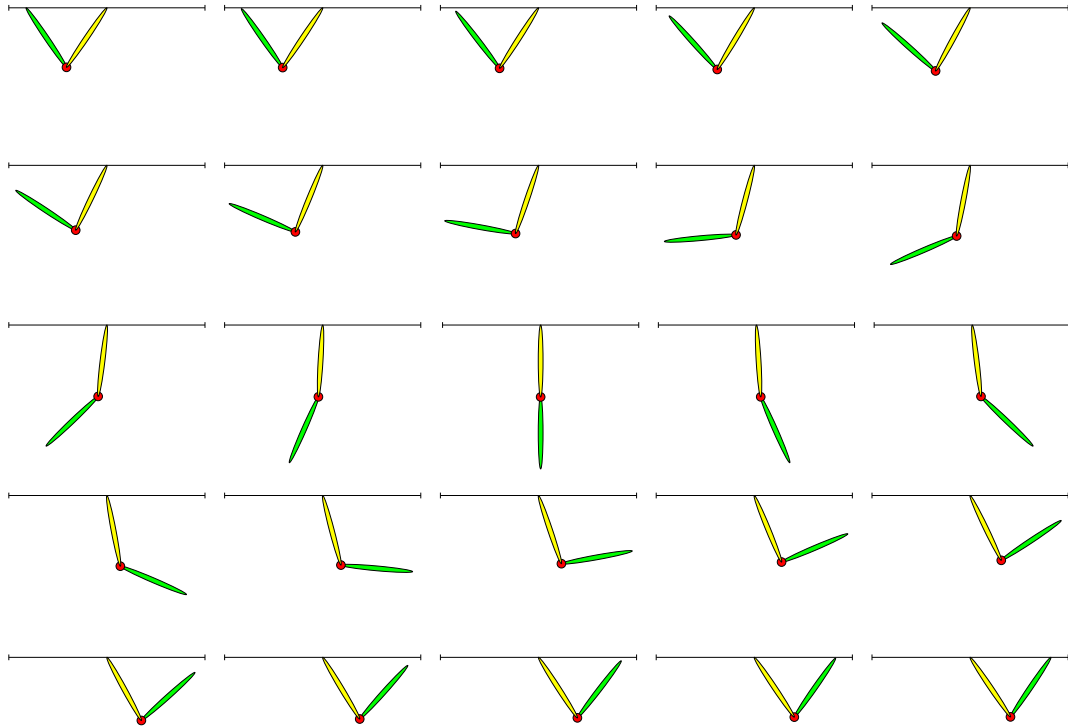
Figure 2.9: A gibbon-like continuous contact motion of the two-link model. The initial conditions are: $\theta_1 = 0$ rads, $\theta_2 = 0$ rads, $\dot{\theta}_1 = 1.5505189108055$ rads/sec, $\dot{\theta}_2 = 11.733043896405$ rads/sec. This motion is further described in Figures 2.10 and 2.11. This motion is the motion labeled "A" in Figure 2.19.
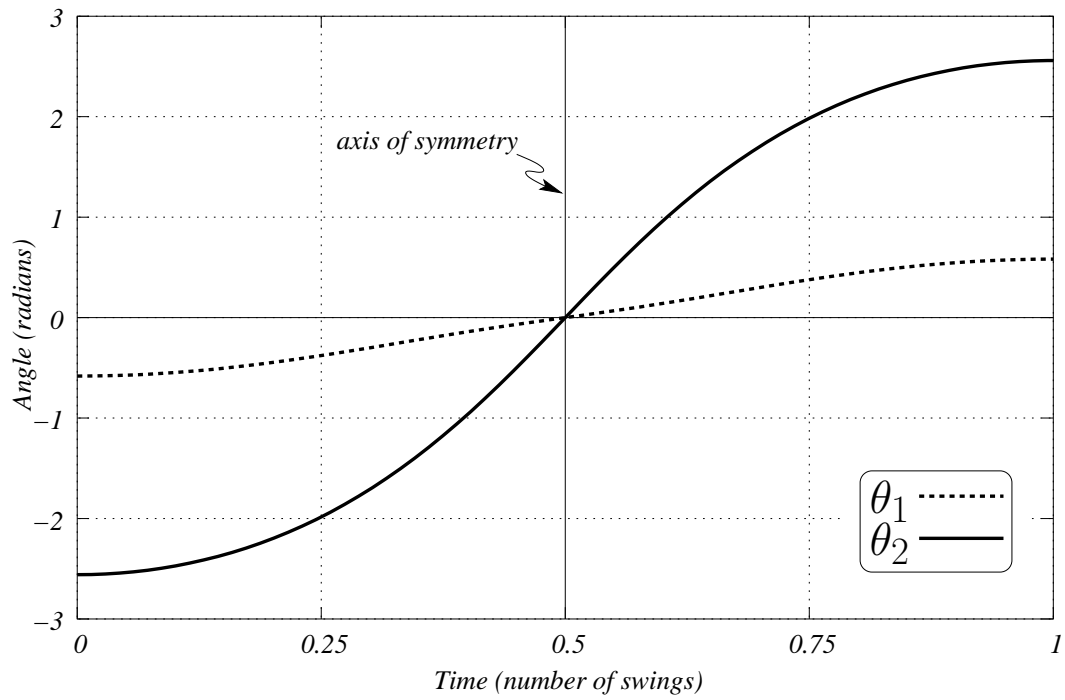
Figure 2.10: Graph of link angles for the motion depicted in Figure 2.9. Note that at the end of the swing the swing hand must be in contact with the ceiling. Both link angles are equal in magnitude at the end and beginning of the cycle but are opposite in sign.
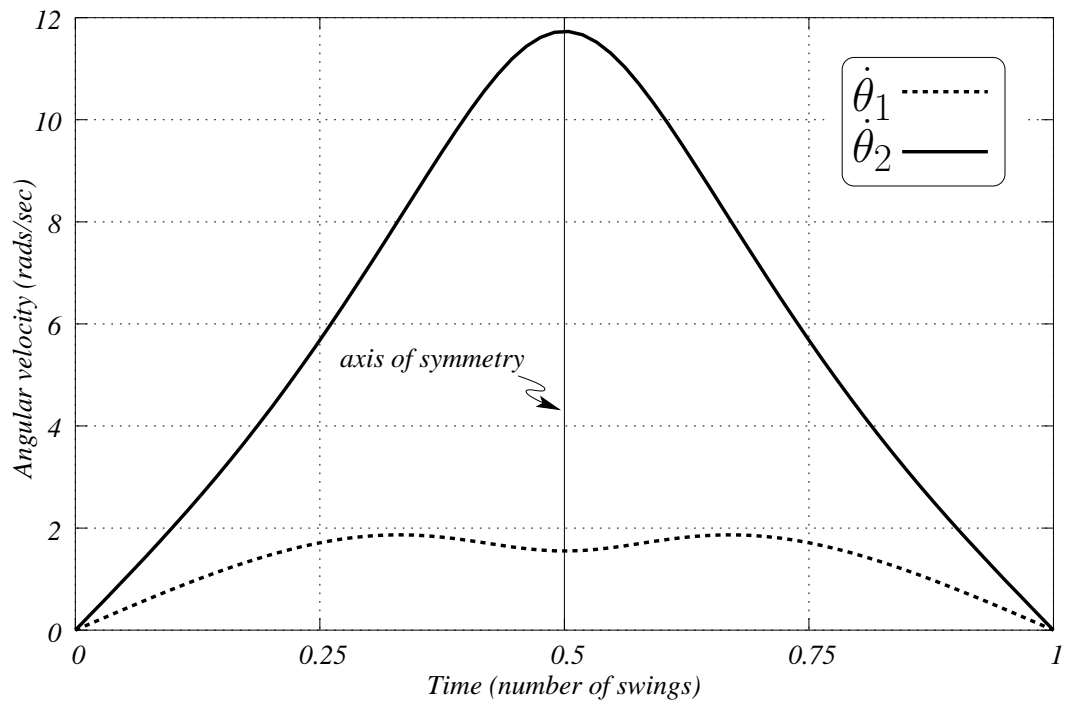
Figure 2.11: Graph of angular velocities for each link during the motion depicted in Figure 2.9. Note that at the beginning and end of the motion, the swing hand is at rest since both links have zero angular velocities at those times. The swing hand being at rest is the condition for a collisionless motion.
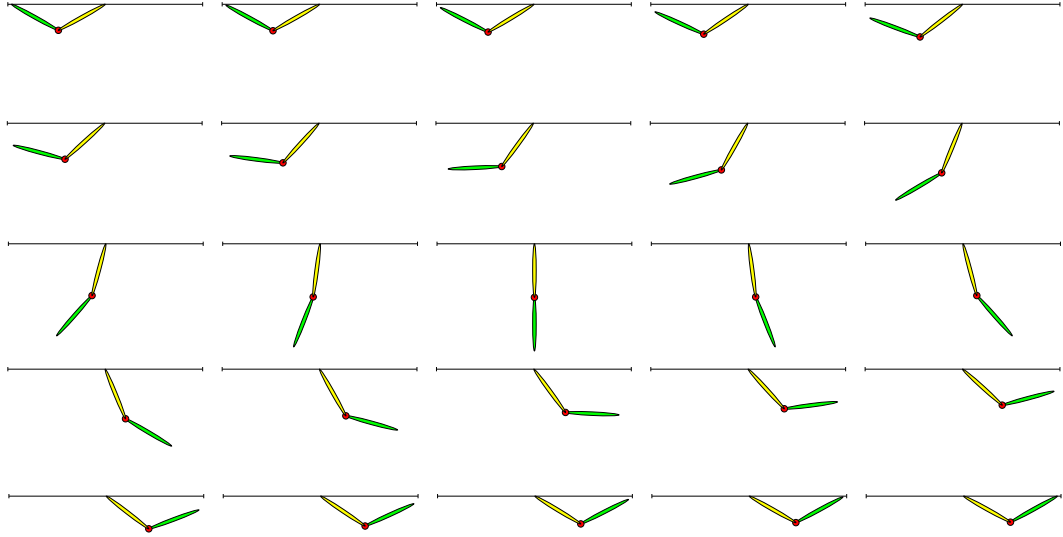
Figure 2.12: Another gibbon-like continuous contact motion for the two-link model. This motion's initial conditions are: θ_1=0 rads, θ_2=0 rads, $\dot{\theta}_1$=3.560582315550 rads/sec, $\dot{\theta}_2$=10.19595757383 rads/sec. This motion is the motion labeled "B" in Figure 2.19.

the links pass through the symmetrical position with one arm straight up and the other straight down. The motion ends when the swing hand arrives at the ceiling just as the swing hand's velocity drops to zero. In this manner the model is able to conserve energy even in the presence of plastic collisions.

To find these motions we used a brute force approach and systematically mapped out a section of the system's initial condition space. Each point on Figure 2.22 represents an initial condition where the system starts with $\theta_1 = \theta_2 = 0$ (and the two values of $\dot{\theta}_1$ and $\dot{\theta}_2$ as derived from the values of ϕ and E/Eref shown in the plot by the position of the point) and ends with both links simultaneously at rest some time later($\dot{\theta}_1 = \dot{\theta}_2 = 0$). We will call these plots where the collisionless motions are represented by points in a reduced state space, *initial condition plots*. We will also refer to a *modified initial condition plot* which has points representing the same motions as in the corresponding initial condition plot, but uses the distance of the swing hand from the ceiling at the moment of zero kinetic energy in the system during the collisionless motion instead of $E/Eref$ to represent the collisionless motions. The initial condition plot of Figure 2.22 does not show all of the motions satisfying the above conditions since one needs to put a limit on the amount of time one waits for the system to reach the desired end state. Instead of using integration time, we limit the number of sign reversals of $\dot{\theta}_1$. For example, Figure 2.22 contains the motions which have two reversals in the sign of $\dot{\theta}_1$ during half of the swing (*i.e.* the first and second sign change of $\dot{\theta}_1$ are ignored and the integration is stopped when $\dot{\theta}_1 = 0$ for the third time). This restriction allows us to examine only the "simpler" periodic collisionless motions. Since Figure 2.22 only
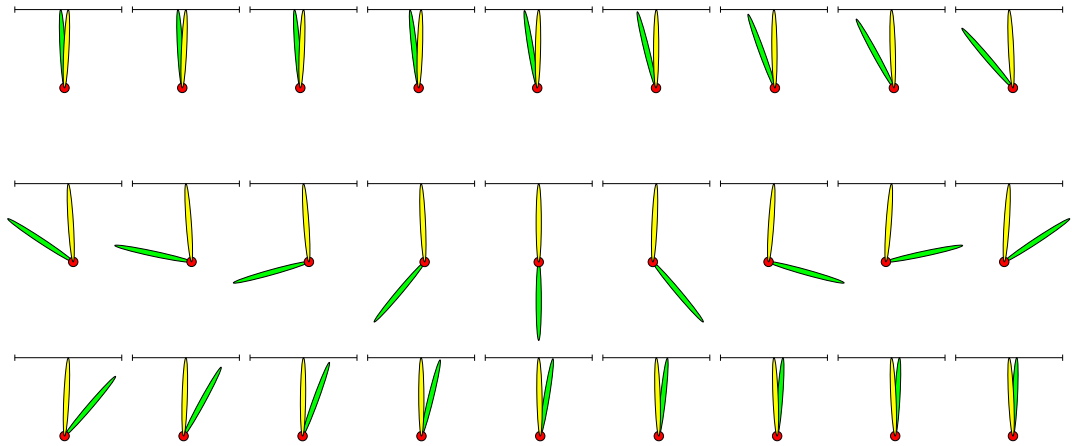
Figure 2.13: A very slowly forward-progressing motion for the two-link model. The initial conditions for this motion are: θ_1=0 rads, θ_2=0 rads, $\dot{\theta}_1$= -0.8161734768013 rads/sec, $\dot{\theta}_2$=11.39054426196 rads/sec
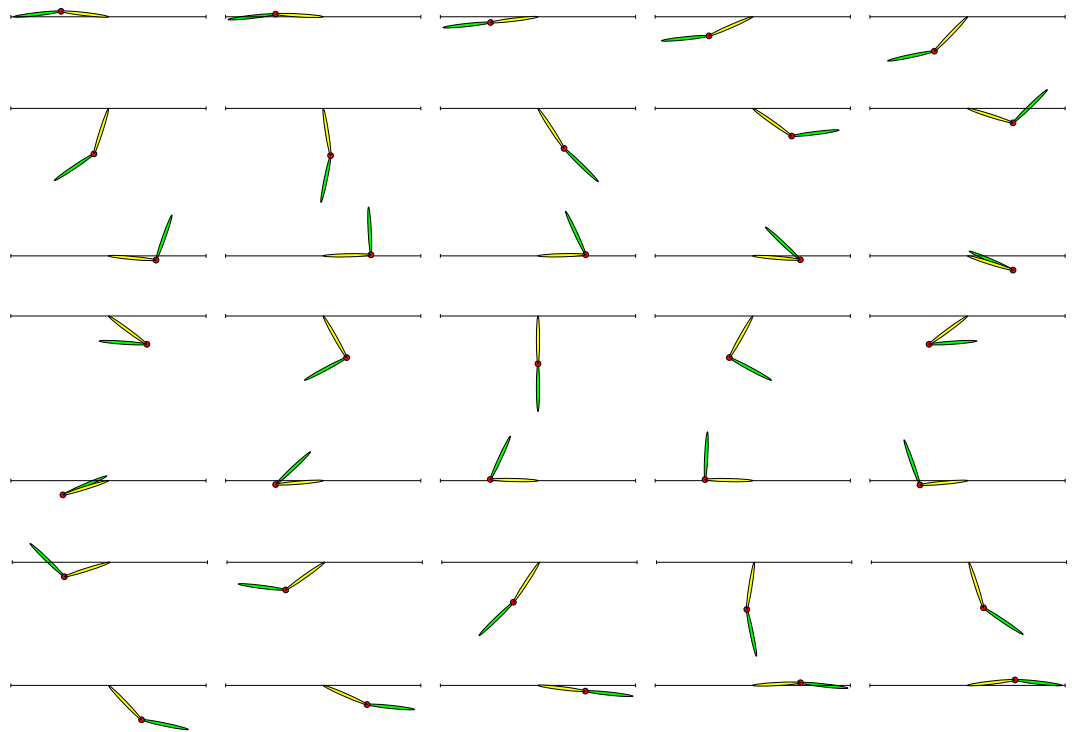
Figure 2.14: A more complicated continuous contact motion for the two-link model. Initial conditions are: $\theta_1 = 0$ rads, $\theta_2 = 0$ rads, $\dot{\theta}_1 = $ -6.533304299333 rads/sec, $\dot{\theta}_2 = 15.24050128207$ rads/sec
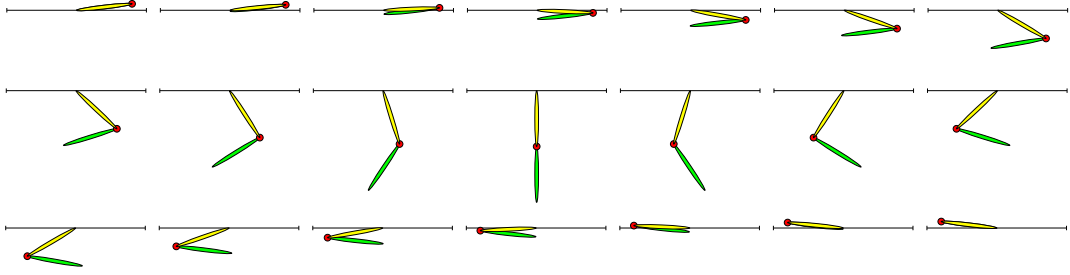
Figure 2.15: A non-forward-progressing motion for the two-link model which satisfies all of the required conditions for a periodicity and lack of collision of the swing hand with the ceiling.. Initial conditions for this motion are: θ_1=0 rads, θ_2=0 rads, $\dot{\theta}_1$=-6.535385384989 rads/sec, $\dot{\theta}_2$=13.52769090018 rads/sec. This motion is the motion labeled "C" in Figure 2.19.
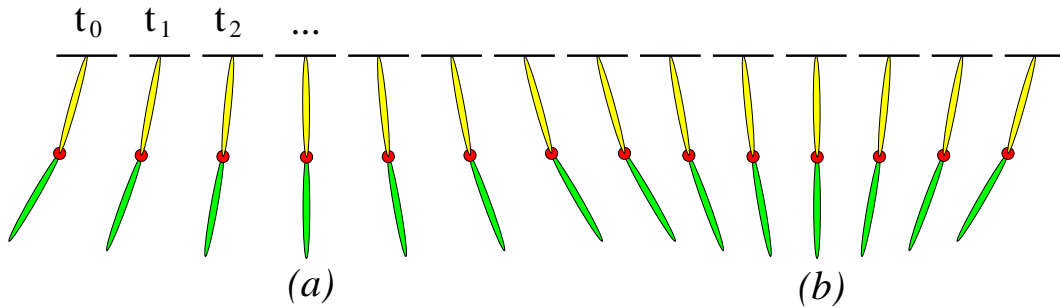
Figure 2.16: Snapshots showing one of the two small amplitude linear normal modes for a double pendulum

describes a small set of the possible initial conditions which would result in a periodic collisionless motion. Even though Figure 2.22 is incomplete, we can be fairly confident that we have not missed any of the *gibbon-like* motions by disregarding the complicated and high energy motions.

Figure 2.22 shows some of the initial conditions which result in periodic motions where the kinetic energy of the system drops to zero at some point during the cycle. The double pendulum is a two degree-of-freedom system which requires four initial conditions (θ_1, θ_2, $\dot{\theta}_1$, and $\dot{\theta}_2$) to specify a state of the system and thus a particular motion. A symmetry argument can be made, similar to the one made for the rigid-body model, to reduce the dimension of our search space. We find collisionless motions by doing a proxy search for symmetric motions. If we can find motions which have a certain symmetry then by necessity (time reversibility of solutions) they are also collisionless. For this model we can also show that all collisionless motions have this symmetry property (see section 2.6.1). The symmetry condition that we seek is one where the motions must pass through the state ($\theta_1 = \theta_2 = 0$) and at some time later achieve ($\dot{\theta}_1 = \dot{\theta}_2 = 0$). These motions will be symmetric

t_0 t_1 t_2 ...

(a) *(b)*
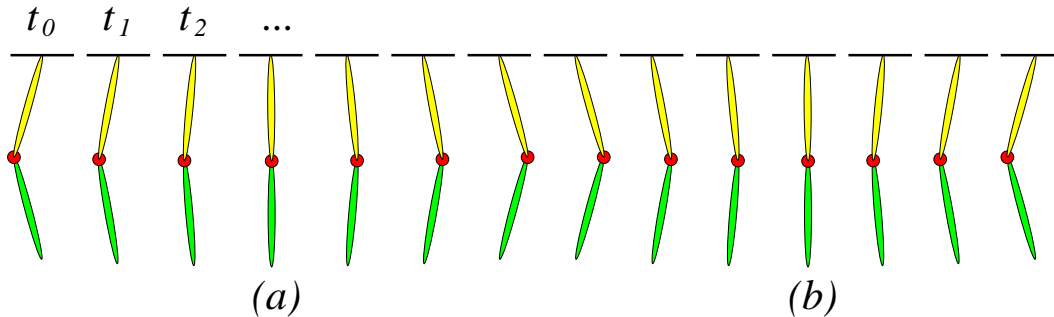
Figure 2.17: A depiction of the double pendulum's other small amplitude linear normal mode.

about the $\theta_1 = \theta_2 = 0$ configuration. Note that motions which match the above two conditions will be collisionless motions for which the swing hand will most likely not reach handhold but will come to rest at some point below the ceiling. Since we want to enforce this symmetry condition we start all candidate motions with both links straight down (*i.e.* $\theta_1 = \theta_2 = 0$). Thus, we just need to specify two initial conditions, the two angular velocities of the two links (*i.e.* $\dot{\theta}_1$ and $\dot{\theta}_2$). The combinations of those two variables which result in a collisionless periodic motion are plotted as points on the initial condition plot. Instead of using the angular velocities in the plots, we execute a simple change of variables and use instead ϕ, a phase angle defined as $\tan(\phi) = \dot{\theta}_2/\dot{\theta}_1$, and a non-dimensionalized energy E, where we use $E_{ref} = mg(l - p) + mg(l + p) = 2mgl$ to non-dimensionalize the system's energy. E_{ref} is half of the largest difference in potential energy possible for the system. This alternative set of initial condition variables allows a thorough exploration of the initial condition space because one of the initial conditions is bounded, *i.e.* $-\pi \le \phi < \pi$ and the other one is bounded on one side (at zero) and we can choose the bound for the other side. Actually, for the continuous-contact motions we seek, we can put an upper bound on the energy initial condition. Since we are requiring that the system come to rest when we switch handholds in order to conserve energy, there will be no solutions with an initial energy larger than $2E_{ref}$.

At low energies Figure 2.22 shows that there are only two motions which meet the above requirements. These motions correspond to the two normal modes of the linearized system, depicted in Figure 2.16 and 2.17. These two normal modes do not have enough energy to get the swing hand up to the height of the next handhold. We need to further require that the end point of the swing arm link reach ceiling height when the kinetic energy of the system drops to zero. Each of the motions represented in Figure 2.22 ends up at rest a measurable distance away from the ceiling elevation. For each of those motions, we can plot ϕ versus the distance of the swing hand below the ceiling height. Intersections of the curves in Figure 2.19, 2.21, and 2.23 with a vertical line at a zero ceiling distance represent a solution which satisfies the conditions for a periodic collisionless motion. However,
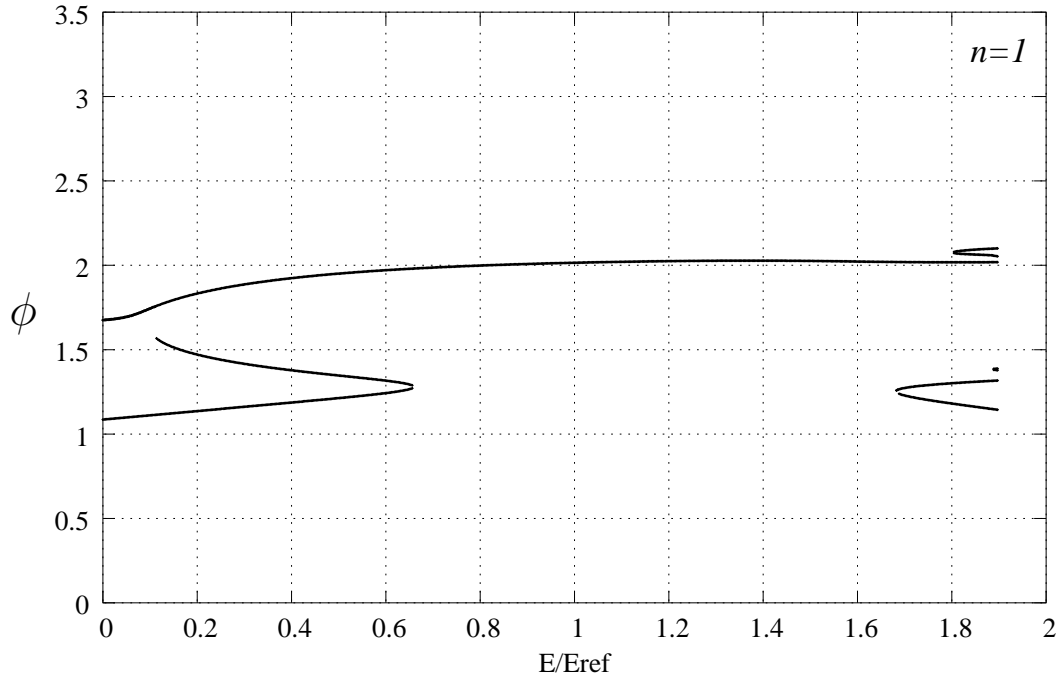
Figure 2.18: Initial condition plot (see definition in text on page 27) for the two-link model beginning with $\theta_1 = \theta_2 = 0$ and the designated values of ϕ and E/E_{ref}. These motions end when $\dot{\theta}_1 = 0$ for the first time, that is they have no reversals in sign of $\dot{\theta}_1$ in the complete motion.

even in that set of motions, about half come up to the ceiling with the swing hand at exactly the same vertical and horizontal position as the supporting arm's hand. An explanation for the existence of two categories of collisionless motions is given in appendix 2.6.4. Now, let's consider the set of motions which do progress horizontally. Most of those swing around many times before coming to rest at the next handhold, like the motion shown in Figure2.14. Thus there are only a few motions (for this model and parameter set) which give gibbon-like brachiation behavior.

2.6.1 Symmetry

Previously in this chapter we showed how a symmetric motion of the type we described will necessarily be collisionless. One might think that this reduces the number of possible collisionless solutions that we will find since we can only find symmetric ones using our proxy search. This is not true for continuous-contact motions for this model. Here we show that all collisionless motions must be symmetric.

We use proof by contradiction to show that collisionless motions for this model
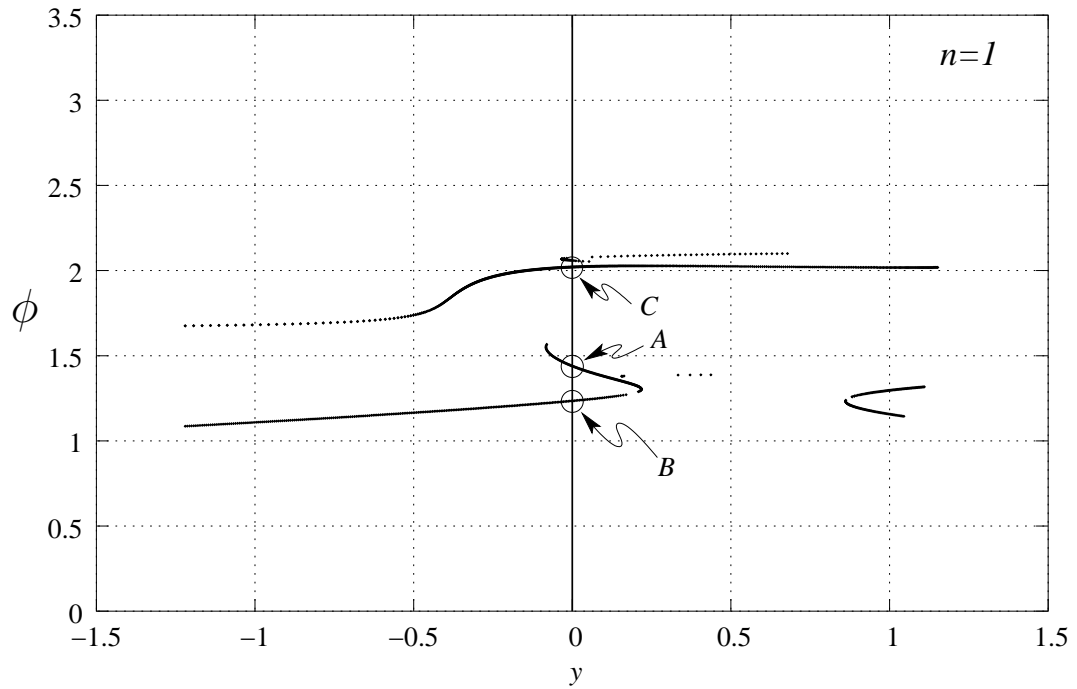
Figure 2.19: Modified initial condition plot (see definition in text on page 27) for the two-link model representing the same motions as in Figure 2.18 Here the horizontal axis of the plot uses the distance of the swing hand above the ceiling when the system is at rest (y), instead of using the non-dimensionalized energy. The motions that are of interest to us are the ones where the swing hand comes to rest at ceiling height $(y = 0)$. In this plot there are four such intersections representing four simple periodic collisionless motions. Three of these motions, labeled A, B, and C, are shown as pictograms in Figures 2.9, 2.12, 2.15, respectively.
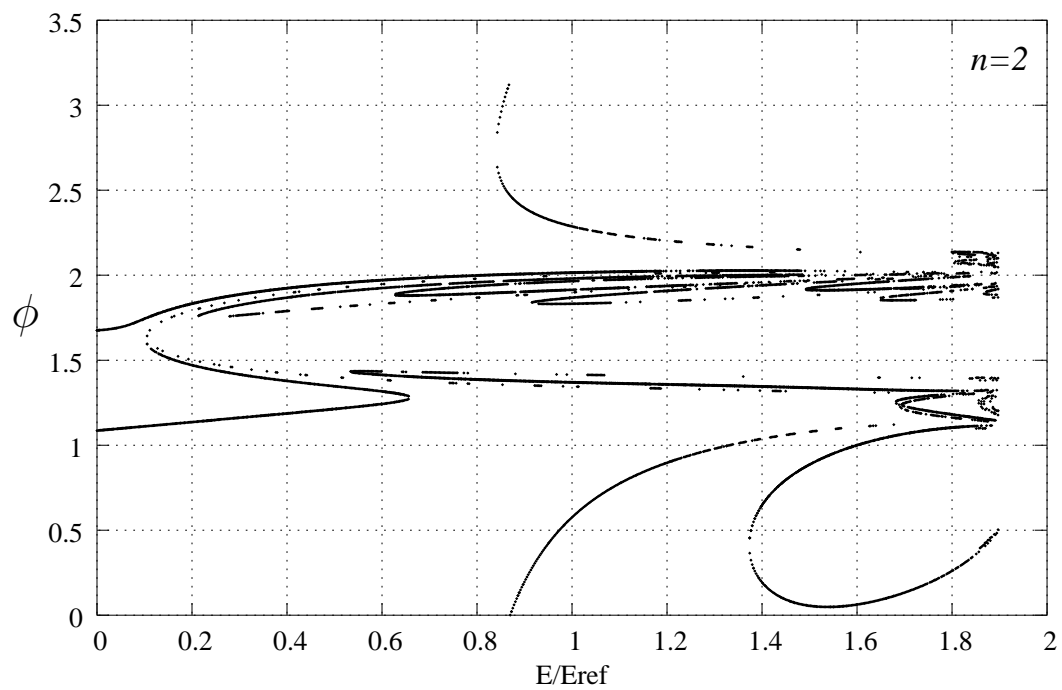
Figure 2.20: Initial condition plot (see definition in text on page 27) for the two-link model showing more complicated motions, *i.e.* ones that have two sign reversals of $\dot{\theta}_1$ during a single swing.
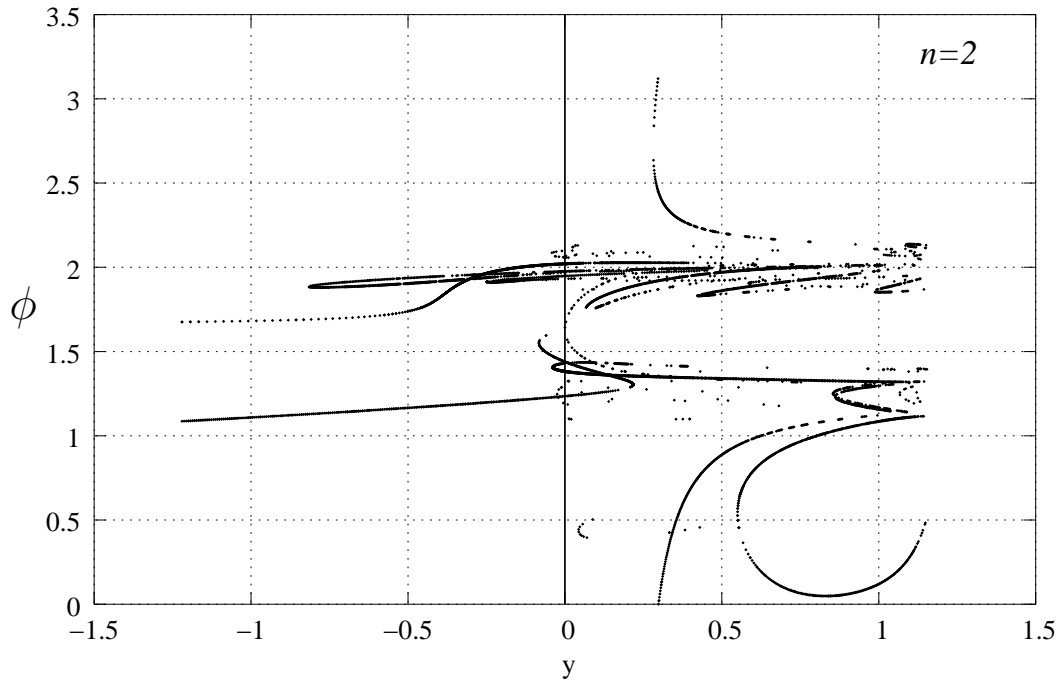
Figure 2.21: Modified initial condition plot (see definition in text on page 27) for the two-link model representing the same motions as in Figure 2.20. Note that the solutions that we found that have no sign reversals of $\dot{\theta}_1$ appear on this plot of motions that have two sign reversals. This is due to the fact that all of these motions are periodic so one just needs to wait until the motions that have no sign reversals to swing back and forth in place and then grab onto the ceiling after it has swung in place twice.
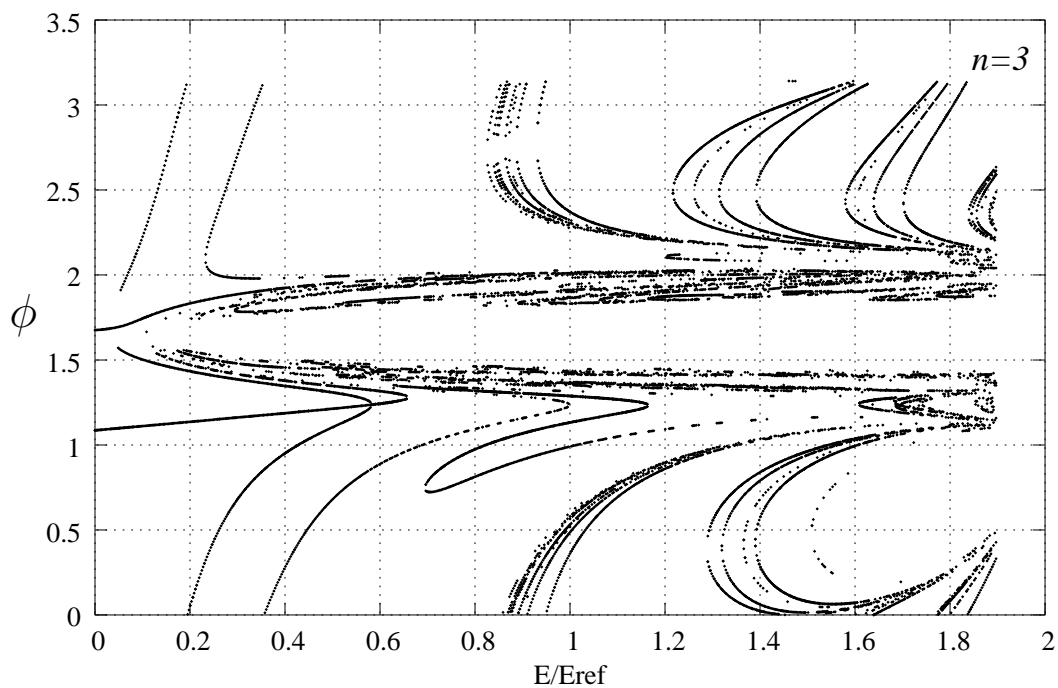
Figure 2.22: Initial condition plot (see definition in text on page 27) for the two-link model showing even more complicated collisionless motions, i.e ones that have four sign reversals of $\dot{\theta}_1$ during a single swing.
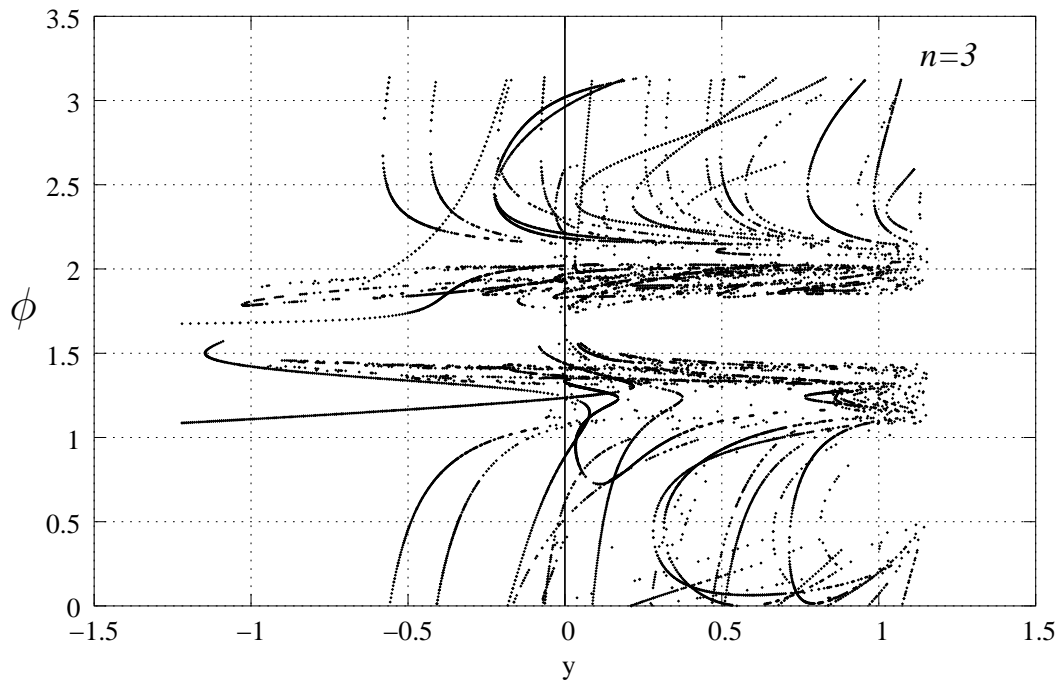
Figure 2.23: Modified initial condition plot (see definition in text on page 27) for the two-link model representing the same motions as in Figure 2.22. Again, note that this plot has the solutions found for zero and two sign reversals of $\dot{\theta}_1$. Note that one simply needs to wait longer, due to periodicity, to turn a two reversal motion into a four reversal motion.
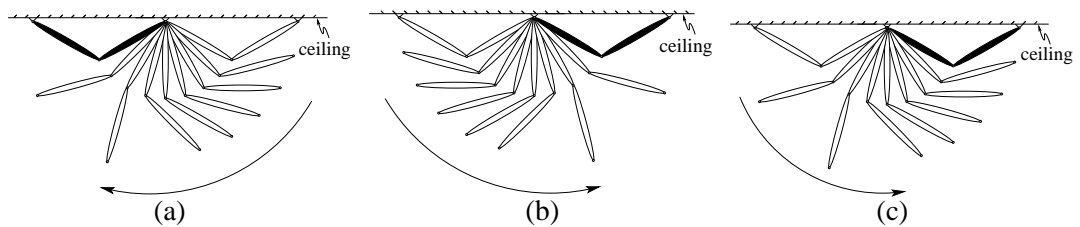
Figure 2.24: (a)Tentative trajectory for system. (b)Trajectory for mirrored initial conditions. (c)The original trajectory under a time reversal.

must be symmetric. First we assume that we have a non-symmetric collisionless motion, shown in Figure 2.24(a). The motion of the system when started from the ending position will be identical to the motion started from the beginning position just mirrored about the support hand since energy is conserved and the kinetic energy of the system is zero at the starting and ending configurations. Figure 2.24(b) shows the same motion with the two hands switched or, if one prefers, the same motion as seen from the other side of the 2-D plane. When we look again at the original system and reverse time, the trajectory for that system would look like Fig 2.24(c) due to the time reversibility of the differential equations. Note though that both of the systems pictured in Figure2.24(b) and 2.24(c) have the same initial conditions. Since the solutions for initial value problems of well-behaved (continuous and first-derivative continuous) ordinary differential equations are unique that means that the two trajectories shown in Figures 2.24(b) & (c) must be the same trajectory. The only way that they can be the same trajectory is for the that trajectory to be mirror reflection symmetric about a vertical line passing through the support-hand.

Another way to see the above argument is to look at the equations of motion for the two-link system, eqn.(2.1)&(2.2), and make the following substitutions: $\theta_1 = -\theta_1$ and $\theta_2 = -\theta_2$. The equations of motion both before and after the substitution are identical.

$$
\begin{aligned}
\theta_1'' = -(&P^2 \sin(2\theta_2 - \theta_1) + P^2 \theta_1'^2 \sin(2\theta_2 - 2\theta_1) + \\
&(2P^3 + 2R^2 P)\theta_2'^2 \sin(\theta_2 - \theta 1) + \\
&(2P^3 - 3P^2 + 2PR^2 - 4R^2)\sin(\theta_1))/ \\
&(P^2 \cos(2\theta_2 - 2\theta_1) - 2R^4 + \\
&(-4P^2 + 4P - 4)R^2 - 2P^4 + 4P^3 - 3P^2)
\end{aligned}
\tag{2.1}
$$

$$
\begin{aligned}
\theta_2'' = (&P^2 \theta_2'^2 \sin(2\theta_2 - 2\theta_1) + \\
&(2P^3 - 4P^2 + 4P + 2R^2 P)\theta_1'^2 \sin(\theta_2 - \theta_1) + \\
&(2P - P^2)\sin(\theta_2 - 2\theta_1) + \\
&(2P^3 + 3P^2 + 2P + 2R^2 P)\sin(\theta_2))/ \\
&(P^2 \cos(2\theta_2 - 2\theta_1) - 2R^4 + \\
&(-4P^2 + 4P - 4)R^2 - 2P^4 + 4P^3 - 3P^2)
\end{aligned}
\tag{2.2}
$$

The above equations have been non-dimensionalized with prime($'$) denoting derivatives with respect to the non-dimensionalized time, τ. The non-dimensional variables are given in the following table:

non-dim'l center of mass location $P = p/l$

non-dim'l radius of gyration $\quad R = \sqrt{I_{cm}/ml^2}$

non-dim'l time $\quad \tau = t/\sqrt{l/g}$
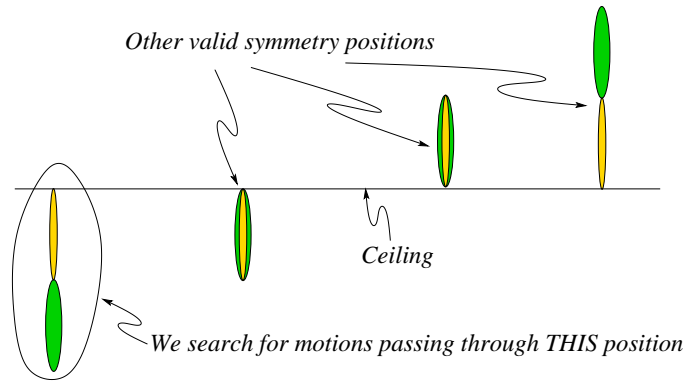
Figure 2.25: The four mirror-image symmetry positions for the mid-swing configuration during a continuous-contact motion of the two-link brachiation model.

The solutions for the motions that are of interest must be symmetric about ($\theta_1 = 0$ *and* $\theta_2 = 0$), ($\theta_1 = 0$ *and* $\theta_2 = \pi$), ($\theta_1 = \pi$ *and* $\theta_2 = 0$), or ($\theta_1 = \pi$ *and* $\theta_2 = \pi$). In other words, the motion of interest must be symmetric about a vertical line going through the support-hand, which was the same conclusion that was reached with the above argument. The four possible symmetry configurations are shown in Figure 2.25. We limit our search by using just one of the four symmetry configurations (*i.e.* $\theta_1 = 0$ *and* $\theta_2 = 0$).

2.6.2 Further restrictions on our search

Collisionless motions of the two-link model require that the swing-hand finish the motion with zero velocity at ceiling height. We enforce this criteria by stating that both links should be at zero angular velocity when the swing-hand reaches ceiling height. This is not the only way for that criteria to be met. There are two sets of configurations for the system where both links have non-zero angular velocity with the swing-hand instantaneously at rest. One set of configurations has $\theta_1 = \theta_2$ and $\dot{\theta}_1 = -\dot{\theta}_2 \neq 0$. This is a "pop-through" motion, similar to the motion of a toggle switch. The other set of configurations has $\theta_2 = \theta_1 + \pi$ and $\dot{\theta}_1 = \dot{\theta}_2 \neq 0$. This configuration has the two links folded back on themselves and moving at the same angular velocity. These two non-static configurations are ignored and our search does not seek them out. Instead we search for configurations that have both $\dot{\theta}_1 = 0$ and $\dot{\theta}_2 = 0$, which result in a zero velocity of the swing-hand. Thus we further limit our search by ignoring the two non-static ending configurations.

2.6.3 Do periodic motions exist?

Most of section 2.6 is concerned with the characteristics of periodic motions for the two-link system without giving thought to whether such motions actually exist.

One argument that can be made for the existence of the periodic motions is based on the premise that when a single initial condition is changed the motion of the system will be different. A function is defined with the two initial conditions as the input and the output being the angular velocity of the support-arm, $\dot{\theta}_1$, and the distance of the swing-hand from the ceiling, a, when the swing-arm reaches zero velocity, $\dot{\theta}_2 = 0$. Thus it can be argued that by changing one of the two initial conditions it is possible to "move" one of the function's outputs to make $\dot{\theta}_1 = 0$. By changing both of the function's inputs it is possible to move both outputs to make both $\dot{\theta}_1 = 0$ and $a = 0$, resulting in a periodic motion which finishes the motion with the swing-hand at ceiling height with zero velocity. This gives no guarantee that one can achieve the desired result. All of the relevant conservation laws must be upheld. For example, one would be unable to find an initial condition set which will result in a final state that has a different energy level than the state at the initial condition. But it seems reasonable that one could obtain a solution by changing only the two initial conditions of the system.

2.6.4   Remarks on the two-link model results

Although Figure 2.23 shows only a few of the collisionless motions that this model can achieve, the motions found can be divided equally into two distinct groups. One group consists of motions in which the swing-hand starts and finishes the motion at two distinct points a non-zero distance apart, allowing the system to move forward by letting go of the ceiling with the support-hand and grabbing on with the swing-hand. The other group consists of the motions in which the system starts and finishes the with the swing-hand at the same location as the support-hand. An explanation for why the motions found tend to divide so well into these two groups comes from the division of the possible initial configurations into two groups. Since both hands must be touching the ceiling, for a given initial potential energy there are only two configurations which will satisfy this requirement. Figure 2.26 shows that for a given energy level one of the possible configurations has both hands in the same location and the other does not. So for every energy level there are two groups of initial conditions, one where the two links overlap and the other where the two links are separated by some angle.

2.6.5   Nonlinear Normal Modes

The periodic motions of the double pendulum are known as nonlinear normal modes. "What is a nonlinear normal mode?" Normal modes of a linear system are the basic motions from which, by superposition, the general motions can be obtained. The double pendulum model at low energies can be well-approximated as a linear system. However, when the energy of the system becomes larger (which is necessary for the swing hand to reach ceiling height) the linearization breaks down and the full nonlinear model must be used. The concept of normal modes as basis functions for general motion does not apply to a nonlinear system. However,
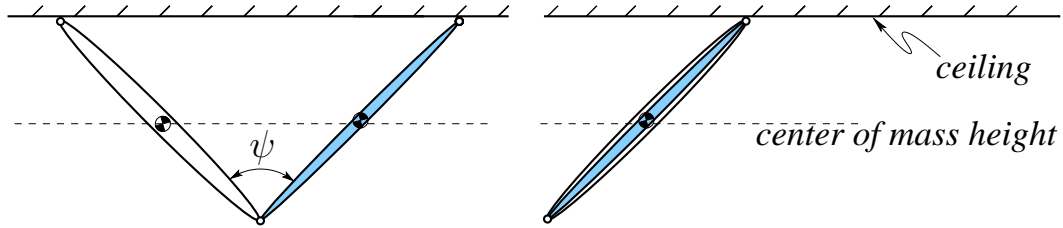
Figure 2.26: Two possible collisionless ending configurations for a given energy level with the swing-hand at ceiling height. One class of configurations has a non-zero relative angle between the two links ($\psi \neq 0$) when switching handholds. The other class of configurations have the links folded back on themselves ($\psi = 0$).

the nonlinear system is capable of motions which have similar characteristics to the normal modes of a linear system. Those similar motions are called nonlinear normal modes. The normal modes of the linearized double pendulum model are periodic motions where both links have a zero angular velocity at the same instant. We used Rosenberg's definition of nonlinear normal modes as a periodic motion with both links achieving zero angular velocity at the same instant [50].

The number of linear modes is equal to the number of degrees of freedom for the system, therefore there are to linear normal modes for the two link model. As the energy of this system increases, the linear approximation becomes less and less accurate. Based on this, a question arises. What happens to these linear modes: do they persist or disappear? As can be seen in Figures 2.18 and 2.20, the linear modes for this system do not disappear as the energy increases, but persist and are joined by other newly created nonlinear normal modes.

2.6.6   Chaotic Motions

As a side note, the rigid body model and the two-link model are well-known as a double pendulum model. The double pendulum has been studied extensively by dynamicists and has become a canonical example of a system which exhibits chaotic behavior. The wild chaotic motions of a double pendulum are beautiful and mesmerizing to observe. However, this system is also capable of periodic motions even at high energy levels, well away from the linear regime of the system.

Since the ape model that we are examining changes handholds, it might not seem to be so closely related to the double pendulum which has a fixed "handhold" for all time. Indeed, the ricochetal two-link model is not so closely related to the double pendulum model. But, the continuous contact model is very similar to the double pendulum model because the initial conditions which result in collisionless periodic motion are identical to those which result in a nonlinear normal mode. For further discussion of nonlinear normal modes please see appendix 2.6.5.

2.6.7 Discussion: Two-Link Model Results

The two-link brachiation model is capable of many collisionless continuous-contact solutions. However, only two of these motions resemble gibbon locomotion. The existence of these collisionless motions is parameter independent. However, the existence of gibbon-like motions is parameter dependent and this is further discussed in Chapter 3. This two link model forms the basis for finding the motions of the three and five link models.

2.7 Three-Link Model

In the previous model the ape's torso and legs were modeled as a point mass at the shoulder, here it is extended into a third link with mass and non-zero moment of inertia.. This three-link model again has two identical arms whose mass and length parameters are based on Figure 3.8. Not that all of the joints not represented in the three-link model are locked (*i.e.* elbows and wrists). The two legs (made up of thighs, shanks, and feet) are compressed to a single point-mass located at the bottom of the torso cylinder.

We examine this three-link model for ricochetal motions only. Given the symmetry properties we have assumed for these motions (that they must pass through the state $\theta_1 = \theta_2 = 0$), we must specify three initial conditions $\dot{\theta}_1$, $\dot{\theta}_2$, and $\dot{\theta}_3$ and a release angle, θ_{rel}. When $\theta_1 = \theta_{rel}$, the support hand releases the ceiling and the brachiator begins the free flight portion of the ricochetal gait. We end our integration when the vertical velocity of the shoulder reaches zero and examine the following state variables θ_1, θ_2, θ_3, $\dot{\theta}_1$, and $\dot{\theta}_2$. We want to find the correct combination of the three initial angular velocities which will result in a motion where (1) the two arm positions are mirror images of each other $[\theta_1 = \pi - \theta_2]$, (2) the two arms are moving with the same angular velocity $[\dot{\theta}_1 = \dot{\theta}_2]$, and (3) the body is in the vertical position $[\theta_3 = 0]$. These three criteria, depicted in Figure 2.28, all need to be met when the vertical velocity of the shoulder goes to zero. If we can find three initial conditions to match the three final conditions, then by symmetry we have found the motion we desire. Figure 2.29 shows such a motion.

As the complexity of the model increases, finding periodic solutions becomes more difficult (root finding procedures fail or lead to odd solutions). So we started with solutions to the two-link model, replacing the point mass with a rigid body with center of mass at the shoulder (which does not change the dynamics at all). Then we repeatedly sought and found solutions with the torso center of mass progressively moved farther from the shoulder [23, 6]. We then slowly moved the connection hinge away from the center of mass, finding periodic zero-energy solutions with each new parameter set.
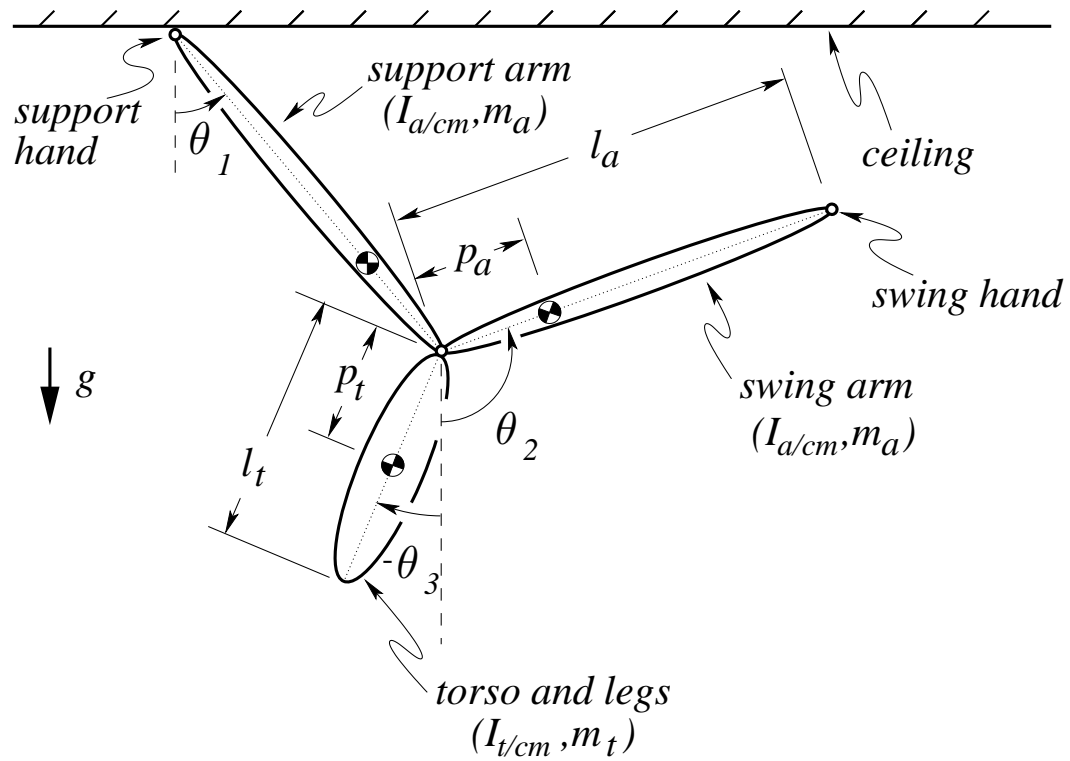
Figure 2.27: Three link model. Parameter values: $l_a = 0.61$m, $p_a \approx 0.2362$m, $m_a \approx 0.8325$kg, $I_{a/cm} \approx 0.01997$m^{2}kg, $l_t = 0.27$m, $p_t \approx 0.1625$m, $m_t \approx 4.5015$kg, $I_{t/cm} \approx 0.03887$m^{2}kg, $g = 9.81$m/s^2
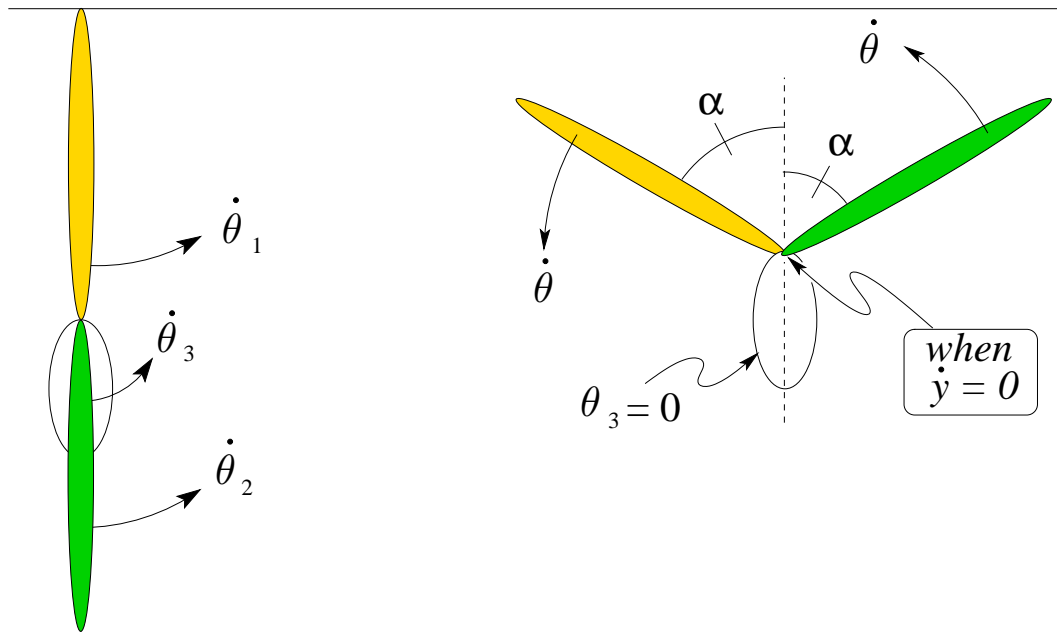
Figure 2.28: This shows the criteria for collisionless ricochetal motions in the three link model. The appendix contains an argument as to the reasons why satisfying these conditions will result in a periodic collisionless motion for this model. We begin with all the links lined up in the straight down position. In this position, there are three initial conditions to specify. We then search for the values of those three initial conditions which result in the system having 1) a symmetrical arm position, 2) equal arm angular velocities, and 3) exactly vertical torso position, at the moment when the vertical component of the shoulder's velocity is zero.
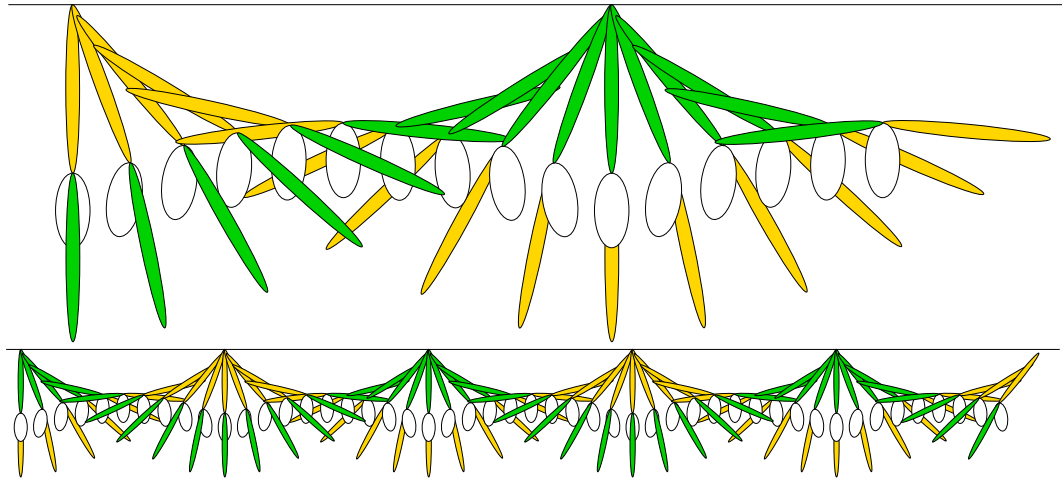
Figure 2.29: A ricochetal motion for the three link model: Initial conditions for this motion are: $\theta_1 = \theta_2 = \theta_3 =$ 0 rads, $\dot{\theta}_1 = 9.991543419533$ rad/sec, $\dot{\theta}_2 = 3.500844111575$ rad/sec, $\dot{\theta}_3 = $ -6.919968841782 rad/sec. The model releases the ceiling when $\theta_1=20°$ (so $\theta_{rel} = 20°$). This motion is further described by the plots in Figure 2.30.

2.8   Five-Link Model

Our most complex brachiation simulation is a five-link model. The five links are made up of two forearms, two upper arms, and a torso. It is exactly equivalent to unlocking the elbows of the three-link model described previously. We used a novel continuation method to track the three-link motion found above into the five-link model in a continuous manner. We assigned an inertia to the amount of bend in the two elbows and then progressively diminished this inertia from an infinite value to zero. At infinite relative-rotation inertia, the model is equivalent to the three-link model. At zero relative-rotation inertia the model is equivalent to the five-link model. Although we were able to successfully use this method to find a collisionless periodic motion, it was not gibbon-like (see Figure 6.19 in Chapter 6). The motion we show here was found using intuition and a negative rotational coupling inertia (see Chapter 6) in jumping from path segment to path segment and ending in this motion with zero coupling inertia.

The counting argument for the existence of symmetric motions in the five-link model is very similar to the one given for the three link model. Assuming that the release angle, θ_{rel}, is fixed we have five initial conditions that can be varied to match five conditions when the vertical component of the shoulder velocity drops to zero. These five conditions are depicted in Figure 2.35.
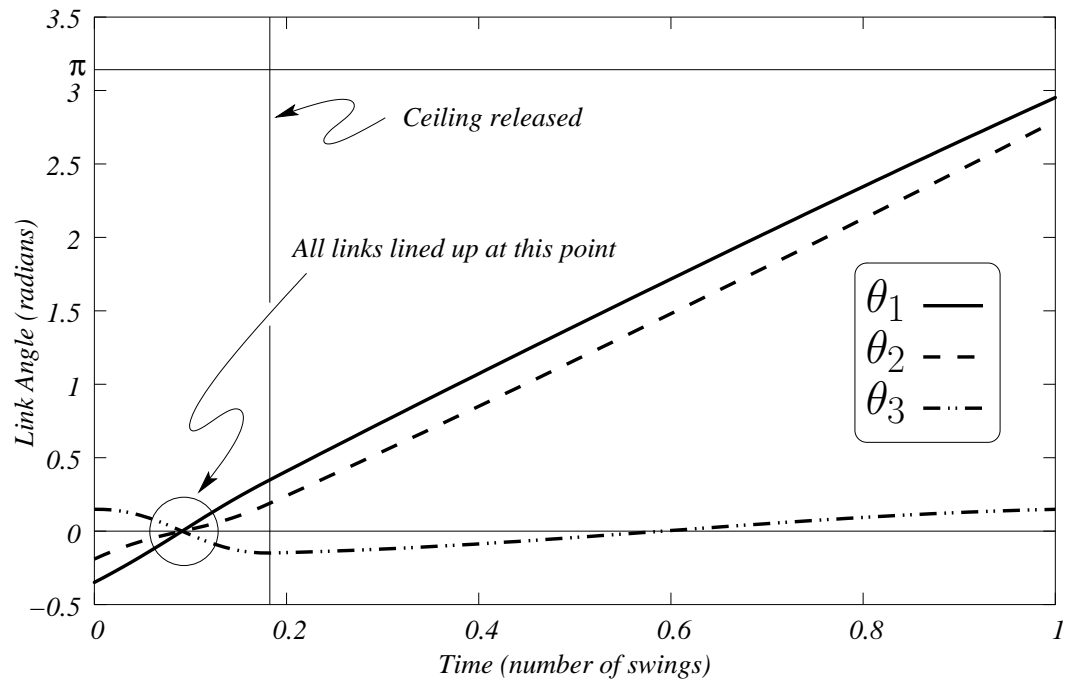
Figure 2.30: Link angle trajectory for the collisionless periodic ricochetal motion of the three-link brachiation model depicted in Figure 2.29. This figure shows a single complete swing starting just as the new hand grasps the ceiling and ends when the other hand just starts to grab the ceiling.
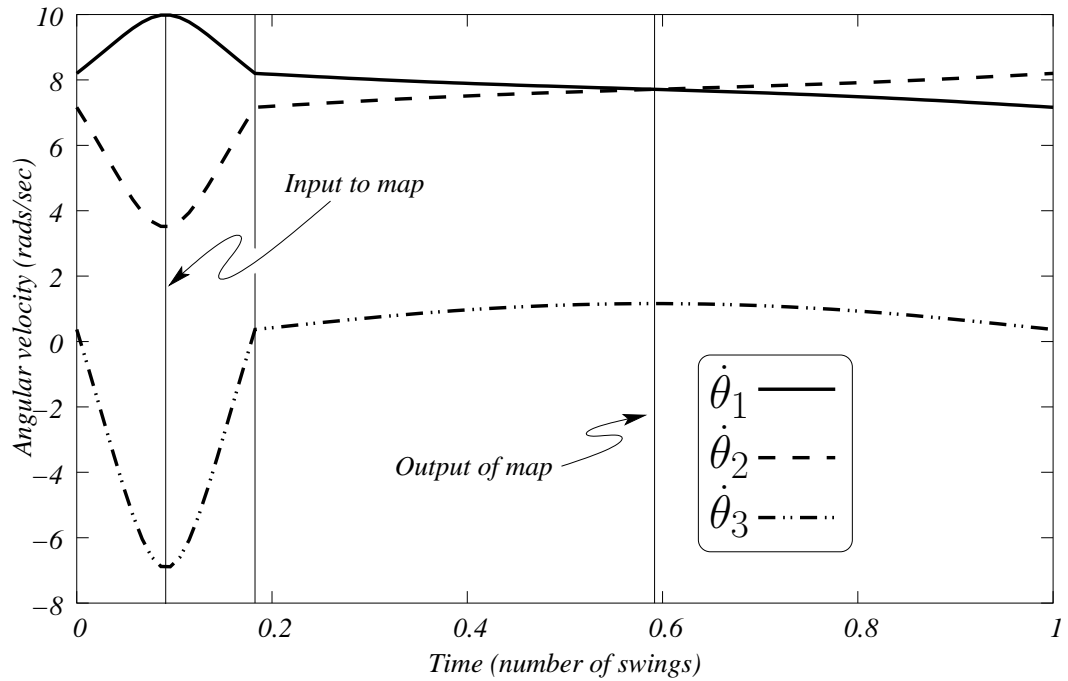
Figure 2.31: Angular velocities of the three links for the motion shown in Figure 2.29. Note the symmetries present in the contact and free-flight portions of the complete motion. We searched for a motion which had these mirror reflection symmetries, which in turn enforced that the motion would be collisionless. Because of symmetries we only needed to integrate our equations of motion for half of the complete cycle, and the input and output of our root-finding function (see Figure 2.28) are shown in the plot above.
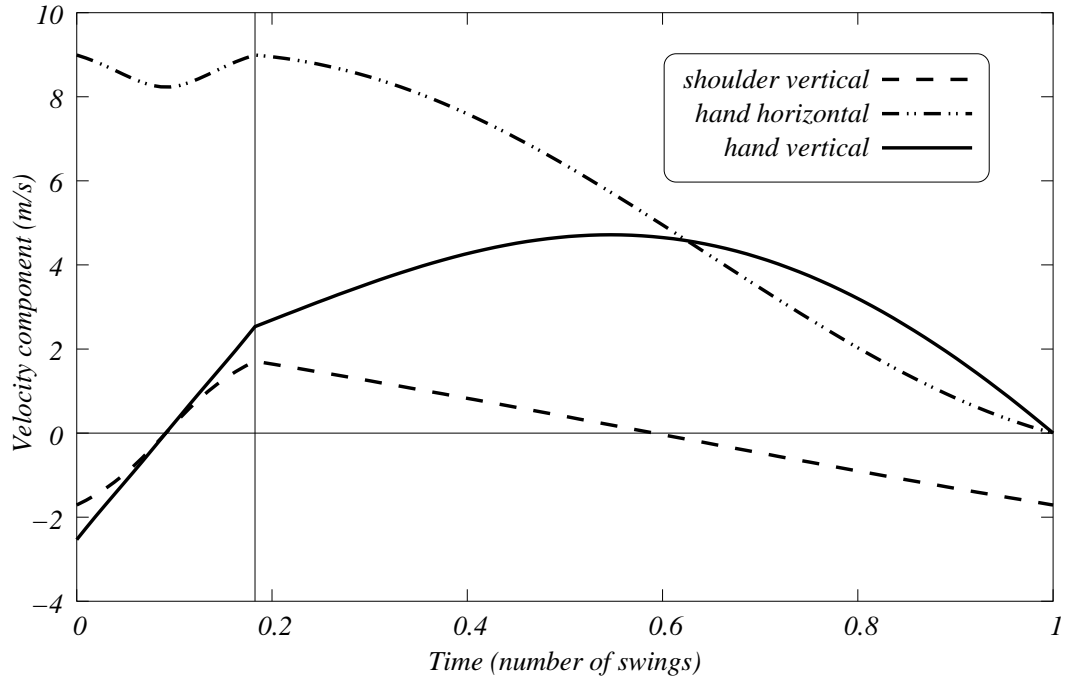
Figure 2.32: Velocity components for the hand and shoulder of the three-link model for the motion shown in Figure 2.29. Note that the slopes of both the horizontal and vertical component are zero, $\dot{x}_{hand}=\dot{y}_{hand}=0$ m/s, when the hand collides with the ceiling. The kink in the velocity components that occurs when the hand releases the ceiling is due to the discontinuity in the force applied by the ceiling on the supporting hand going from some non-zero magnitude to zero magnitude.
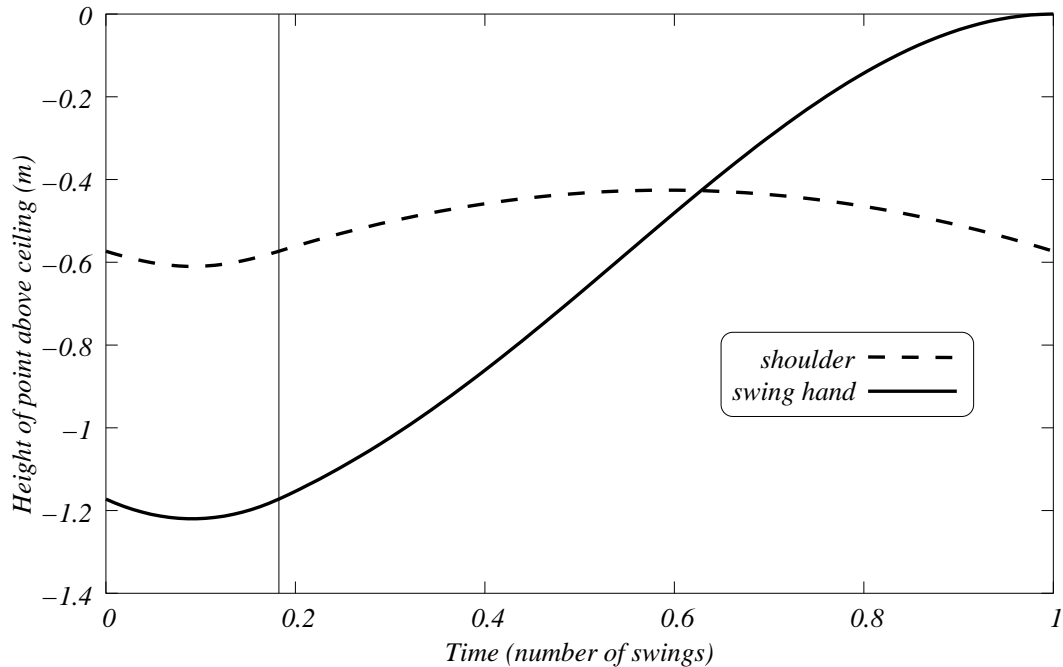
Figure 2.33: Vertical and horizontal distance of the swing hand from its impending handhold versus time for the three-link model during the motion shown in Figure 2.29.

2.9 Discussion

We have observed the following:

> *If a motion seems intuitively plausible and is consistent with basic momentum and energy considerations, a solution to the dynamics equations with those motions exists.*

This is not a theorem, or even the basis of a candidate theorem. But has been the rule, rather than the exception for a host of passive-dynamic walking and brachiating models. The counting arguments buttress the concept; if finding solutions is equivalent to solving n equations for n or less conditions it is reasonable to hope to find solutions. But there are, of course, exceptions. In the next chapter, we will show that not all mass and geometry parameters will give life-like collisionless solutions.

The claims in this chapter are two-fold, mathematical and relevant for explaining animal motion.

1) We claim here that the governing equations of rigid-body mechanics have solutions with (mathematically) zero energy cost. One may distrust a numerical solution to an essentially mathematical question. So in our numerics we have taken care with convergence, event detection, and root finding and thus we believe that
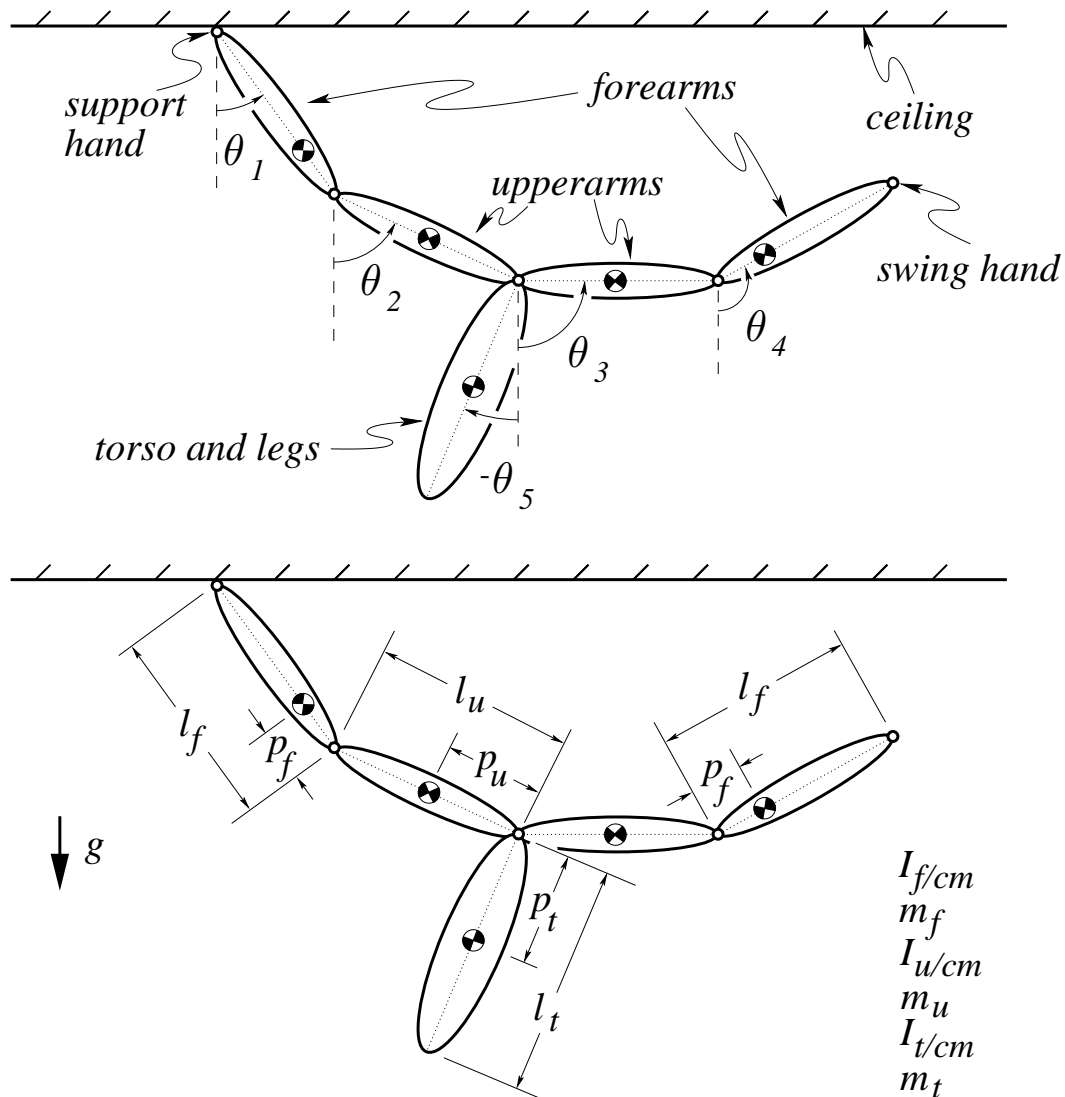
Figure 2.34: Five link model. Parameter values: l_f = 0.37m, $p_f \approx 0.1477$m, $m_f \approx 0.3613$kg, $I_{f/cm} \approx 0.002979$m^{2}kg, l_u = 0.24m, $p_u \approx 0.12$m, $m_u \approx 0.4712$kg, $I_{u/cm} \approx 0.002336$m^{2}kg, l_t = 0.27m, $p_t \approx 0.1625$m, $m_t \approx 4.5015$kg, $I_{t/cm} \approx 0.03887$m^{2}kg, g = 9.81 m/s^2
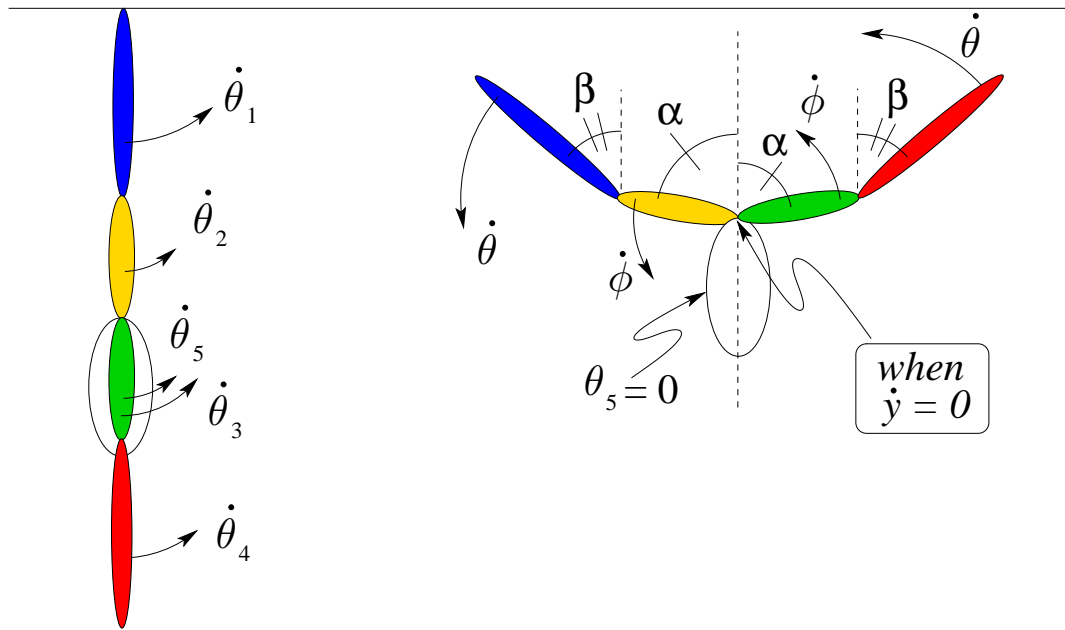
Figure 2.35: Criteria for collisionless ricochetal motions for the five link model. The position on the left shows the input state for the map used to find the motion. The position on the right shows the output from the map which would result in a periodic collisionless motion. Note that the map evaluates when the vertical component of the shoulder's velocity is equal to zero.
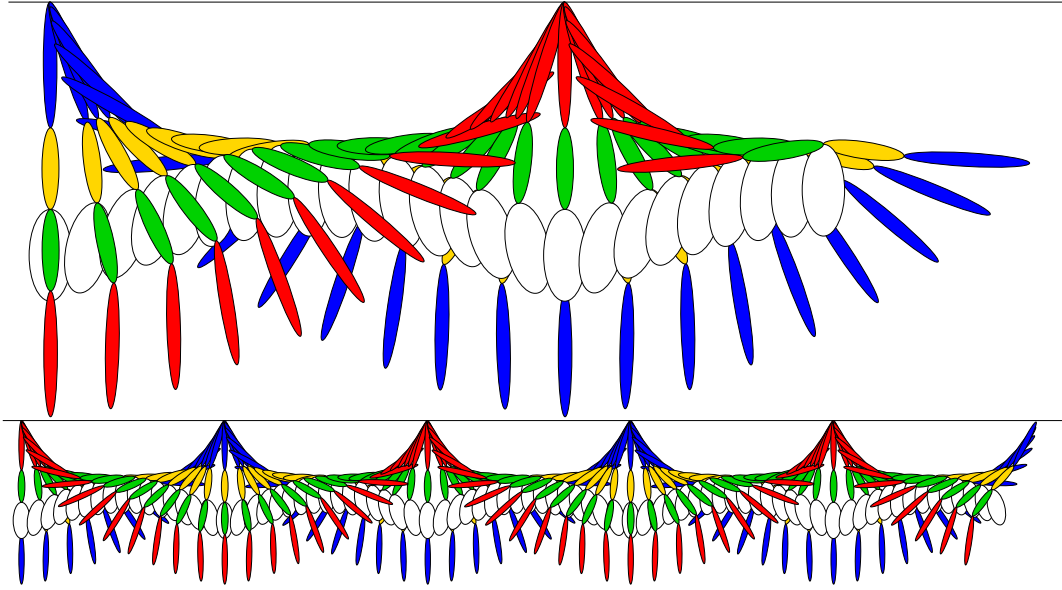
Figure 2.36: Snapshots of a periodic collisionless ricochetal motion of the five-link model. Note that the beginning is on the left of the figure with the model halfway through the swing portion of the gait and the end is on the right of the figure with the model just finishing the free flight portion of the ricochetal gait and just grabbing on to the next handhold with the swing hand at zero velocity (lower plot). Note that here we have the model (in the upper plot) shown on the right side of the figure halfway through the free flight portion of the ricochetal gait. This motion is further described by the plots in Figure 2.37. The state of the system at mid-swing for this motions is: $\theta_1 = \theta_2 = \theta_3 = \theta_4 = \theta_5 = 0$, $\dot{\theta}_1 = 13.696793227$ s^{-1}, $\dot{\theta}_2 = $ -2.4791517485 s^{-1}, $\dot{\theta}_3 = 7.9261511913$ s^{-1}, $\dot{\theta}_4 = $ -1.7030280005 s^{-1}, $\dot{\theta}_5 = $ -5.6362892519 s^{-1}, with $\theta_{rel} = 22.3°$.
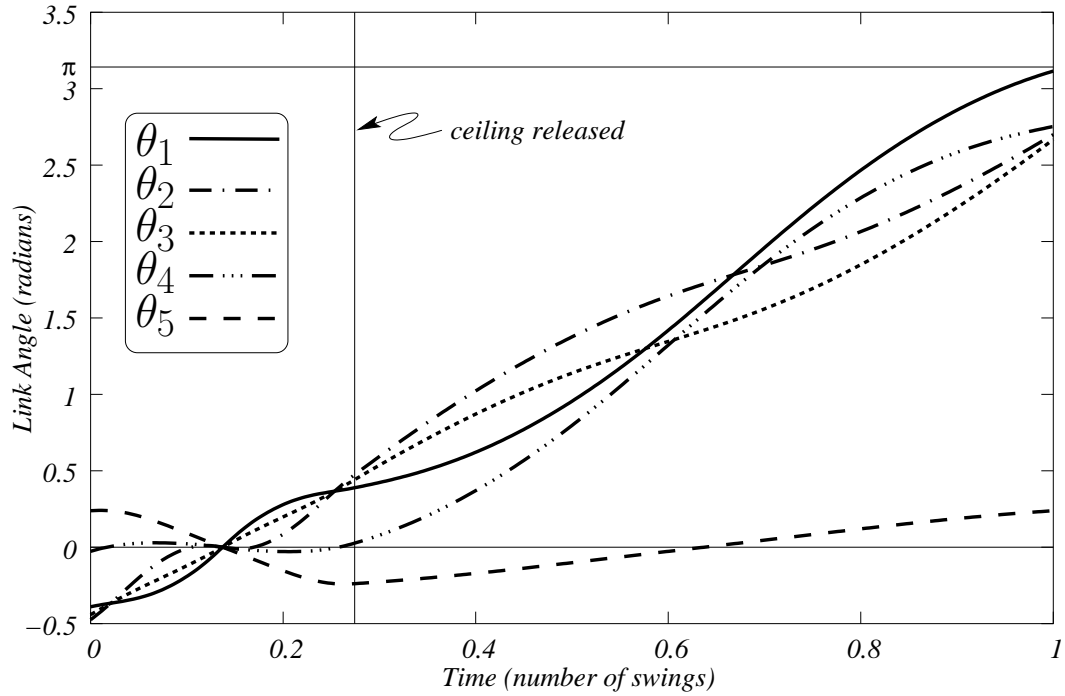
Figure 2.37: Graph of link angles for a single swing of the ricochetal motion of the five-link model shown in Figure 2.36.

our solutions correspond to proper mathematical solutions. We have presented parameters and initial conditions with many digits so others can check this claim with their own numerics.

2) The zero-energy-cost solutions that solve the governing equations for the models, particularly the solutions of the 5-link model, are somehow beautiful. They are also reminiscent of the motions of real gibbons. Thus some version or other of the following class of vague hypotheses is supported: animals make use of natural dynamics, animals minimize muscle use, or animals minimize muscular work.
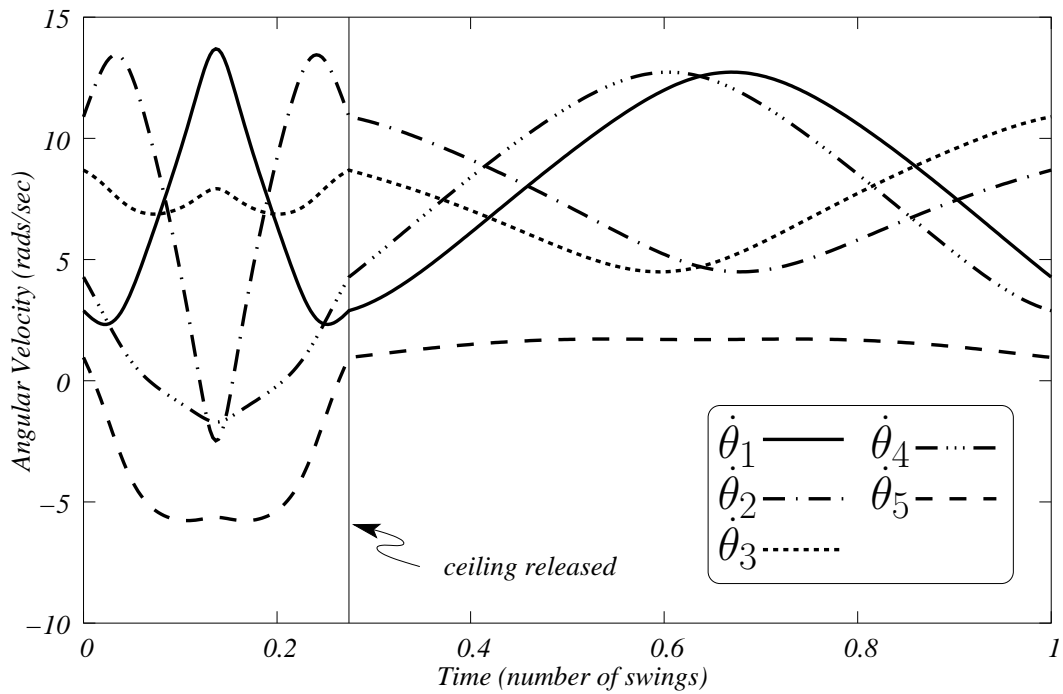
Figure 2.38: Graph of the angular velocities of the links for a single swing of the five link model for the same ricochetal motion shown in Figure 2.36. Note that the swing phase and the free-flight phase of the motion are symmetric about their respective mid-points.
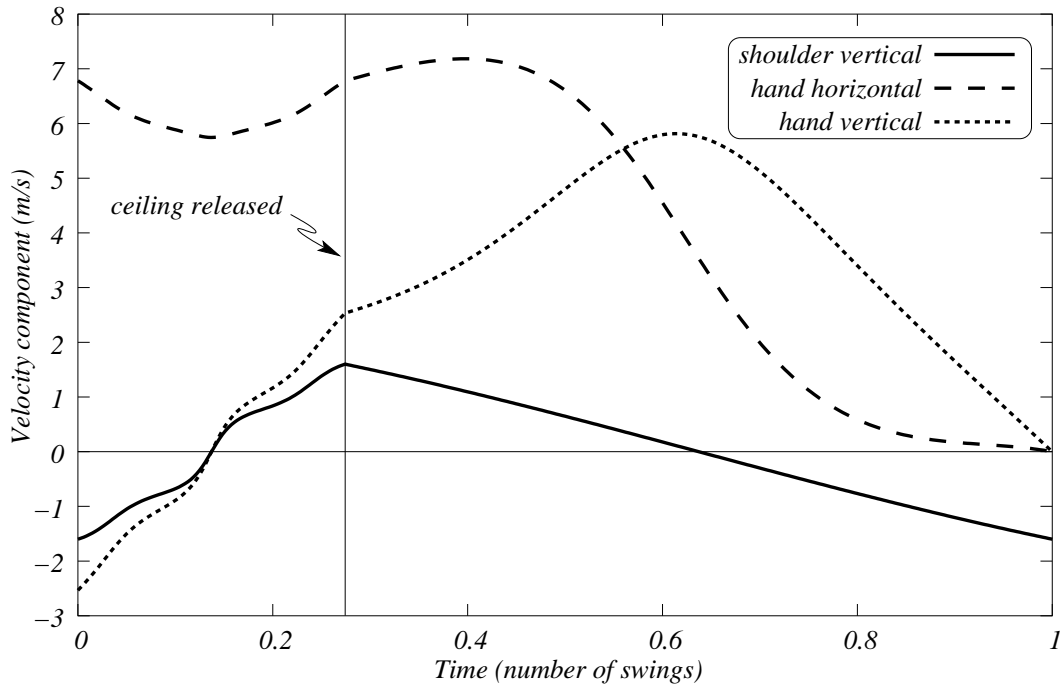
Figure 2.39: Graph of the vertical component of velocity of the shoulder and the vertical and horizontal components of velocity of the swing hand for a single swing of the five-link model for the motion shown in Figure 2.36. Note that both components of the swing hand's velocity go to zero at the end of the cycle (when the swing hand reaches the ceiling, as can be seen in Figure 2.40).
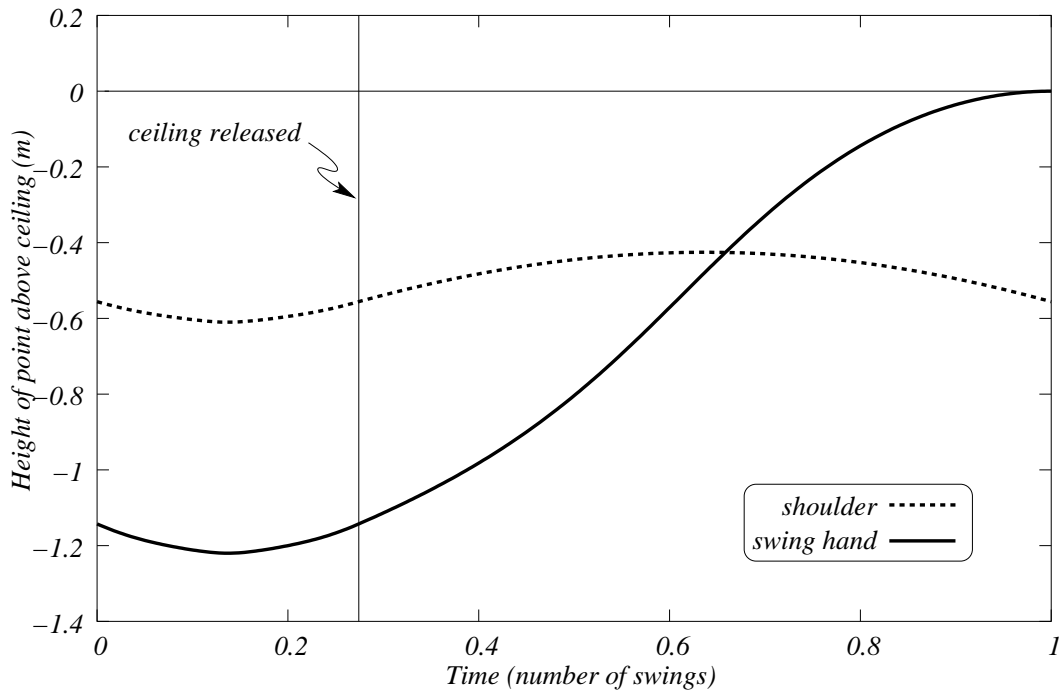
Figure 2.40: Graph of the distance of the swing hand and shoulder from the ceiling for a single swing of the five-link model for the motion shown in Figure 2.36.

Chapter 3

Mass and Geometry Parameters for Brachiation Models

3.1 Introduction

Any rigid-body model requires not only a topological description (what is connected to what) but also a physical description which defines each rigid body's important characteristics (mass, length, center of mass location, and moment of inertia). Determining reasonable values to assign for each of the limb's parameters can be difficult. If a complete parameter study is desired, the most reasonable approach is to non-dimensionalize the parameters to find the smallest number of parameters which change the behavior of the system. Then, instead of a point to be chosen in the large dimensional parameter space, one instead must choose a subspace with a range for each non-dimensional parameter. Choosing a range of values for each parameter allows us to probe the behavior of the model without a detailed determination of the system's parameters. However, if one then wants to determine if the model gives a good approximation to the actual animal, a comparison must be made between the animal's parameters and the model's parameters. This brings us back to the problem of determining a set of parameters for the animal.

Length: The length of an animal's large limbs are usually fairly straightforward to determine. Measuring the length of a limb that is approximately 0.25 meters in length can be done non-invasively with a relative error on the order of 5–10%. More accurate measurements can be done using a skeleton of the animal since the actual bone can be measured. However, there is a limit to how accurately one can measure the length of the limb. This limit has to do with the fact that modeling the joints as pin or hinge joints is, in detail, wrong. The joints, such as the knee and elbow even when they are moved solely in a 2D plane do not move as pin joints when one is measuring things at a sub-millimeter level. Therefore, attempting to measure the length of a limb to sub-millimeter accuracy is pointless.

Mass, Center of mass, Moment of Inertia: Determining a link's mass, center of mass location, and moment of inertia tensor is more difficult than deter-

mining length. There are two main ways to determine these values, direct measurement and volumetric estimation. Direct measurement requires that a dissection be performed on a cadaver and the limbs weighed, balanced, and other measurements performed (like pendulum experiments) to determine the limb's center of mass location, and moment of inertia. Volumetric estimation is less intrusive than direct measurement and basically consists of taking many distance measurements of the limb in various places and developing a three dimensional mathematical volume with an assumed density. The total mass, center of mass location, and moment of inertia of this mathematical solid can then be determined by calculation. Hatze [24] gives an example of the second method by outlining a procedure for determining a subject-specific parameter set which requires 242 measurements. These measurements can then be transformed into a 17-link rigid-body model of a human. It can be argued that there is much more room for error in determining the parameters when using volumetric estimation since there are more assumptions involved and one is propagating errors through a series of calculations. However, the advantage of not having to kill one's subject is an large advantage of this indirect method.

For the rest of this chapter, we focus on determining a set of parameters for our gibbon models. Gibbon brachiation has not been studied as much as human bipedal walking and thus there is less parameter data available. Fortunately, many dissections of adult and juvenile gibbons have been performed and the limb geometry of gibbons has been well documented, most notably by Schultz [53]. Unfortunately, many of these records are incomplete from our point of view since almost none of them include limb mass and moment of inertia data. Thus, for this research we have been forced to develop a more complete parameter set for an "average" adult gibbon.

This chapter begins by summarizing the relevant parameter data from several studies of gibbon anatomy as well as from some computational studies of gibbon brachiation. We also study the response of two-link model to three different sets of parameters. A new set of gibbon parameters based on anatomic data and volumetric estimation is presented at the end of this chapter.

3.2 Mathematical Models

3.2.1 Preushoft and Demes

Preushoft and Demes [47] model continuous-contact brachiation of a gibbon and siamang using a single rigid body pendulum. They relate the period of oscillation of this pendulum with the average forward speed of a brachiating gibbon. They use a volumetric estimation method for obtaining the parameters used in their model. The support arm is modeled as a right circular cylinder. It is attached to another cylinder which models the torso, legs, and swing arm of the gibbon. They give two sets of parameters, one for a "cylindrical" gibbon and the other for a "cylindrical" siamang. The sizes of the cylinders are based on data from the

Table 3.1: Parameters for a cylindrical **gibbon** given by Preushoft and Demes in [47] (see Figure 3.2(a)).

| forelimb: | height = 0.55m | diameter = 0.06m | mass = 0.75kg |
| body: | height = 0.60m | diameter = 0.25m | mass = 5.07kg |

Table 3.2: Parameters for a cylindrical **siamang** given by Preushoft and Demes in [47]

| forelimb: | height = 0.65m | diameter = 0.08m | mass = 1.34kg |
| body: | height = 0.70m | diameter = 0.30m | mass = 9.36kg |

'lar-group' gibbons given by Napier and Napier [42] and Schultz [53]. They also assume that the mass of both forelimbs is 25% of the total mass. This figure is based on their observations of a juvenile chimpanzee.

For the sake of consistency in all of the simulations presented in this thesis, we only examined parameters for the gibbon, specifically, the *Hylobates lar*, instead of the siamang (a significantly larger animal, as can be seen in 3.2).

Rigid-body model

The rigid-body model (section 2.5) uses the parameters given in Table 3.1 but with the forelimb mass reduced to zero. Note that the moment of inertia of a cylinder about its center of mass is given by $I_{cm} = \frac{1}{12}m(3r^2 + l^2)$, where m is the mass of the cylinder, r is the radius of the cylinder, and l is the length of the cylinder. The parameters from Preushoft and Demes result in the following parameters for the rigid-body model of section 2.5 and shown again, for convenience, in Figure 3.1.

$l_{arm} = 0.55$ m

$p = 0.30$ m

$m = 5.07$ kg

$I_{cm} \approx 0.1719$ kg $\cdot$ m^2

As can be seen from the results given in section 2.5 several gibbon-like collisionless periodic motions exist for this model.

Two-link model

The two-link model increased the model complexity of the rigid-body model. The continuous-contact motions of this model were thoroughly examined. A short historical account of the parameter set used for this model is given below.

To obtain parameters for the two link model, I did the following. The cylindrical forearm parameters given by Preushoft and Demes [47] were used for the support arm and the swing arm (see Figure 3.2). Since the swing arm was included in the parameters for the body cylinder, I subtract the mass of the swing arm from the
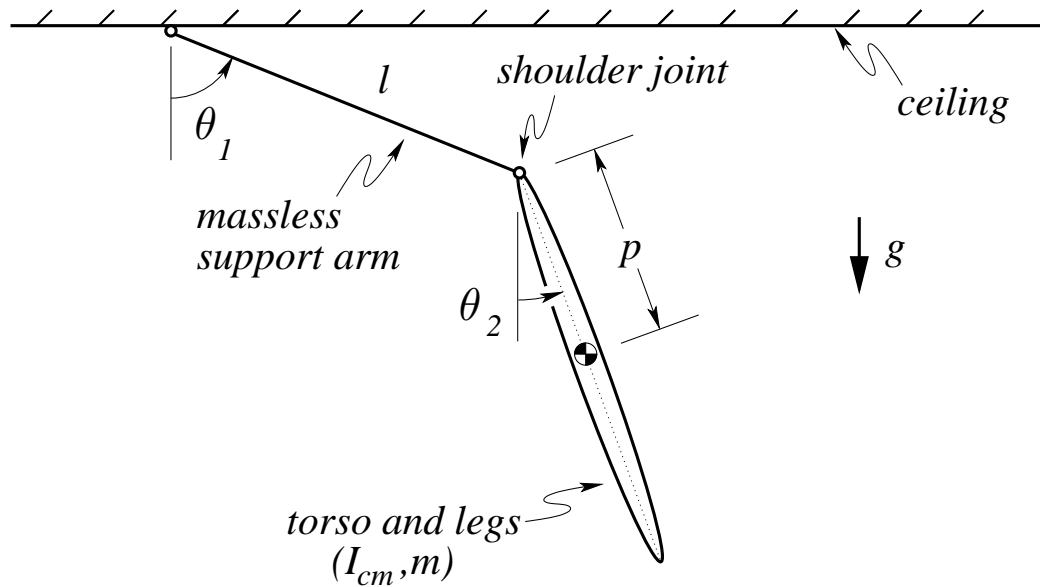
Figure 3.1: Single rigid body model of section 2.5.

(a)

(b)
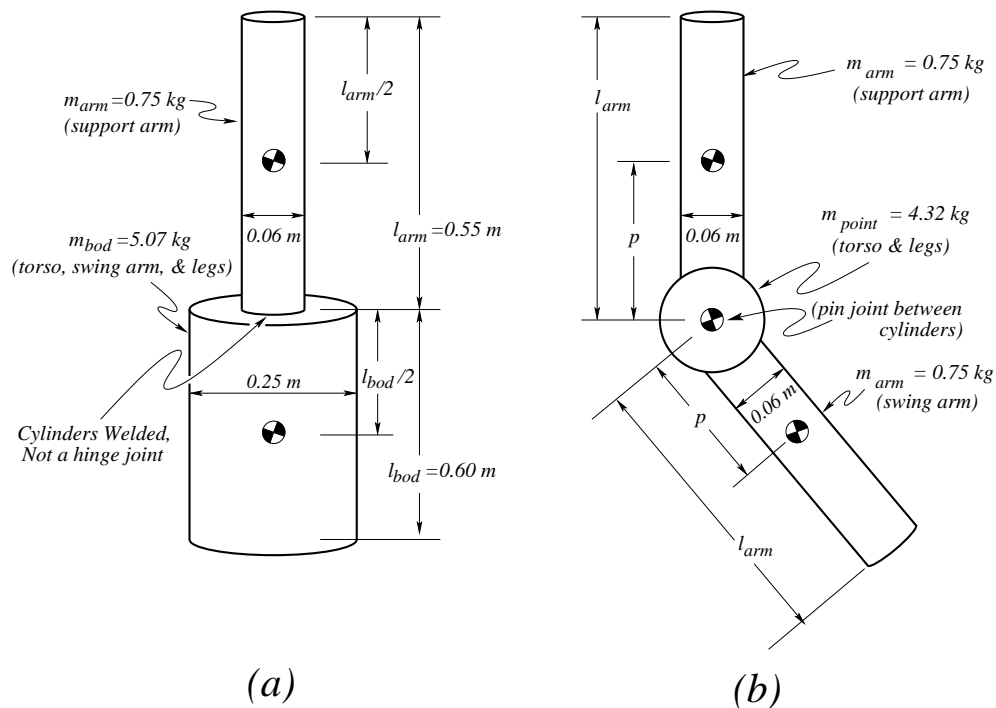
Figure 3.2: (a) Parameters for the cylindrical gibbon given by Preushoft and Demes in [47]. (b) Diagram of two link model with parameters derived from the cylindrical gibbon model in (a).
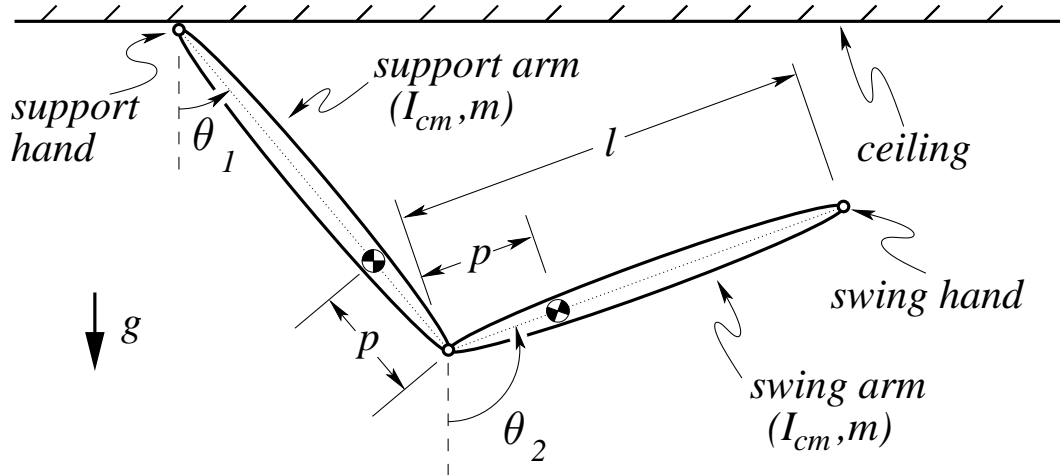
Figure 3.3: The two-link brachiation model of section 2.6.

body cylinder mass. The resulting body mass, minus the swing arm, makes up the point mass that I add to the central hinge of the two link model.

To incorporate the point mass into the parameters for the model, one could add the whole point mass to the swing arm, or the support arm, or split it in half and add half the point mass to the swing arm and half to the support arm. Although, the parameters will be different depending on what one chooses to do, the solutions to the equations of motion will be exactly the same. For convenience, I chose to split the point mass evenly between the two arms. This results in the following mass and geometry parameters for the two links.

$$m_{point} = m_{bod} - m_{arm}$$

$$p = \frac{m_{arm}\frac{l_{arm}}{2} + \frac{m_{point}}{2}0}{m_{arm} + \frac{m_{point}}{2}}$$

$$I_{cm} = \frac{1}{12}m_{arm}(3r_{arm}^2 + l_{arm}^2) + m_{arm}(\frac{l_{arm}}{2} - p)^2 + \frac{m_{point}}{2}p^2$$

$l = 0.55$ m
$p \approx 0.070876$ m
$m = 2.91$ kg
$I_{cm} \approx 0.061176$ kg $\cdot$ m^2

Although, these parameters admits many periodic collisionless motions for this model, none of them are gibbon-like. Of the two motions at ceiling height, shown in Figure 3.4, one oscillates in place and the other swings up to and grabs onto the ceiling with both links above the ceiling. This prompted me to examine the parameters that I was using, to see how realistic they were.
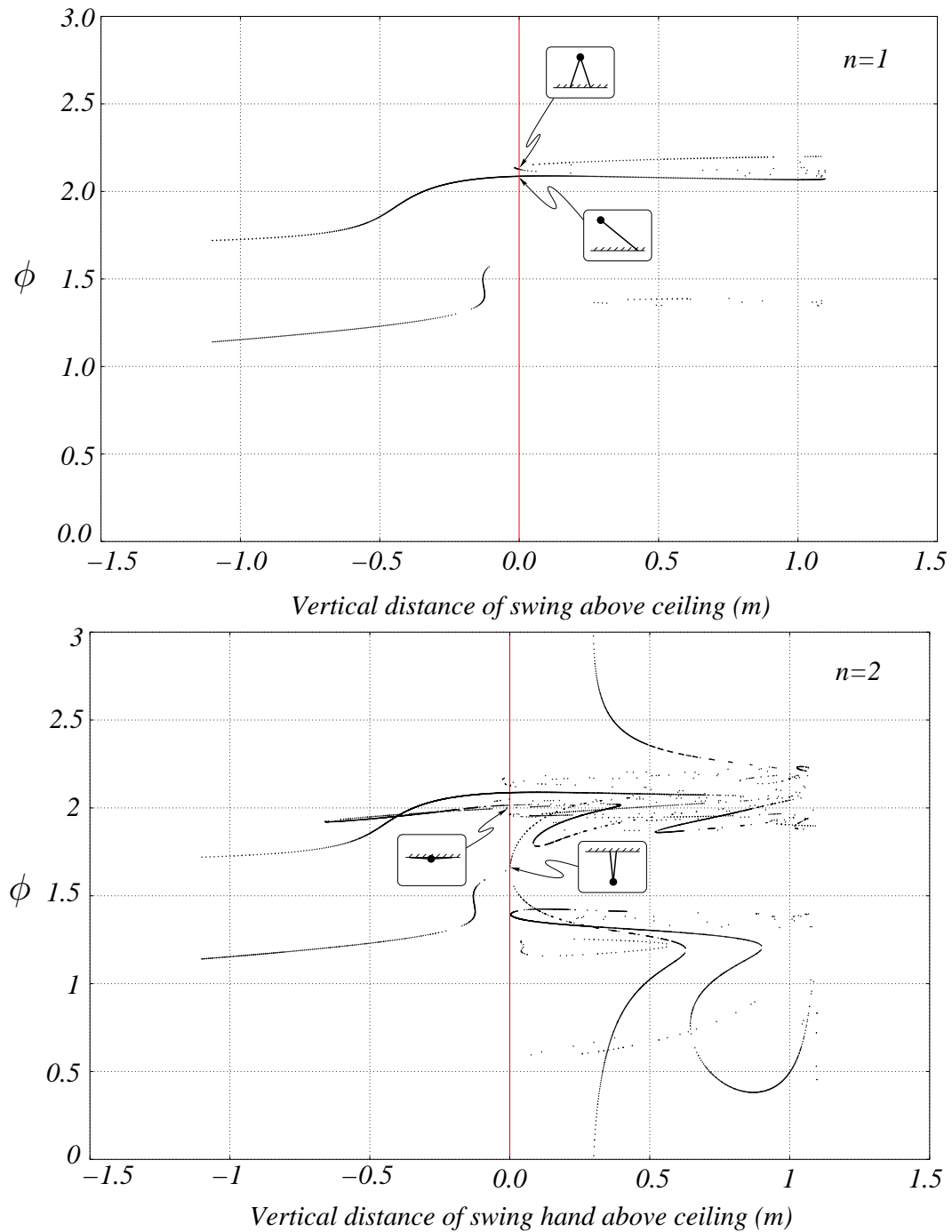
Figure 3.4: Periodic motions of the two link model using the parameters from Preuschoft and Demes [47]. The inserts show the approximate configuration of the system when the kinetic energy is zero. The top figure contains periodic motions with no reversals in sign of $\dot{\theta}_1$ in a half cycle. The bottom figure has motions that have one sign reversal of $\dot{\theta}_1$ in a half cycle.

Table 3.3: Parameters for a cylindrical gibbon given by Swartz in [60]

forelimb:	height = 0.50m	diameter = 0.045m	mass = 0.75kg
body:	height = 0.55m	diameter = 0.114m	mass = 5.25kg

3.2.2 Swartz

Like Preushoft and Demes [47], Swartz [60], modeled the continuous-contact gait of gibbon using a single rigid body pendulum. However, she disagreed with the parameters for the rigid body pendulum that Preushoft and Demes used in [47]. Swartz pointed out that the parameters given in [47] give unrealistic densities of 0.172g/cm^3 for the body and 0.483g/cm^3 for the forelimb. She states that densities for nonhuman mammals are comparable to human densities, which are 1.038g/cm^3 for the body and 1.001g/cm^3 for the forelimb. Note that both of these densities are close to the density of water (1.0g/cm^3), which is understandable given that our bodies are primarily composed of water. Swartz then proposed a modified set of parameters based on Schultz's measurements of hylobatid skeletons and her own direct radiographic measurements. These values give densities of 0.943g/cm^3 and 0.935g/cm^3 for the forelimb and body respectively.

Transforming these parameters for the two-link model, using the same method as before, one obtains the following:

$l = 0.50$ m

$p \approx 0.0625$ m

$m = 3.0$ kg

$I_{cm} \approx 0.05088$ kg $\cdot$ m^2

These mass and geometry parameters are very similar to Preushoft and Demes parameters. This can readily be seen by non-dimensionalizing the equations of motion. For the two link model, there are really only two parameters (a non-dimensional center of mass location, and a non-dimensional radius of gyration) that will result in different periodic solutions. The Preushoft and Demes parameters result in a non-dimensional center of mass location $P = p/l \approx 0.1289$ and a non-dimensional radius of gyration $R = (\sqrt{I_{cm}/m})/l \approx 0.2636$. Swartz's arm parameters gives us $P = p/l = 0.125$ and $R = (\sqrt{I_{cm}/m})/l \approx 0.2605$. The fact that these non-dimensional parameters are so close, they differ by 3% and 1% respectively, means that the parameters given to the two-link model will result in almost identical periodic solutions to the equations of motion. This fact is readily apparent by comparing the periodic motion plots in Figure 3.5 with Figure 3.4.

We now examine a two-link gibbon model which consists of two cylindrical arms and a point mass body at the central hinge. The mass of the cylinders is
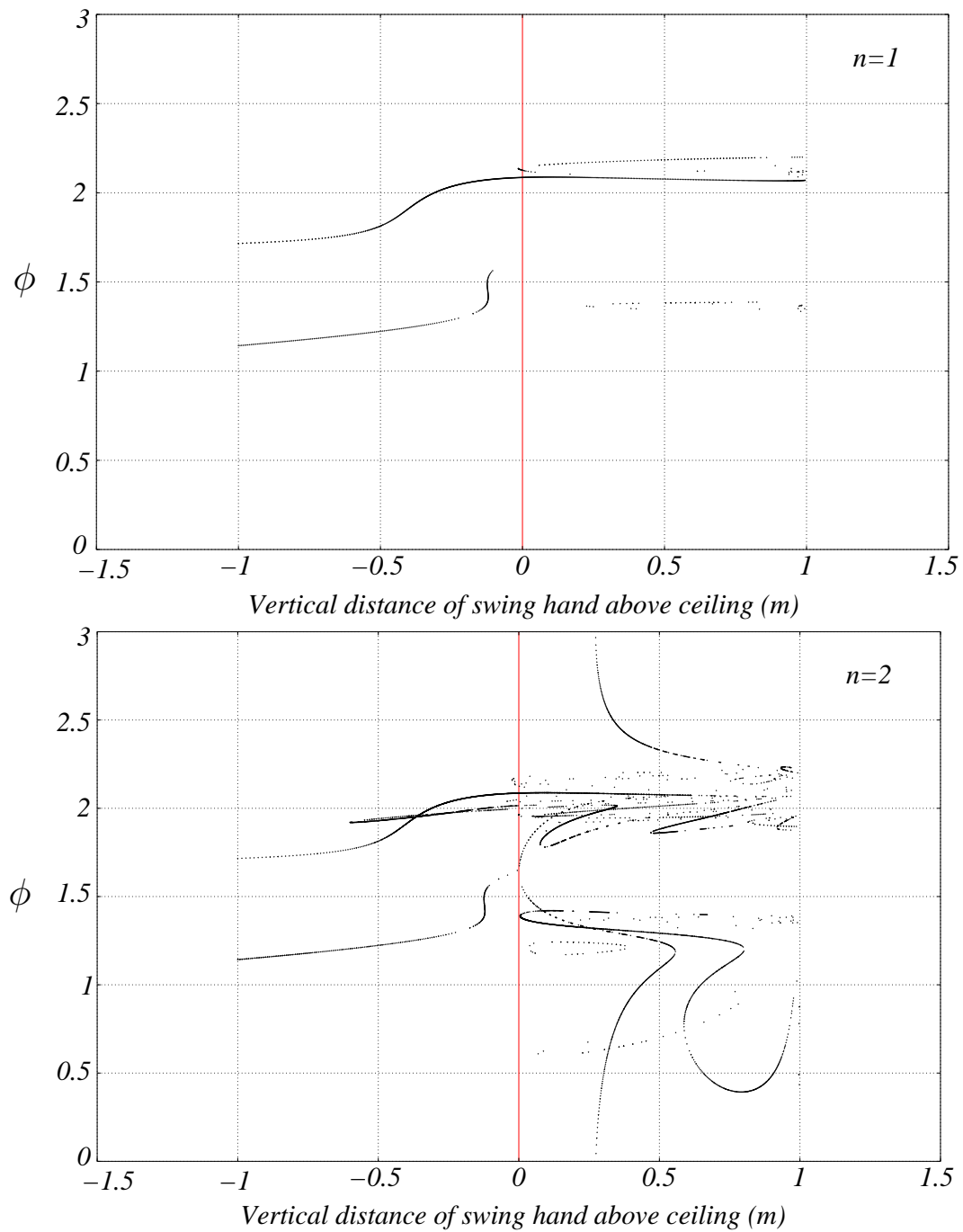
Figure 3.5: Periodic motions of the two-link model using the parameters from Swartz [60]. The inserts show the approximate configuration of the system when the kinetic energy is zero. The top figure contains periodic motions with no reversals in sign of $\dot{\theta}_1$ in a half cycle. The bottom figure has motions that have one sign reversal of $\dot{\theta}_1$ in a half cycle.

12.5% (1/8) of the total mass gives the following non-dimensional parameters.

$$m_{arm} = \frac{1}{8}(m_{point} + 2m_{arm})$$

$$m_{arm} = \frac{m_{point}}{6}$$

$$m = m_{arm} + \frac{m_{point}}{2}$$

$$m = \frac{2m_{point}}{3}$$

$$p = \frac{m_{arm}\frac{l}{2}}{m}$$

$$p = \frac{l}{8}$$

$$\mathbf{P} = \frac{p}{l} = 1/8 = \mathbf{0.125}$$

If we then assume that the cylinders are very slender, i.e that $3r^2/l^2 \ll 1$, then the cylinder can be well approximated by a rod for the calculation of it's moment of inertia about the center of mass. The slenderness ratios of the Preushoft and Demes arm parameters is $3r^2/l^2 = 0.009$ and for the Swartz arm parameters, $3r^2/l^2 = 0.006$.

$$I_{cm_{cylinder}} = \frac{1}{12}m(3r^2 + l^2)$$

$$I_{cm_{rod}} = \frac{1}{12}ml^2$$

$$I_{cm} = \frac{1}{12}m_{arm}l_{arm}^2 + \frac{m_{point}}{2}p^2 + m_{arm}(\frac{l}{2} - p)^2$$

$$I_{cm} = \frac{13m_{point}l^2}{288}$$

$$\mathbf{R} = \frac{\sqrt{I_{cm}/m}}{l} = \sqrt{\frac{39}{576}} \approx \mathbf{0.2602}$$

Although these two sets of parameters (basically the same) admit many collisionless periodic solutions, none of them are gibbon-like. Unfortunately, non-gibbon-like motion are not the goal. At this point, one might be tempted to change the model's parameters until one obtains desirable results. However, this is not an objective way to conduct research. If the model has many modifiable parameters then almost any behavior can be obtained. This procedure can be almost exactly compared to the problem of curve-fitting, or matching mathematical functions to experimental data. On the other hand, to fully examine a given model, a study of the effects of changing parameters on its behavior is required. Since there are only two non-dimensional parameters for the two-link model, it is a tractable model to do some parameter studies.
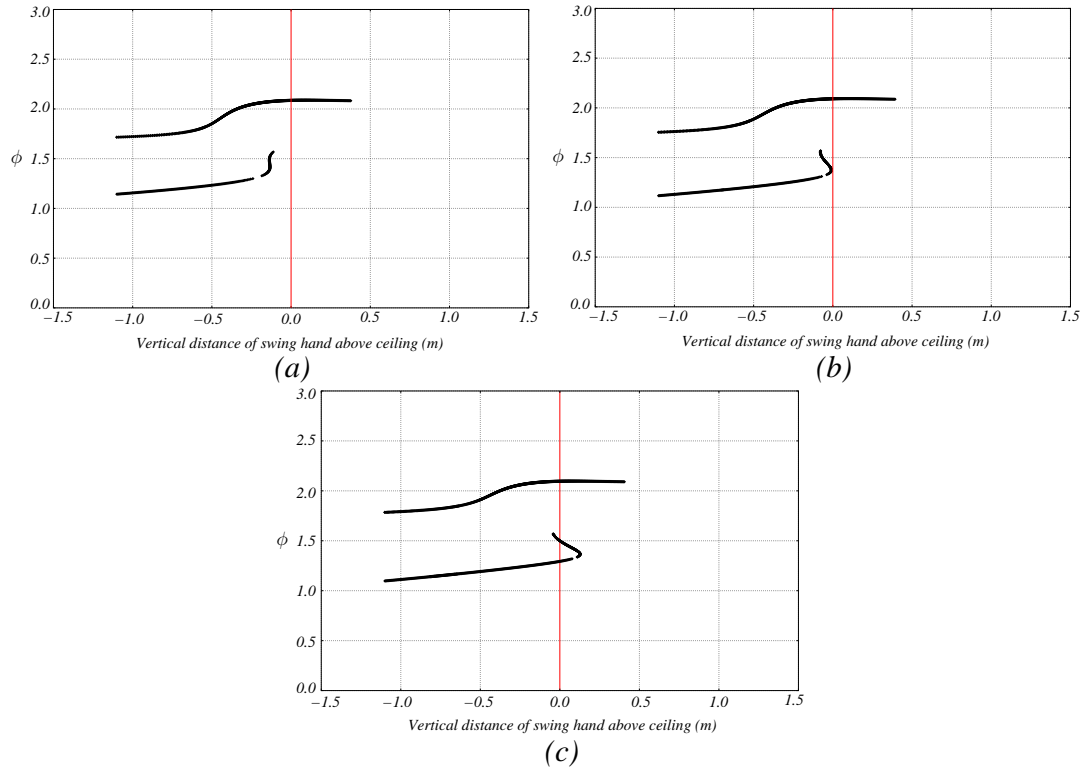
Figure 3.6: Periodic motion plots for the two-link model with single cylinder arms [total mass = 6kg] (a) with both arms having 1/4th (25%) of the total mass (b) both arms having 1/3rd (33.3%)of total mass (c) both arms having 2/5th (40%) of total mass.

One possibly questionable assumption used to develop the parameters for the two-link model was the assumption by Preushoft and Demes that for a gibbon, the mass of the arms is 25% of the total mass since that was what they measured for juvenile chimpanzees. What happens to the behavior of the two-link model if that parameter is varied? Increasing the mass of the body in relation to that of the arms resulted in the central curve in Figure 3.4 moving to the left. By doing the opposite, increasing the arm mass in relation to the body mass, that curve moves to the right as seen in Figure 3.6

Although Figure 3.6(c) gives two motions that are simple and progress forward (underneath the ceiling) instead of oscillating in place, the ratio of mass in the arms compared to the body is almost twice the value given in the literature. The unrealistic value of the modified parameters (with the arms consisting of slightly less than half of the total mass) led me to conclude that the original value of the arm/body mass ratio was not the cause of the two-link model having no gibbon-like collisionless motions. At this point a more objective, and realistic set of gibbon parameters was needed. The more complicated brachiation simulations would require a more detailed set of parameters than what was given by Preushoft and
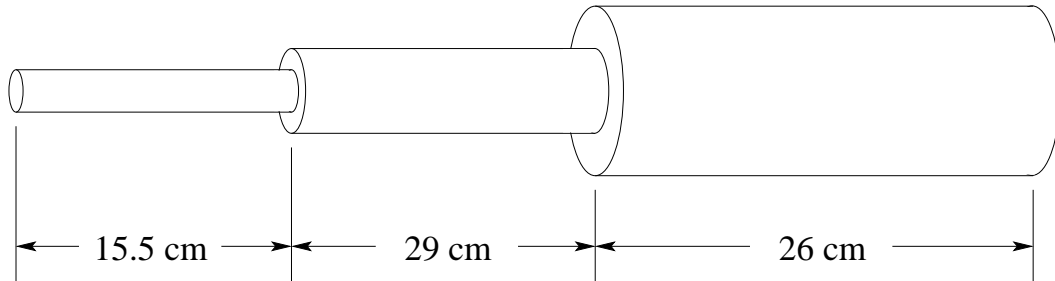
Figure 3.7: Preushoft and Demes three segment siamang arm [48].

Demes [47] or Swartz [60]. This led to another Preushoft and Demes paper and a closer study of the published data on gibbon anatomy.

Preushoft and Demes, in a later paper, [48] model a gibbon's arm by breaking it apart into three cylinders (upperarm or Humerus, forearm or Radius,and hand) of differing lengths and diameters. They were interested in the effect of varying length and diameter of these cylinders on the muscle forces required to move the arm. This was done to explain the existence of an upper limit on a gibbon's arm is due to muscle strength. Since the are interested in the effect of different parameters on muscle force, they give a range of values for the cylinders. However, they begin the calculations with the dimensions of a siamang arm(they give only lengths of the cylinders)(hand length = 15.5cm; forearm length = 29.0cm; and upper arm length = 26.0cm). A siamang is significantly larger than a gibbon, so these numbers give only a clue to the limb segment proportions of a gibbon.

3.3   Anatomical gibbon measurements

This section summarizes some of the relevant published measurements of gibbon anatomy. Although the data sets are comprehensive in some areas they are also completely lacking in others, most notably there is no information concerning the center of mass locations and moments of inertia tensors for the individual limb segments of the gibbons. It is conceivable but unlikely that center of mass location data might have been collected (since the measurement on an isolated limb is fairly straightforward [1]) and not reported. However, it is extremely unlikely that the moment of inertia tensor was measured since this is a rather difficult and complex experiment requiring a good grasp of rigid body dynamics and several well thought out rigid-body pendulum experiments. Before the age of ubiquitous computer use (approx. 1960), this data would have been fairly useless as well, since mathematical models which would require this level of detail would be intractable

---

[1]The isolated limb must simply be balanced by moving the location of line support underneath it. This must be done a minimum of three times to obtain the center of mass location in three-dimensions.

using solely analytical approaches. However, the data sets do give a good starting point for the development of our model using a volumetric estimation approach for determining a reasonable set of parameters for our gibbon models.

3.3.1   Schultz

Schultz [54] published a large amount of data on the limb proportions of gibbons. The things that he measured ranged from the length of the tibia to the average number of hairs per square cm on the scalp, back, and chest of a gibbon. The data given for the limb lengths for an adult Hylobates is summarized below.

```
(Radius length)/(Humerus length) x 100 = 112.4
(Tibia length/Femur length) x 100 = 88.2
(Humerus+Radius)/(Femur+Tibia) x 100 = 128.5
(Chest circumference)/(Trunk height) x 100 = 148.8
(Chest breadth)/(Chest depth) x 100 = 118.2
(total lower limb length)/(trunk height) x 100 = 146.5
(total upper limb length)/(trunk height) x 100 = 237.8
(total upper limb length)/(total lower limb length) x 100 = 158.8
```

3.3.2   Erikson

Erikson [18] also performed some measurements of gibbon anatomy. He gives ratios for lengths of different limbs for Hylobates. These non-ratio numbers are in proportion to the trunk length which was normalized to 100 units.

```
(Humerus+Radius)/(Femur+Tibia) = 132
Radius/Humerus = 108
Trunk = 100
Humerus+Radius = 184
Hand length = 243-184 = 59
Femur+Tibia = 139
Foot length = 191-139 = 52
```

3.3.3   Napier and Napier

Napier and Napier [42] published the following mass and dimension data for Hylobates. They also give relative limb lengths for several species of apes, including Hylobates, which is shown below.

	males	females
mass range:	4.300-7.928kg (41 ♂)	4.110-6.800kg (30 ♀)
head and body length range:	40.3-63.5cm (62 ♂)	40.8-62.2cm (38 ♀)

```
Brachial Index = (Radius length)/(Humerus length) x 100.
Crural Index = (Tibia length)/(Femur length) x 100.
```

```
Intermembral Index=(Humerus+Radius length)/(Femur+Tibia length)x100.
```

```
For the Hylobates they give:
Brachial Index = 113 (avg from 66 measurements)[range: 105-124]
Crural Index = 88 (avg from 66 measurements)[range: 78-94]
Intermembral Index = 129 (avg from 55 measurements)[range:121-138]
```

3.4 A new set of parameters

At this point I stopped by search for gibbon mass and geometry parameters. For the reasons that I gave above, I did not hope to find measured moment of inertia data and although the data given above is incomplete, there is enough information to devise a reasonable, if not completely rigorous, set of mass an geometry parameters. The rest of this section gives a detailed listing of the method I used to determine the parameter set used in the brachiation models.

Although I was able to find several values for the limb length ratios of a gibbon, it was difficult to find a scaling for those ratios to set the actual lengths of each limb. Erikson [18] gave some numbers which allowed me to set the lengths of the upperarm(Humerus) and the forearm(Radius), normalized to trunk length. Then, along with the crural index (Femur/Tibia) and the data given by Erikson, I was able to set values for the lengths of the thigh(Femur) and shank(Tibia), normalized to trunk length. At this point I have Humerus length = 88.5, Radius length = 95.5, hand length=59, Femur length = 74.5, Tibia Length = 62.25, and foot length = 52 (all numbers are normalized to the trunk length which is 100 units long). Setting the sum of the Humerus and Radius to 0.50m (the value that Swartz gives for the support limb length), gave me a conversion (0.002717 m/unit) from the trunk-length-normalized dimension to meters.

I could not find any values for the diameters of any of the limb segments, only a (chest diameter)/(trunk height) ratio which was given in Schultz [54]. Using this diameter, I get a circumference of about 0.4 m which corresponds to a diameter of about 0.13 m.

I shortened the hand length from the number that Erikson's ratios gave me (0.16m) because he states that his length is for the whole hand. When the hand is grasping the handhold this distance is less since gibbon's don't swing with the fingertips glued to the underside of the support. I felt that (0.11m) would be a reasonable compromise.

I felt that the density given by Swartz for the limb segments seemed a reasonable value to use. If I had limb mass data I could use the density to determine the radii of the various cylindrical segments. However, the only mass data that I found was for the total mass of the gibbon, although, both Swartz and Preushoft and Demes do give values for the mass of their cylindrical arm.

At this point I measured a radiographic image of a complete adult female Brachyteles arm that was given in [18]. The image showed the bones clearly along

Table 3.4: Approximate values for each of the segments parameters given the geometry shown in Figure 3.8. Note that for the thighs, shanks, feet, we merge the two cylinders into a single rigid body. $I_{cm} = m/12(3r^2 + l^2)$ is the moment of inertia of the body part about its center of mass. The center of mass is located in the middle of each cylindrical body segment.

body part	length(m)	radius(m)	volume(m^3)	mass(kg)	$I_{cm}(\text{kg} \cdot \text{m}^2)$
hand	0.11	0.01	0.3456 x 10^{-4}	0.03456	0.0357 x 10^{-3}
forearm	0.26	0.02	3.267 x 10^{-4}	0.3267	1.873 x 10^{-3}
upperarm	0.24	0.025	4.712 x 10^{-4}	0.4712	2.334 x 10^{-3}
torso	0.27	0.065	35.84 x 10^{-4}	3.584	25.56 x 10^{-3}
thigh	0.20	0.02	2.513 x 10^{-4}	0.2513	0.8629 x 10^{-3}
2 thighs	0.20	——	——	0.5027	1.726 x 10^{-3}
shank	0.17	0.0175	1.636 x 10^{-4}	0.1636	0.4064 x 10^{-3}
2 shanks	0.17	——	——	0.3271	0.8128 x 10^{-3}
foot	0.14	0.01	0.456 x 10^{-4}	0.04398	0.0729 x 10^{-3}
2 feet	0.14	——	——	0.08796	0.1458 x 10^{-3}

with the soft tissue of the arm. This gave me some approximate radii for the hand, forearm, and upperarm.

```
upperarm length = 0.24m
upperarm diameter = 0.05m
forearm length = 0.26m
forearm diameter = 0.04m
1/2 hand length = 0.11m
1/2 hand diameter = 0.02m
```

The only radii left to determine were those for the thigh, shank, and foot, for which I simply guessed at, based on the radii of the arm segments and the total mass of a gibbon.

All of the parameters that I finally arrived at are depicted in Figure 3.8.

The parameters for the two link model are easily derived from the model depicted in Fig. 3.8. The hand, forearm, and upper arm cylinders are kept in a straight line and glued to each other so that no relative motion between links is possible. The torso, 2 thighs, 2 shanks, and 2 feet cylinders are all compressed upward toward the shoulder into a point mass located at the shoulder pin joint. If the point mass at the shoulder is split in half and half is stuck onto the end of one arm link and the other half stuck to the other arm link then the list below gives rounded values for the model's dimensional parameters.

$l = 0.61$ m

$p \approx 0.0638$ m

$m \approx 3.083$ kg
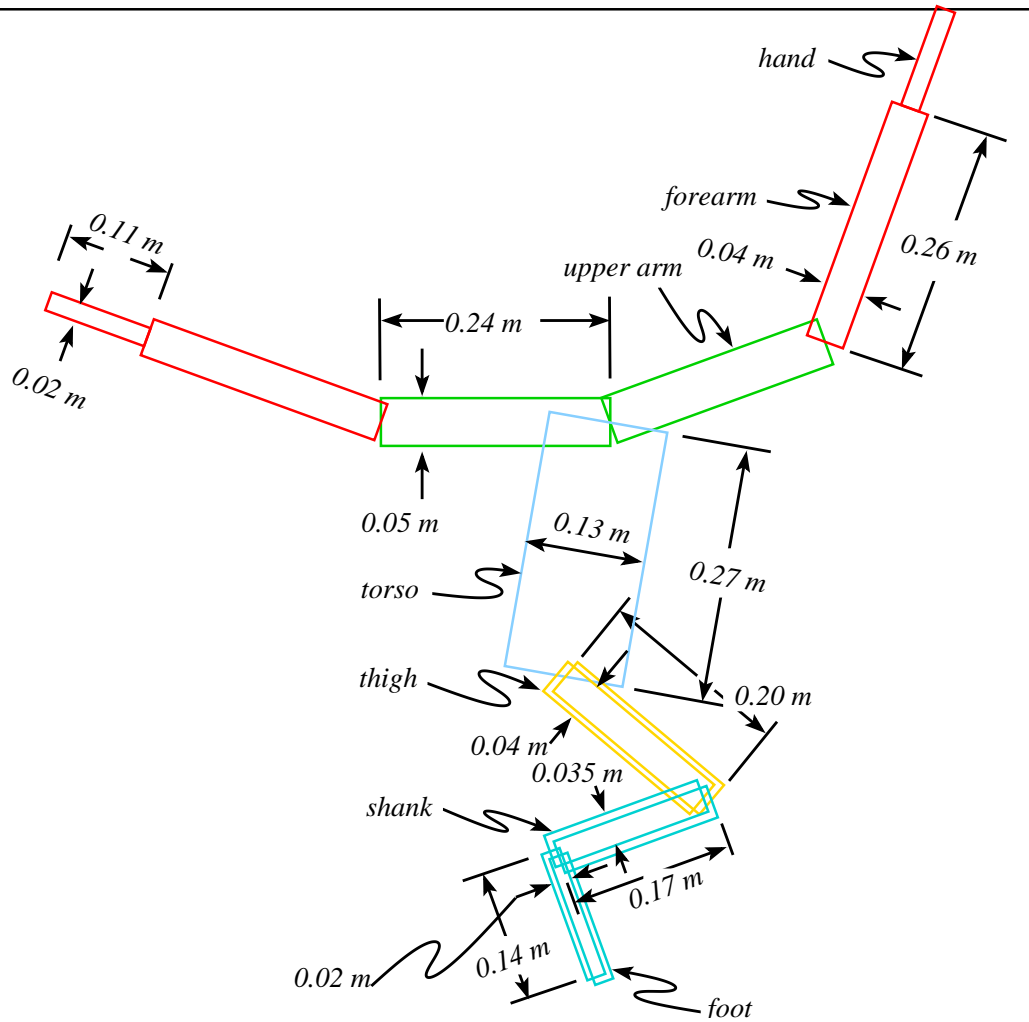
Figure 3.8: Cylindrical Body Segment Gibbon for Visualizing Parameters. The density used for all cylinders was 1000 kg/m^3 [60].

$I_{cm} \approx 0.0539$ kg $\cdot$ m^2

These values give a non-dimensional center of mass location to be $P = p/l \approx$ 0.105 and a non-dimensional radius of gyration to be $R = \frac{\sqrt{I_{cm}/m}}{l} \approx 0.2168$. The arm mass is approximately 0.8325 kg and the total mass of the gibbon is approximately 6.167 kg (close to the average total mass of a Hylobate given by Napier and Napier [42]). These masses result in an arm to total mass ratio of about 13.5%, which is very close to the 12.5% given by Preushoft and Demes in [47].

As can be seen in Figure 3.9, we obtain the simple forward progressing motions of the two-link-model with these more realistic mass and geometry parameters. It is almost unfortunate that this two-link model is so sensitive to the mass and geometry parameters. It is much more comforting to have a model which exhibits the same behavior for a wide range of system parameters. However, different parameter values will result in different behavior and given the approximate nature of our model as a gibbon, it is pleasing to find motions similar to brachiation for any set of parameters which can be argued as reasonably close to an actual gibbons. For example, Coleman and Mombaur's 3D passive walker walks stably, but mass distribution is completely non-anthropomorphic with the mass located down near the feet and away laterally from leg.

One last comment about the parameters. They were not obtained by curve-fitting (*i.e.* they were not adjusted until the desired behavior was seen in the model). Instead they were obtained by examining the published anatomical measurements, previously published model parameters, and approximations. Thus, the predictive nature of these results (that a gibbon's coordination strategy incorporates passive motions to a large extent) is an objective one.

3.5 Three and Five Link Model Parameters

The lower limbs are more difficult to accurately represent in these models because assumptions must be made as to the posture of the legs and whether to keep the posture fixed while moving. Most gibbons ricochetally brachiate with their legs tucked up underneath their body but use different postures for the continuous contact gait. For the three and five link models we assume the legs are tucked up under the body and model that by shrinking the thighs, shanks, and feet to a single point-mass on the bottom of the torso.

3.5.1 Three-Link Model

The parameters for the three-link model are more complicated to derive from the model shown in Fig 3.8. The difficulty lies in how to contract the many segments of the torso and legs into a reasonable single rigid body. The posture of the lower body is different in the two gaits and also moves during the motion. There are some who believe that the gibbon raises and lowers their legs to "pump" energy
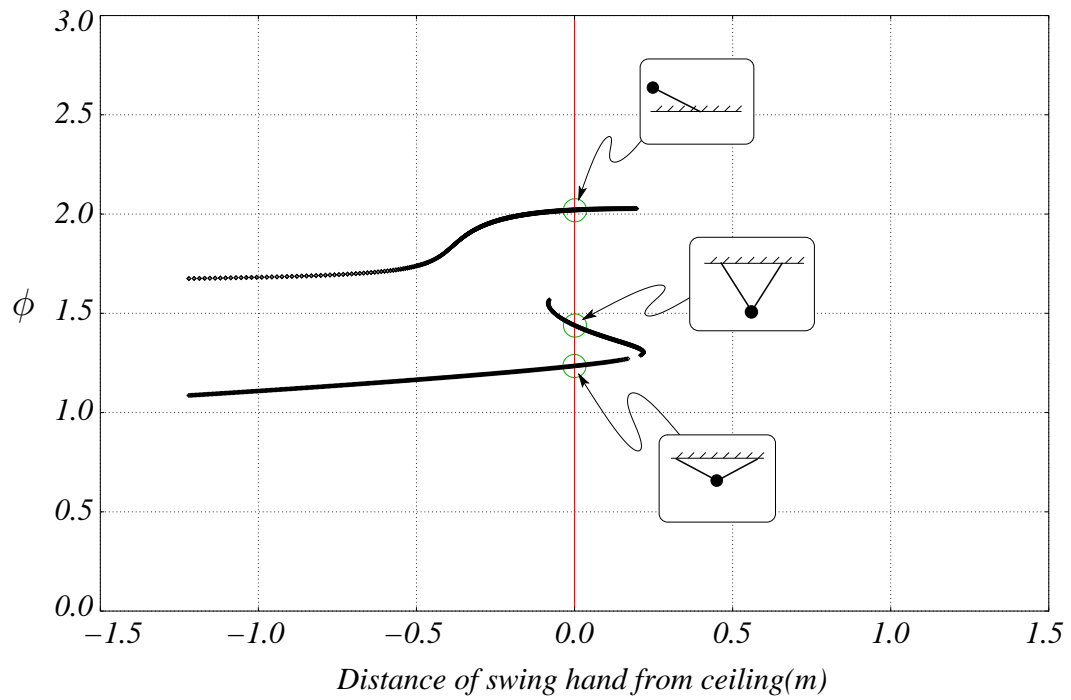
Figure 3.9: Periodic motions of the two link model using the three cylinder tapered arm parameters that were based on data in the literature [54, 18, 42].

Table 3.5: Approximate value for the rigid bodies used in the three link brachiation model shown in Figure 2.27. The arm link is constructed from the body parts shown in Figure 3.8 by locking the elbow and wrist joints so that the upperarm, forearm, and hand is in a straight line. The body link consists of the torso with the 2 thighs, 2 shanks, and 2 feet compressed to a single point mass and glued to the bottom of the torso cylinder. The center of mass locations are given as distances from the central shoulder hinge.

rigid body	length(m)	center of mass(m)	mass(kg)	$I_{cm}(kg \cdot m^2)$
arm	0.61	0.2362	0.8325	0.01997
torso and legs	0.27	0.1625	4.5015	0.03887

into the movement [19]. Active pumping of the lower limbs will have an effect on the dynamics of the system. Thus reducing the legs and torso to a single rigid body appears to be a cruder approximation than reducing each arm to a single rigid body. For the present work we approximate the lower body by keeping the torso as a cylinder and compressing both thighs, both shanks, and both feet into a point mass which is glued to the bottom of the torso cylinder. We could have also keep the legs as cylinders and locked the hip joints, knee joints, and ankle joints in the tucked up position but we did not choose that option.

3.5.2 Five-Link Model

The parameters for the five link model are a simple extension of those used in the three link model. In the five link model the arm links both have an "elbow" pin joint between the upperarm and the forearm. The forearm and the hand are still locked together with no relative rotation allowed between those links.

3.6 Discussion

The set of mass and geometry parameters used in a model of an animal can have a large impact on the types of passive motions that it can execute. McGeer found that anthropomorphic parameters gave some of the "best" periodic motions for his knee-jointed walking model [36]. This also seems to be the case for the passive models of brachiation, at least for the two-link model doing continuous-contact brachiation. There is certainly much that could be done to improve the accuracy of the set of parameters that was given in this chapter. Not only could more measurements be made to reduce the amount of approximations and guesses involved in determining the parameters, but the whole cylindrical approximation assumption could be replaced with simple rigid bodies with their actual moments of inertia. The constant density assumption could also be improved since the density of muscle, bone, and other body tissues are different. However, given there

Table 3.6: Approximate value for the rigid bodies used in the five link brachiation model shown in Figure 2.34. The forearm link is constructed from the body parts shown in Figure 3.8 by locking the wrist joint so that the forearm and hand is in a straight line. The body link consists of the torso with the 2 thighs, 2 shanks, and 2 feet compressed to a single point mass and glued to the bottom of the torso cylinder. The center of mass locations for the torso and upperarms are given as distances from the central shoulder hinge along the given rigid body. The center of mass location for the forearm is measured from the elbow joint.

rigid body	length(m)	center of mass(m)	mass(kg)	$I_{cm}(kg \cdot m^2)$
forearm	0.37	0.1477	0.3613	0.002979
upperarm	0.24	0.12	0.4712	0.002336
torso	0.27	0.1625	4.5015	0.03887

are so many things which we did not include in our model, such as restricting it to two-dimensional motion, neglecting air resistance, etc. it is quite unlikely that the model would benefit from additional accuracy in model parameters. This set of parameters simply gives rough idea of the mass and geometry properties of a gibbon.

Chapter 4

Extended Rimless Wheel Model

4.1 Introduction

A rimless wheel is a single rigid-body having equally spaced radial spokes, which moves in a two-dimensional environment. Imagine a wooden wagon wheel with the wood and metal rim around the circumference removed and leaving a central hub with the wooden spokes protruding from it. How does such an object move about? This question was asked by McGeer ([34], [35], [36] and he in turn refers to Margaria's work [32]) and later thoroughly answered by Coleman [14] where he examined all of the possible rolling and tipping motions that such an object can have when interacting with a floor without slip. In Coleman's work, as in the work presented in this chapter, collisions were modeled as perfectly plastic. This model was studied originally to provide a link between the simple passive dynamic walking models and a rolling disk. The rimless wheel, like the passive walkers, has sticking collisions between the ends of the spokes and the ground. The rimless wheel is also capable of stable downhill locomotion. As one increases the number of spokes in the rimless wheel it approaches a continuous circular disk. Although the rimless wheel can only locomote indefinitely down a ramp due to the collisional energy loss, the continuous disk is able to roll forever at constant speed across a level floor (assuming no slip occurs between the disk and the ground). In this chapter we will extend the 2D rimless wheel model to include a second rigid-body which is coupled to the rimless wheel via a torsional spring. We call this model the extended rimless-wheel model. The motivation for studying this model is to draw a closer connection between the collisionless walking model presented in chapter 5 and Chatterjee *et al.* 's one-dimensional hopping block model [8]. The walking model consists of three rigid-bodies with two torsional springs and is able to locomote across level ground indefinitely by avoiding collisions between the feet and the ground. Chatterjee *et al.* 's hopping block model consists of two point masses connected by a spring and is capable of incessant vertical hopping by avoiding collisions between the lower mass and the ground by velocity matching. The hopping block model is essentially a one-dimensional model and is therefore not capable of locomotion in a 2D environment. If it were allowed to move in
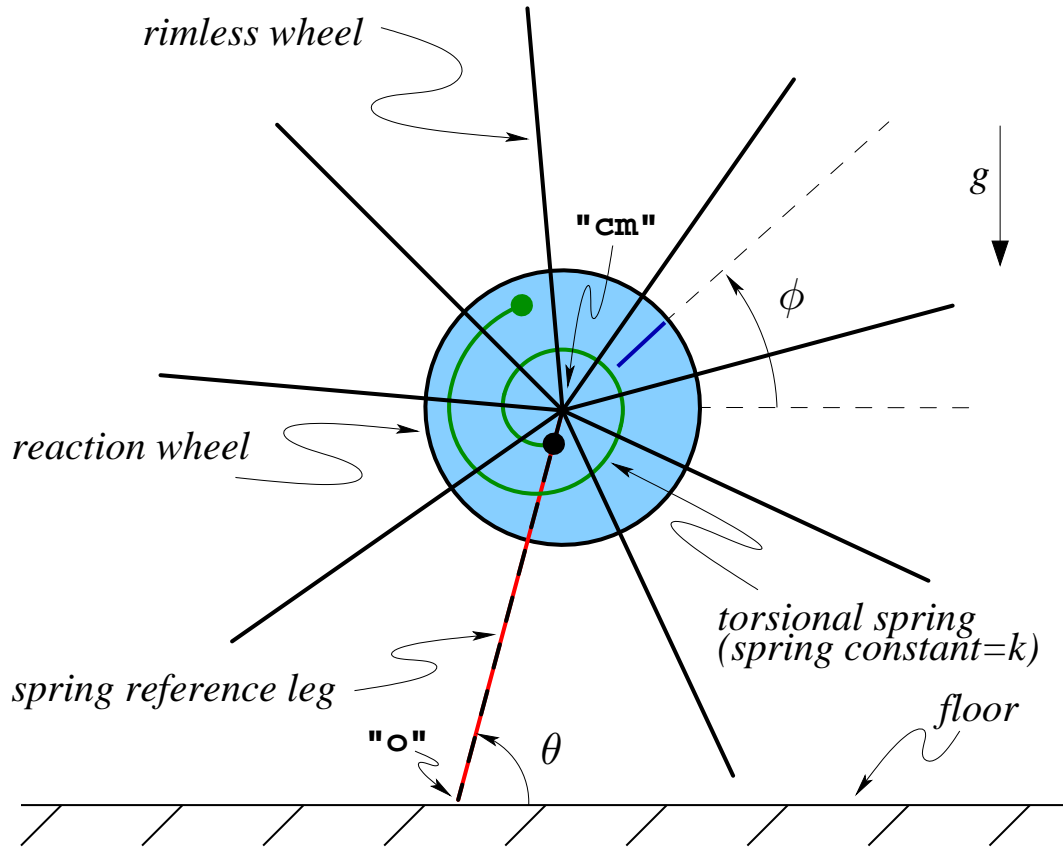
Figure 4.1: Rimless wheel model. This model is an extension of the 2D rim-
less wheel model that appears in Coleman's PhD thesis [14]. The
addition of the reaction wheel and torsional spring allow this
model to move across a horizontal support without collisions.

two dimensions then the model would now have 4 degrees of freedom instead of
the original 2 degrees of freedom. It quite probable that this 2D hopping block
system could be able to locomote in a collisionless manner but we instead chose
to construct and examine the extended rimless-wheel which has only two degrees
of freedom and is much closer in spirit and design to the three-link collisionless
walking model. As we shall see, this two degree-of-freedom extended rimless-wheel
model is also very close in spirit and behavior to Chatterjee *et al.* 's hopping block
model.

Figure 4.1 gives a representation of the extended rimless-wheel model. The
rimless wheel model, like the other models presented in this thesis, can only lose
energy via the plastic collisions that occur between the new stance "leg" and the
ground. Avoiding these collisions is key in conserving the model's energy. This
chapter will show that the extended rimless-wheel model can traverse a horizontal
support with the same lack of energy dissipation as a rolling disk.

Both the rimless-wheel model presented here and the hopping block model of

Chatterjee *et al.* [8] have only two bodies which are connected via a spring. As we shall see, one can consider the extended rimless-wheel model as a rotational analog to the hopping block model. We will examine two classes of motions using our extended rimless-wheel model. One class will consist of motions where the support constraint is instantaneously transferred to the new supporting leg when it contacts the floor (only one leg is in contact with the ground a any time). The other class of motions have a double-stance phase where two legs can be in simultaneous contact with the ground for a finite amount of time. We will see that these two classes will both have collisionless motions with different characteristics.

4.2   Symmetry and counting arguments

As in the brachiation models discussed in chapter 2, we search for motions with a certain symmetry which enforces that those motions will by collisionless. In this model, the symmetry property is slightly different than in the brachiation or walking models. The reason for the difference is that the rimless wheel rotates by a finite amount with each step. Thus the symmetrical motion that we seek must also contain this discrete indexing of the rimless-wheel's rotation. Figure 4.2 depicts a set of conditions that, if met, will result in a collisionless periodic motion. At the beginning of the motion, we have only one state that we can specify, the angular velocity of the reaction wheel ($\dot{\phi}$). The map is then evaluated when $\theta = \pi/2$ and the output from the map is the value of ϕ. Thus our mapping, $\mathbb{R}^1 \to \mathbb{R}^1$ is quite simple.

Note that the conditions require that the system start with the spring relaxed. This is a necessary condition because if one starts with $\phi \neq \theta$ and finds a motion that satisfies the ending conditions of the map, then the motion, although collisionless, will not be periodic since the torque that is applied to the rimless wheel at the end of the step from the torsional spring will be opposite in sign than it was at the beginning of the step.

4.3   Collisionless Periodic Motions

Figure 4.3 shows several snapshots of a periodic collisionless motion equally spaced in time. The figure shows the symmetry of the motion with the symmetrical position halfway through the step marked with a "*". One undesirable feature of this motion is that at the moment weight-shift occurs, the old stance foot immediately passes through the floor before it lifts up and the rimless wheel reverses its rotation. This feature of the motion makes it extremely difficult to physically construct a device which would have such a motion since it would require a rather sophisticated mechanism to allow the swing foot to pass below its previously constrained height when the constraint changes feet.

One might conjecture that other collisionless periodic motions might exist for this model where the incommoding foot does not approach the ground from below

Spring starts and ends in relaxed state

$\phi = \theta$

$\phi = \theta$

$\dot{\theta} = 0$

$\theta = 90^o$

Initial configuration

Desired configuration at end of mapping
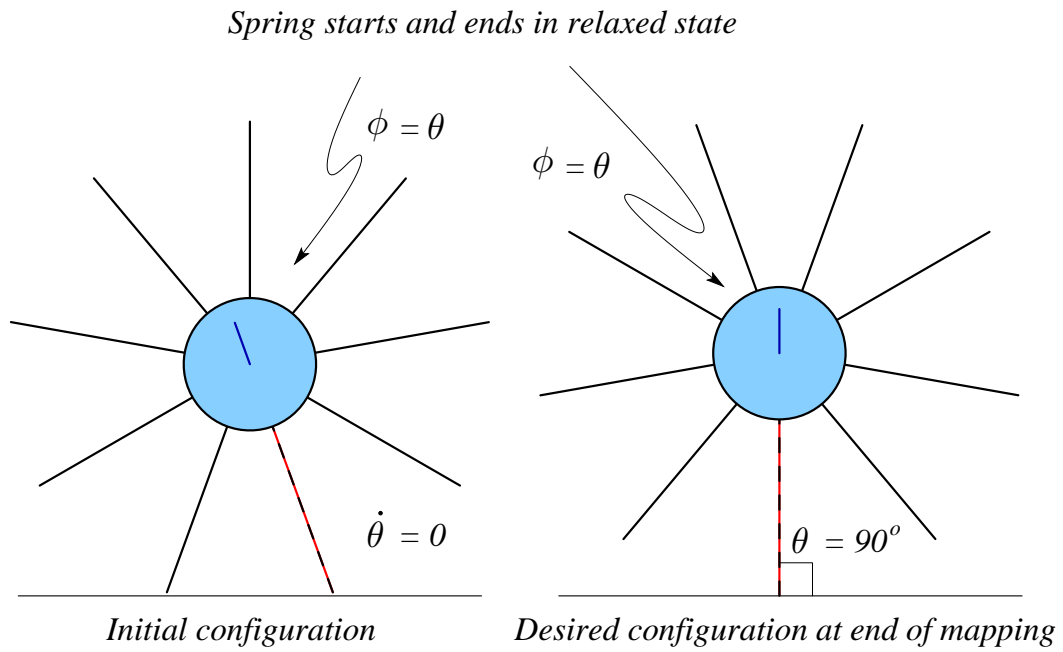
Figure 4.2: Conditions for a symmetrical, collisionless, periodic motion for the rimless-wheel-model. The system begins with two feet on the ground, the rimless wheel at rest($\dot{\theta} = 0$), and no potential energy stored in the spring($\phi = 0$). The state of the system halfway through a single step consists of the stance foot being perpendicular to the ground($\theta = \pi/2$) and the spring in a relaxed state ($\phi = \theta$).
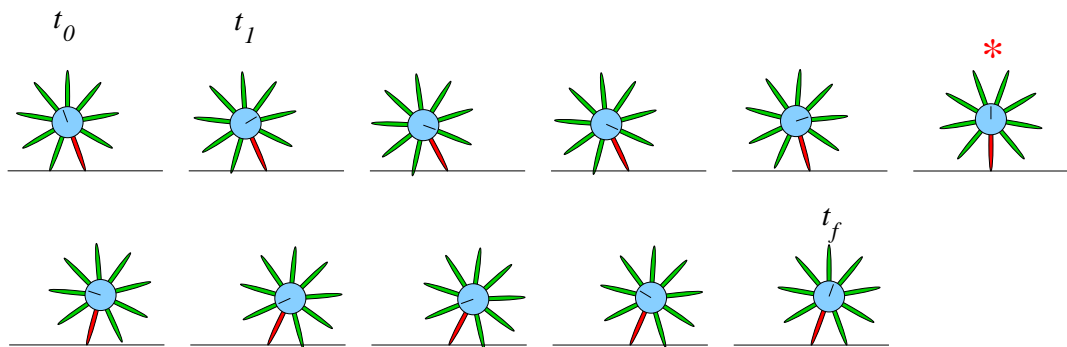
Figure 4.3: A pictogram of a collisionless periodic motion that satisfies the symmetry conditions given in Figure 4.2. Note that the swing foot passes through the ground at the beginning and end of the motion.
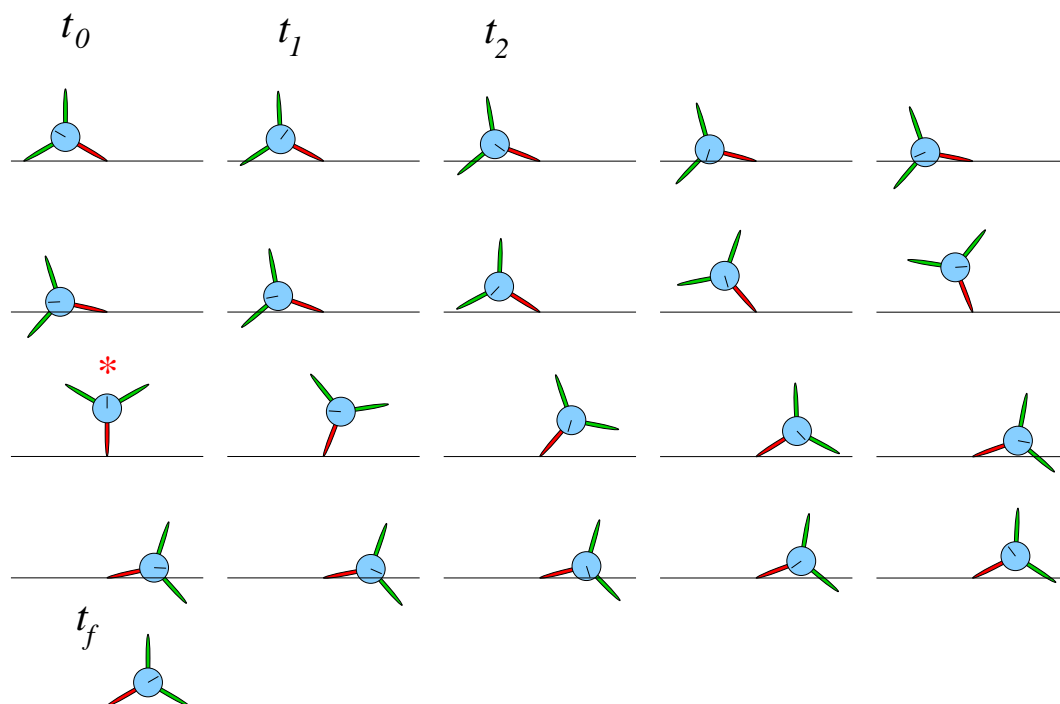
Figure 4.4: A pictogram of a collisionless periodic motion that satisfies the symmetry conditions given in Figure 4.2. Note the larger ground penetration present in this motion with only 3 legs on the rimless wheel. This motion is further described by the plots given in Figures 4.5-4.7.
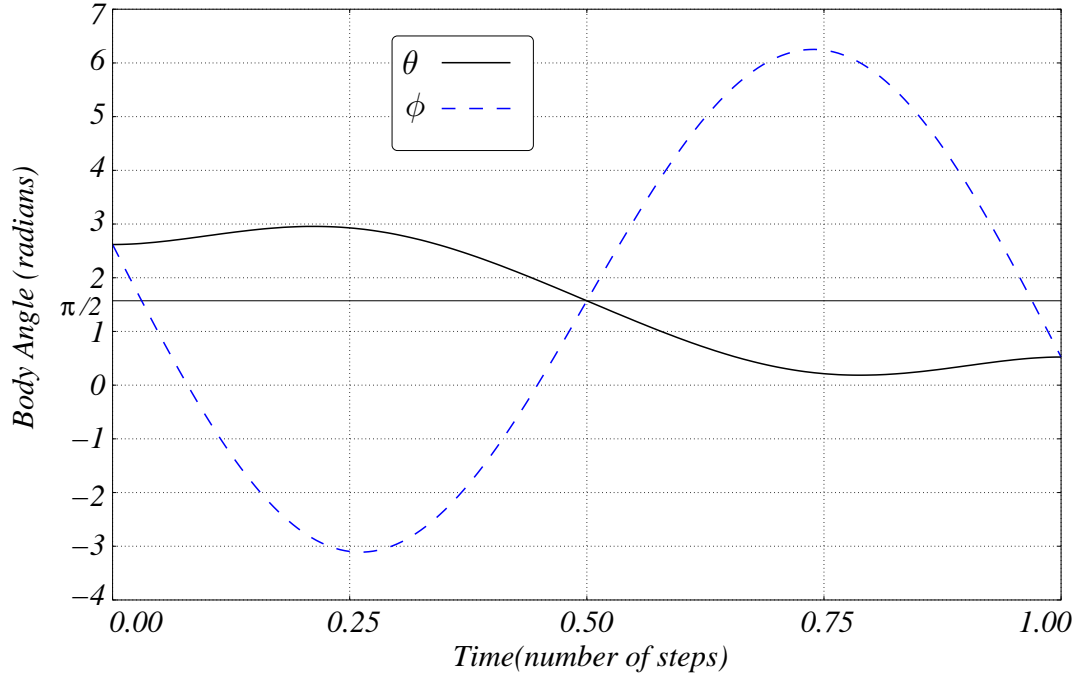
Figure 4.5: Plot of the angles for the two bodies (3 leg rimless wheel) in the motion depicted in Figure 4.4. The parameters for this motion are: $numb_{legs}$=3, l_{leg}=1.0m , m_{leg}=1.0kg, $I_{leg/cm}$=1.0m^{2}kg, m_{torso}=0.1kg, $I_{torso/cm}$=1.0m^{2}kg, K=3.0Nm/rad, g=9.81m/sec. The initial conditions for this motion(after doing convergence tests) are: $\theta(0) = \frac{5\pi}{6}$ rads, $\phi(0) = \theta(0)$, $\dot{\theta}(0) = 0$ rads/sec, $\dot{\phi}(0)$ =-10.177410583917 rads/sec
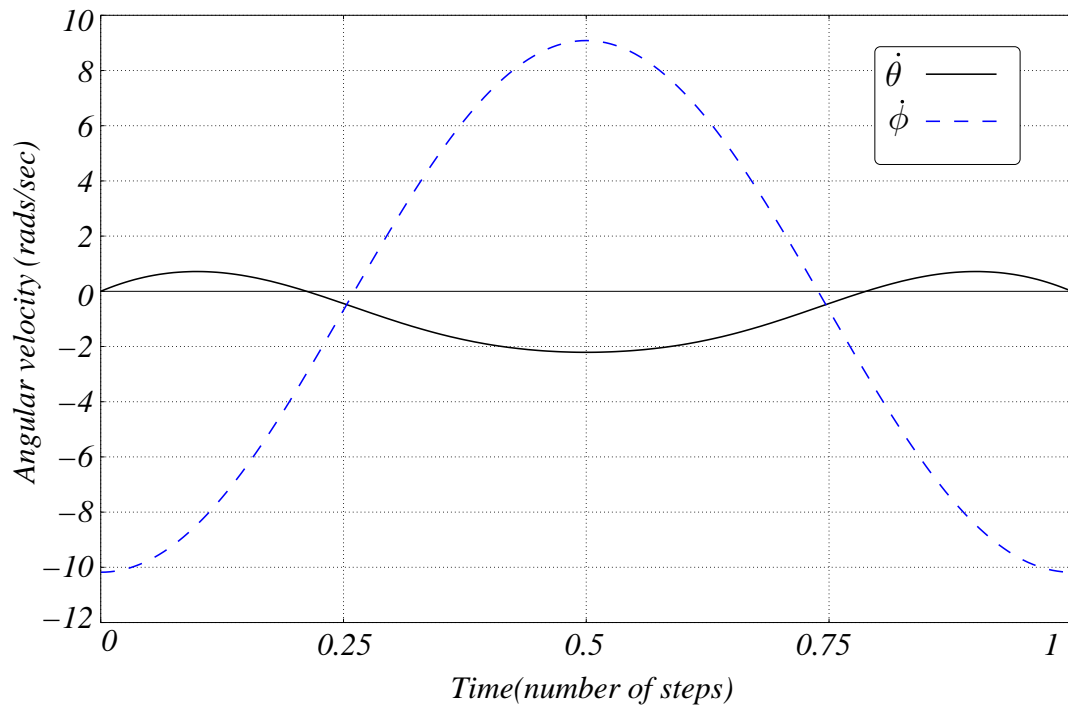
Figure 4.6: Plot of the angular velocities of the the two bodies (for the 3 leg rimless wheel model) in the collisionless motion depicted in Figure 4.4. Note that the rimless-wheel begins and ends the step with zero angular velocity, which is the condition for avoiding collisions with the ground.
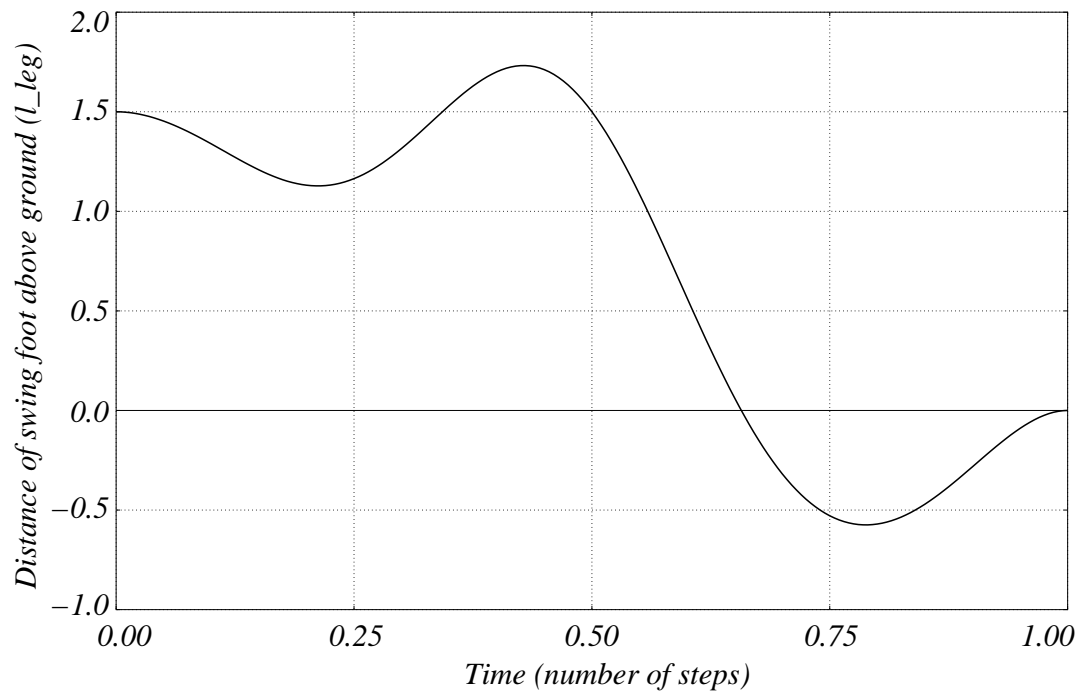
Figure 4.7: Plot of the incoming foot's height above the ground for the motion depicted in Figure 4.4(3 leg rimless wheel). Note the large amount of ground penetration by the incoming foot, as well as the fact that the foot makes contact with the ground from below the floor.
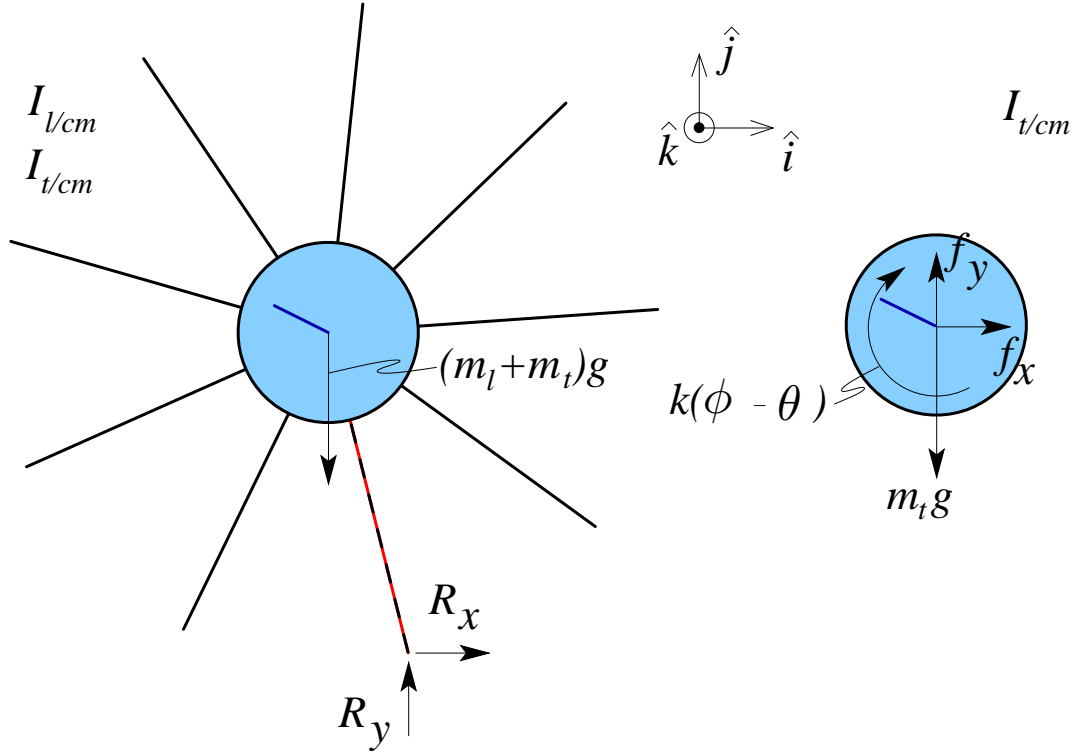
Figure 4.8: Free body diagrams of the rimless-wheel-model. A free body diagram of the whole model appears on the left. On the right is a free body diagram of just the reaction wheel, with the rimless wheel cut away.

and thus allow physical models to be constructed. Unfortunately, for this model this is not the case. This can most easily be shown by examining the system's equations of motion. The non-dimensional equations of motion for the system can be derived from angular momentum balance applied to the free body diagrams shown in Figure 4.8.

The non-dimensional equations of motion are:

$$
\begin{aligned}
-cos(\theta) + \kappa(\phi - \theta) &= (R_l{}^2 + 1)\theta'' \\
-\kappa(\phi - \theta) &= R_t{}^2\phi''
\end{aligned}
\tag{4.1}
$$

where κ is a non-dimensional spring constant defined as $\kappa = k/((m_l + m_t)gl)$. R_l and R_t are non-dimensional radii of gyration of the rimless-wheel(leg) and the reaction-whee(torso) respectively and are defined as $R_l = \sqrt{I_{l/cm}/((m_l + m_t)l^2)}$ and $R_t = \sqrt{I_{t/cm}/((m_l + m_t)l^2)}$. All derivatives noted as $(') = d()/d\tau$ are derivatives taken with respect to a non-dimensional time,τ where $\tau = t/\sqrt{(l/g)}$.

As can be seen from the equations of motion given in equation 4.1, if the motion begins with both feet on the ground (which implies that $\pi/2 < \theta(0) < \pi$),

the rimless wheel at rest($\dot{\theta}(0) = 0$), and the spring relaxed($\phi(0) = \theta$), then $\ddot{\theta}(0) > 0$ since ($\kappa \geq 0$, $R_l \geq 0$ and $cos(\theta(0)) < 0$). A positive $\ddot{\theta}(0)$ means that given the starting configurations with which we must begin, there is no possible initial value of $\dot{\phi}$ that will not result in the new swing foot immediately passing through the floor when the constraint on the feet is instantaneously switched. The only way to make $\ddot{\theta}(0)$ negative is to begin with the torsional spring loaded (*i.e.* with $\phi(0) \neq \theta(0)$) as can be seen from equation 4.2.

$$\phi - \theta < \frac{cos(\theta)}{\kappa} \tag{4.2}$$

However, starting with the spring in a loaded configuration violates the particular symmetry that is being sought since such a motion will end with the spring wound up the same amount as when it started but in the wrong direction. Thus, this model is not capable of physically-realizable collisionless periodic motions where the ground support instantaneously changes feet at the moment of collision.

4.4   Extended double stance

The motions that were sought previously, where the support foot changes instantaneously are a different class of motions than is possible in the hopping block model of Chatterjee *et al.* [8]. The model in [8] only has a single "foot" and thus there cannot be an instantaneous change of foot support. The rimless-wheel-model that is presented here is capable of extended contact motions where both feet are simultaneously in contact with the ground for a finite period of time.

There are some subtle issues concerning ground contact which must be discussed before we can go further with this extended double-stance model. What is the nature of a floor constraint and what are the conditions for releasing the foot contact constraint?

The foot contact release issue concerns the non-intuitive motion that results from removing a pivot constraint when the normal (to the ground) or vertical component of the ground reaction force drops to zero. In many models of physical systems the point on the system where the constraint is removed may immediately pass through the ground. This was discussed by McGeer in [37] and will also be discussed in the collisionless walking-model chapter (chapter 5). In the extended rimless-wheel model, this issue does not arise since the two contact points are on the same rigid body. The friction force on the trailing foot can be neglected since it does not enter into the equations of motion.

Previously, when we used an instantaneous support transfer, we ignored and did not discuss an important property of a floor constraint, that it is a one-way support. Unlike the gibbon models in chapter 2 who could grab onto the ceiling support and provide reaction forces in any direction, the feet of the rimless-wheel model do not grab onto the floor. This means that the floor is able to provide
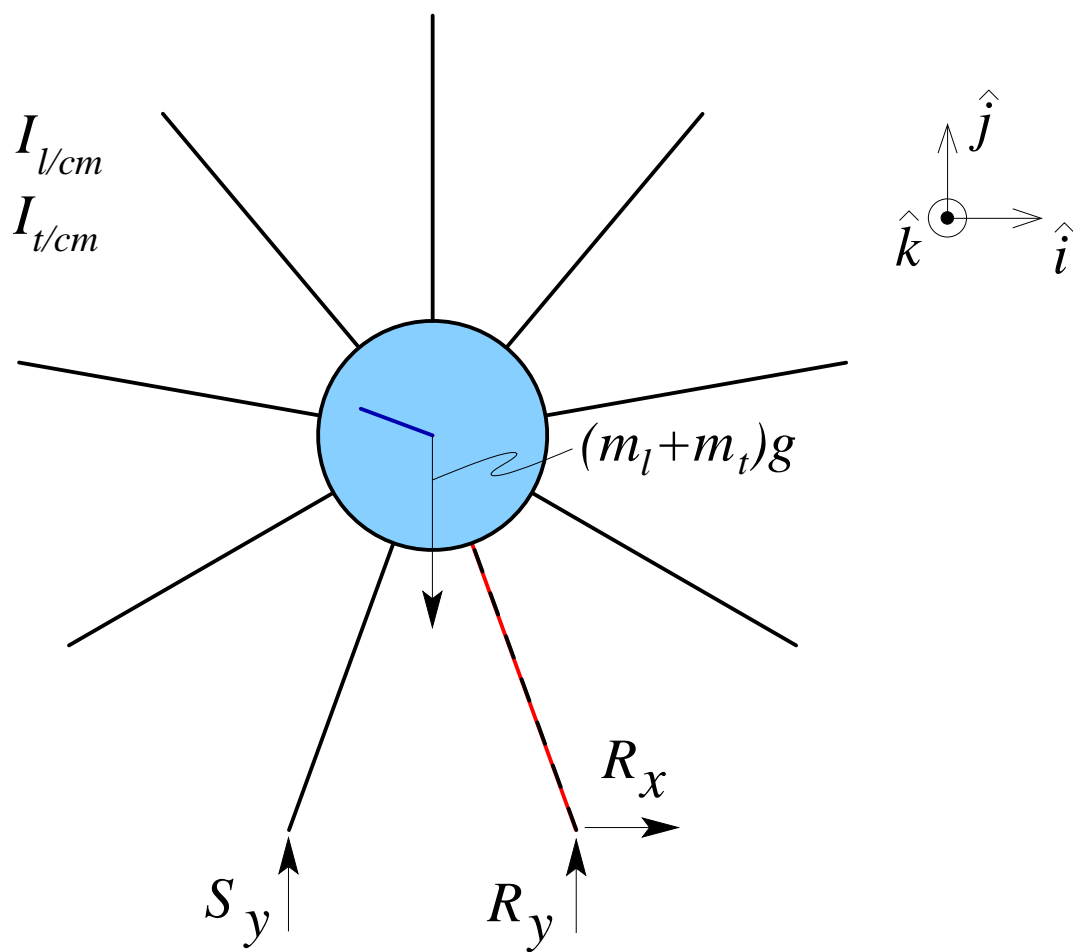
Figure 4.9: Free body diagram of the rimless-wheel-model during a time of extended double stance assuming a frictionless contact between the trailing foot and the ground.

Table 4.1: General criteria to be met at the end of a step for a collisionless
motion. Note that condition 3 is automatically met for this model
if condition 2 is met since the body which makes contact with the
ground has only one degree of freedom.

1) vertical position of foot at floor level.
2) vertical component of the foot's velocity is zero.
3) horizontal component of the foot's velocity is zero.
4) vertical component of the foot's acceleration is zero.
5) vertical component of the foot's jerk is negative.

a force on the foot to keep it from passing through it but is not able pull down
on a foot and keep it from lifting off of it. Previously, we were only concerned
with the incoming foot arriving with a zero velocity (some of the extra conditions
stated below were assumed to be met by the instantaneous support). These extra
conditions are given by Chatterjee *et al.* in [8]. In short, we would like the foot
to start above the floor, reach the floor elevation with zero velocity, and then (if
the floor constraint was not enforced) pass through the floor. If a foot arrives
at the floor with zero velocity, it will lift off from the floor if there is a positive
vertical component of the foot's linear acceleration. This also means that since we
want to approach the floor from above, we need the vertical component of the foot's
acceleration to be zero[1] at the same point that the its elevation and velocity is zero.
Since we want the foot to pass though the floor if there were no floor constraint,
the sign of the vertical component of foot's jerk[2] needs to be negative. If the foot's
jerk has a positive vertical component and its height, velocity and acceleration
are all zero, then the foot would lift off the floor instead of maintaining contact.
Table 4.1 gives the criteria that must be met for a motion to be collisionless in the
general case.

These five conditions can be written as:

$$y_{foot} = 0, \quad \dot{y}_{foot} = 0, \quad \dot{x}_{foot} = 0, \quad \ddot{y}_{foot} = 0, \quad \dddot{y}_{foot} < 0,$$

Diagrams of the vertical position of the incoming foot versus time for various cases
without enforcing the floor constraint are shown in Figure 4.10. These diagrams
are based on ones which appear in Chatterjee *et al.* [8].

Since the rimless wheel is a single rigid body in 2D with two position constraints
(stance foot's horizontal and vertical position is fixed) it has only a single degree
of freedom. Thus the vertical component of incoming foot's position, velocity,

---

[1]If the vertical component of the foot's acceleration were positive, then we would
lift off from the floor again. If it were negative then we would be approaching the
floor from below. Therefore, we need the curve of the vertical component of the
foot's velocity to have an inflection point at the point of zero vertical velocity.

[2]Jerk is defined as the rate of change of acceleration with respect to time
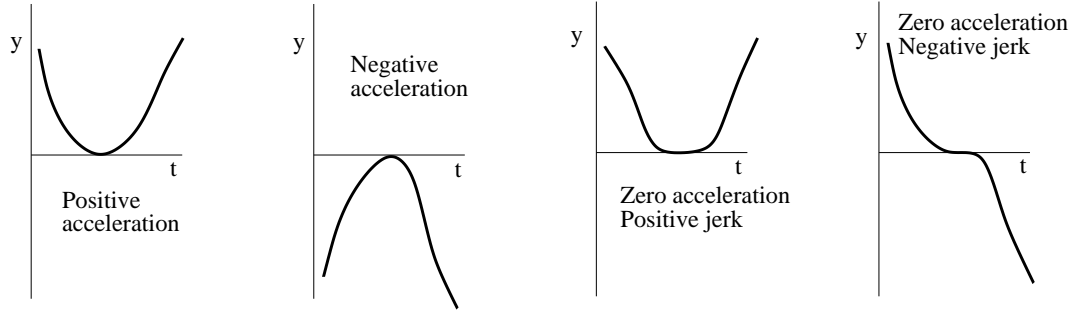
Figure 4.10: Sketches of the vertical position of the incoming foot versus time for various cases. All cases concern the value of the vertical component acceleration and jerk of the foot when the vertical position and velocity of the foot is zero. These diagrams are based on the ones which appear in Chatterjee *et al.* [8].

acceleration, and jerk given in equations 4.6 are all tied to the rimless wheel's angular position, velocity, acceleration, and jerk.

$$\boldsymbol{r}_{p/o} = (d\cos\beta)\hat{\mathbf{i}} + (d\sin\beta)\hat{\mathbf{j}} \tag{4.3}$$

$$\beta = \theta - \frac{\pi - \psi}{2}$$

$$\psi = \frac{2\pi}{\text{number of legs}}$$

$$d = 2l(\sin\frac{\psi}{2}))$$

$$\dot{\boldsymbol{r}}_{p/o} = (-d\dot{\theta}\sin\beta)\hat{\mathbf{i}} + (d\dot{\theta}\cos\beta)\hat{\mathbf{j}} \tag{4.4}$$

$$\ddot{\boldsymbol{r}}_{p/o}\boldsymbol{j} = (-d\ddot{\theta}\sin\beta - d\dot{\theta}^2\cos\beta)\hat{\mathbf{i}} + (d\ddot{\theta}\cos\beta - d\dot{\theta}^2\sin\beta)\hat{\mathbf{j}} \tag{4.5}$$

$$\dddot{\boldsymbol{r}}_{p/o}\boldsymbol{j} = (-d\dddot{\theta}\sin\beta - 3d\ddot{\theta}\dot{\theta}\cos\beta + d\dot{\theta}^3 sin\beta)\hat{\mathbf{i}}$$
$$+(d\dddot{\theta}\cos\beta - 3d\ddot{\theta}\dot{\theta}\sin\beta - d\dot{\theta}^3 cos\beta)\hat{\mathbf{j}} \tag{4.6}$$

For the extended rimless-wheel model, the five conditions given in equation 4.4 get reduced to the four conditions shown in equation 4.7.

However, if we instead look for a symmetric motion of a specific type we can reduce the number of necessary criteria from four to one. This is possible because the lifting motion of a foot played backward in time are exactly the conditions we seek. The symmetric motion we want starts with two legs on the ground and the spring wound up some amount and ends halfway through the cycle with the stance leg being vertical ($\theta = \pi/2$) just as the spring reaches its relaxed state ($\phi = \theta$). The fixed points of this one dimensional map results in collisionless motions which meet all of the four criteria listed above.

$$\left(\beta = 0 \Rightarrow \theta = \frac{\pi - \psi}{2}\right), \quad \dot{\theta} = 0, \quad \ddot{\theta} = 0, \quad \dddot{\theta} < 0 \tag{4.7}$$
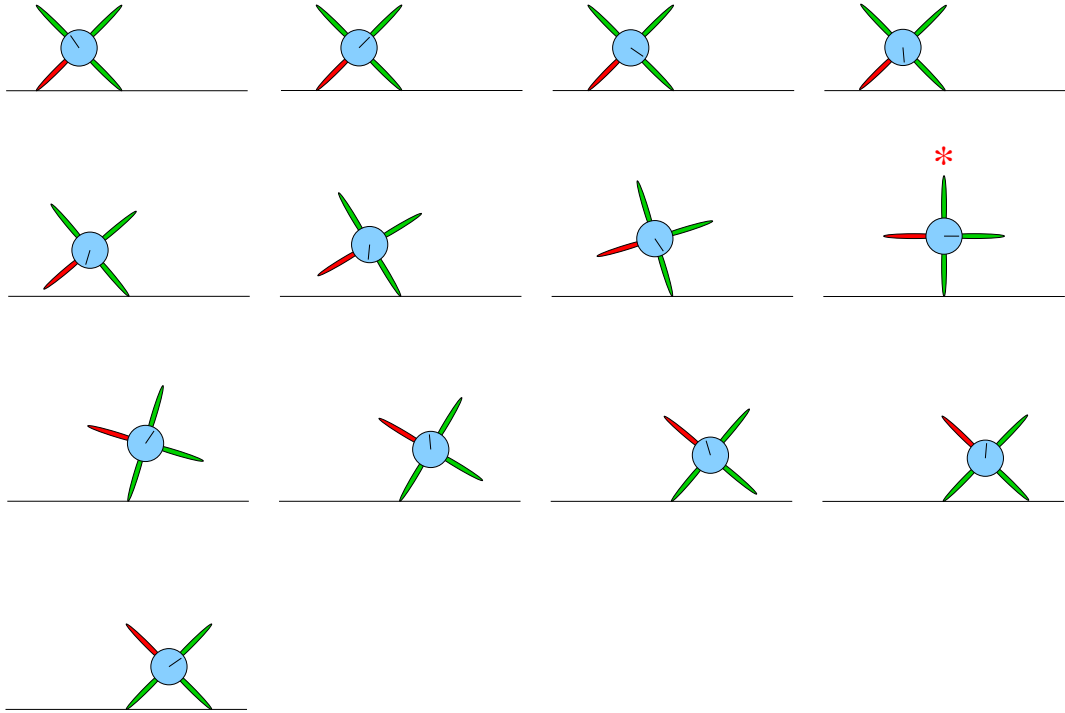
Figure 4.11: Snapshots of a collisionless periodic motion for the rimless-wheel-model with an extended double stance phase. This parameters used in this model for the motion are: number of legs $= 4$, $l_{leg} = 1.0$m, $m_{leg} = 0.1$kg, $I_{leg/cm} = 3.0$kgm^2, $m_{torso} = 0.1$kg, $I_{torso/cm} = 1.0$kgm^2, $K = 1.0$Nm/rad. This initial conditions for this motion are: $\theta = 3\pi/4 rads$, $\phi = \theta$, $\dot{\theta} = 0 rads/sec$, $\dot{\phi} = -2.64770369207$.

4.5 Discussion

Although a single rimless-wheel is unable to traverse a perfectly horizontal support indefinitely unless the number of spokes is infinite, the extended rimless-wheel can do so. The interaction between the oscillations of the reaction-wheel and the rimless-wheel can combine in such a manner as to allow the rimless wheel to achieve a symmetric motion. We have shown that by achieving this symmetric motion which requires only a single condition, one necessarily achieves the four conditions required for collisionless periodic motions. This seemingly gratuitous stroke of luck is due simply to the fact that the way the model must leave the double stance configuration is exactly the way in which we desire for it to enter into the next double-stance configuration. In other words, the four conditions that we have specified are, for this model, non-independent conditions. The collisionless motions which have an double-stance phase, nicely echo the results of the Chatterjee *et al.* 's hopping block results. Lastly, the simplicity of this model make it extremely
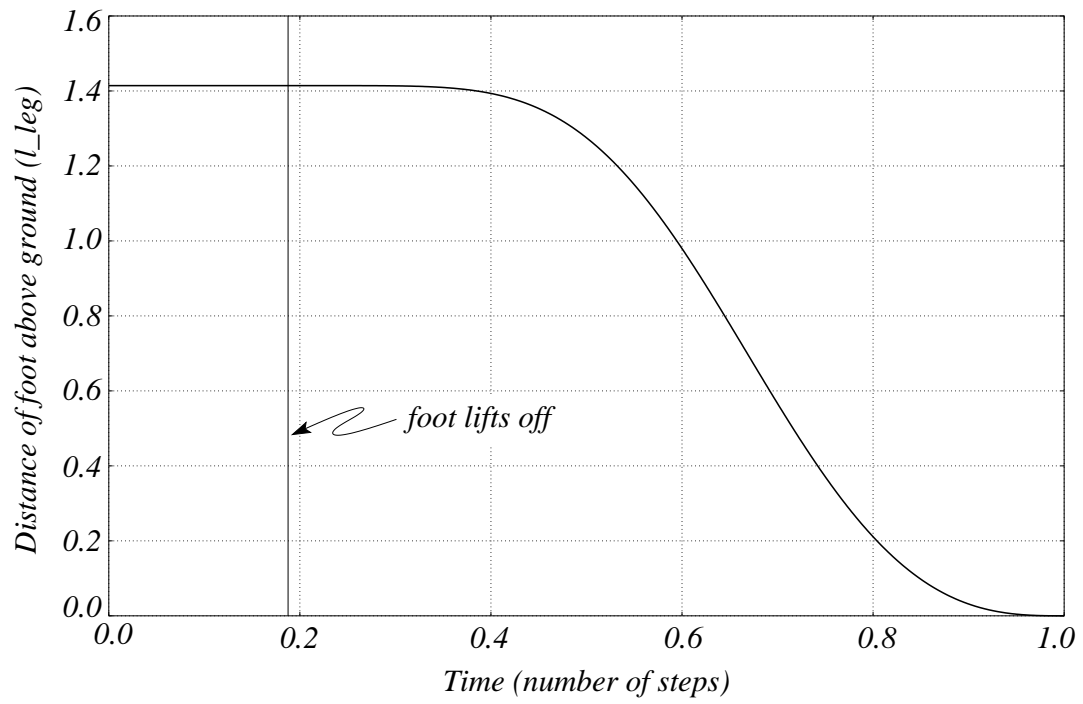
Figure 4.12: Height above the ground of the incoming foot. Note that the foot arrives at a zero distance with a zero slope, which means that it's vertical velocity is zero when it touches the floor.
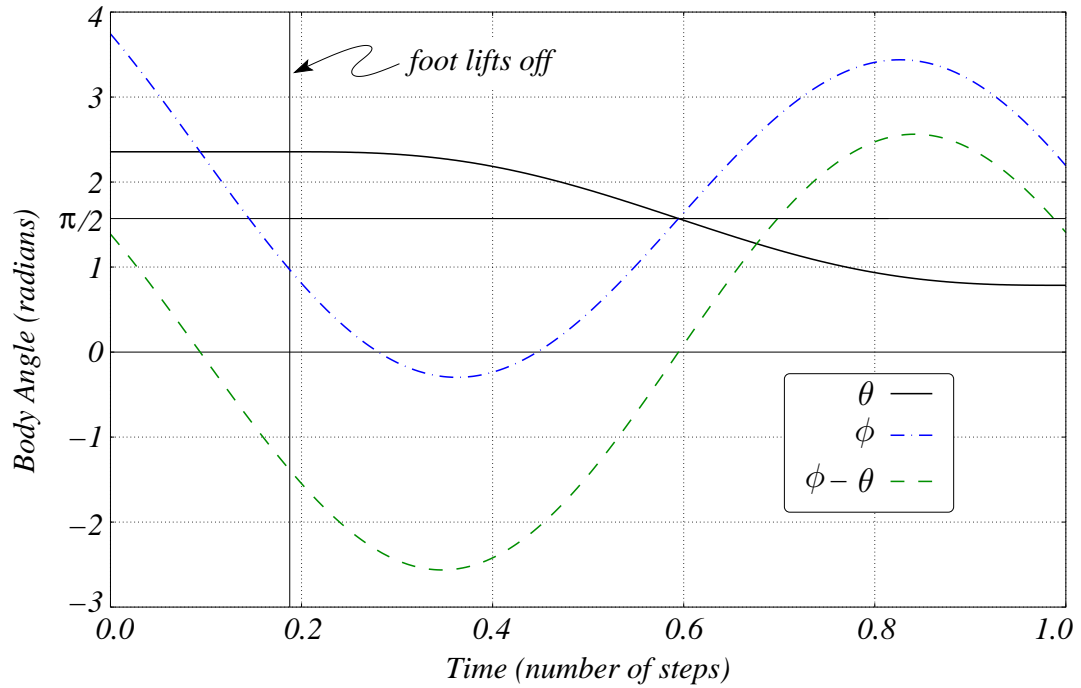
Figure 4.13: Plot of the angles of the rimless-wheel and reaction-wheel for the collisionless periodic motion depicted in Figure 4.11. Note the constant value of θ during the double-stance phase at the beginning of the step. Also note that θ and $\phi - \theta$ are symmetric about the mid-double-stance and mid-single-stance points. (This plot is actually for the step that happened just before the one shown in Figure 4.11 as can be seen by the reference leg and line.)
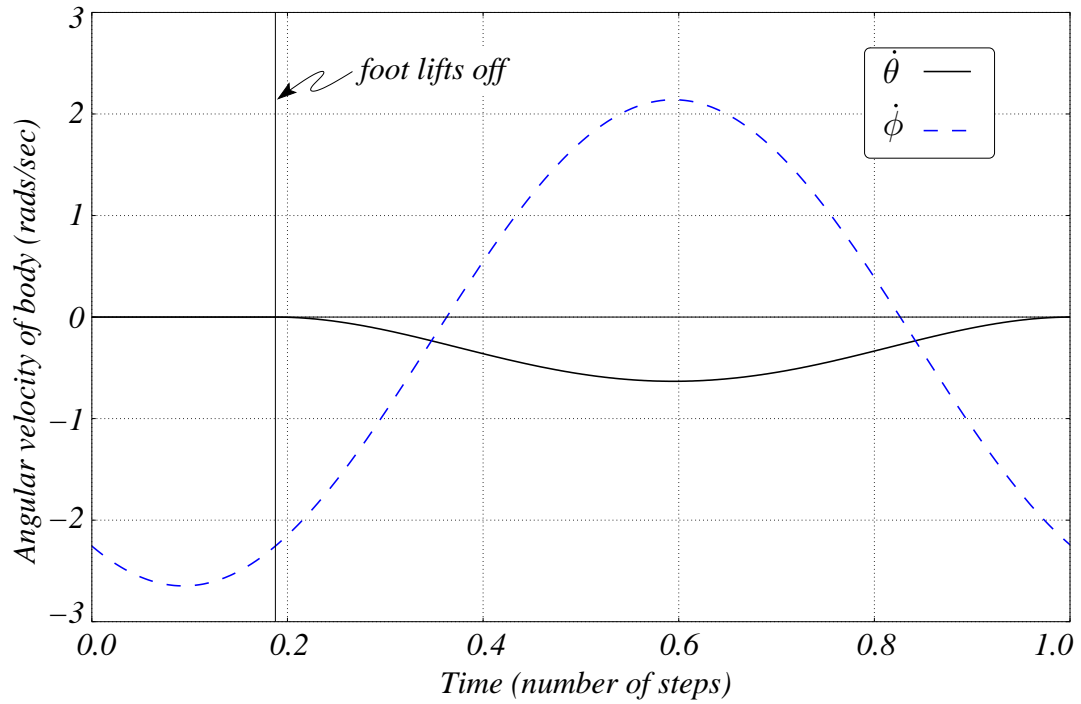
Figure 4.14: Plot of the angular velocities of the two bodies in the motion shown in Figure 4.11. Note that the rimless-wheel starts and ends the motion with zero angular velocity and that the angular velocity curves are symmetric about same two mid-stance positions.
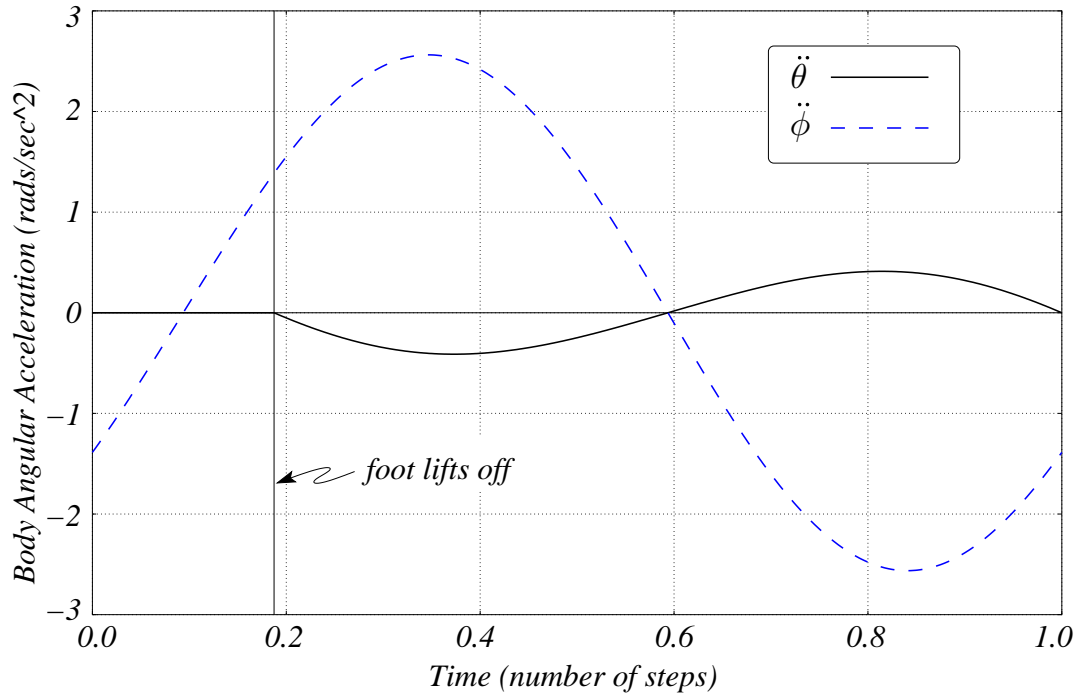
Figure 4.15: Angular acceleration of the two bodies for the collisionless mo-
tion shown in Figure 4.11. Again, the curves are symmetric
about each of the two mid-stance positions. Note that the an-
gular acceleration of the rimless-wheel is zero at the end of the
step. Also, one can clearly see that the slope of the angular
acceleration of the rimless-wheel curve is negative at the end of
the step.

appropriate for the construction of a device which is capable of achieving these collisionless motions. Note, that some sort of external stability mechanism must be created for the physical device to function, but this controller has to only control a single variable at a point in the map. It may also be possible for this model to roll stably down a shallow ramp. This conjecture comes from an extrapolation of the one-sided stability properties of the hopping block model of Chatterjee *et al.* [8].

The collisionless motions shown in this chapter cannot be stable since any error from the given trajectory will result in a collisional energy loss. Once the system loses energy it cannot be gained back since there is no mechanism for pumping energy into the system. If one cannot achieve the same system energy as before, the motion can not be periodic. Thus the collisionless motions cannot be stable. This, however, does not rule out the possibility of adding a simple controller and actuator to a physical extended rimless-wheel model.

Chapter 5

Walking

This chapter consists of a paper by the author and Andy L. Ruina that is in review for Physical Review E. The last part of the chapter on the Chebyshev mechanism was not included in the paper due to the length restrictions of the journal.

5.1 Abstract

We have found periodic collisionless motions for a rigid-body walking model. Unlike previous bipedal designs, this model can walk on level ground at non-infinitesimal speed with zero energy input. The model avoids collisional losses by using internal oscillations of the upper body, relative to the legs. This avoidance of foot-strike collision losses by means of synchronized internal oscillations may help in the design of energy-efficient robots and explain aspects of animal locomotion efficiency.

5.2 Introduction

Locomotion over level ground does not, fundamentally, have a lower bound for energetic cost, since the key relevant force, from gravity, is orthogonal to the net displacement. For example, no energy is required to move a weight across a frictionless horizontal surface. Nature and engineers have designed low friction hinges, and air-friction losses are small for walking. If one neglects minor losses from joint and air friction, is it possible to design a system that can walk with no energy input?

The dominant energy sinks in walking are in the actuators when they absorb rather than perform work (*eccentric* muscle contractions) and through collisions when a foot hits the ground. At such a collision, energy is lost by a combination of mechanisms (heat at the collision point, dissipation in muscles and soft tissues, etc.) the details of which do not affect mechanics predictions, so long as the rigid-body modeling is accurate both before and after the collision [9]. Our model will have

no actuators, so energy cannot be lost by work being done on the actuators. Thus, finding a zero-energy-cost walking machine is equivalent to finding a collision-free walking machine. The following are various ways to seek zero-energy-cost walking.

Kinematic mechanisms. Over 150 years ago Chebyshev designed many mechanisms that guided their endpoints on nearly straight line paths for a portion of their trajectories [12][1]. Using four copies of an approximate-straight-line-mechanism (Fig. 5.1), Chebyshev achieved almost perfectly smooth walking. Chebyshev's aim was a near straight trajectory for the carriage, not zero dissipation. Therefore, a very small collision remains in his design. With a slight cost in levelness of carriage motion, the mechanism could be redesigned to achieve a foot impact velocity of zero. Opening the rules of play further to include more general mechanisms, say with cams or chains, designing a 'kinematic' walker with no foot impact is trivial. Such kinematic (or one-degree-of-freedom) designs do not achieve our present goals of finding an essentially dynamic design with zero dissipation. We desire to increase our understanding of the mechanics of machines that have, like walking people and animals, more than one degree of freedom.

Compliant contact. To avoid collisions, one could consider using massless springs on the bottom of the feet. These springs could be compliant in a telescoping manner along the leg or compliant in both spatial directions (2D). If a telescoping leg spring is used, the foot velocity, at contact, must be parallel to the leg orientation for no impact to occur, a class of solutions we chose not to pursue. If a spring which is compliant in both directions is used, then one runs into the problem (similar to the ground contact issue addressed in the appendix) of having energy stored in the elastic element when the vertical component of the ground reaction force drops to zero. Thus using springs on the bottom of the feet does not easily lead to an energy-free and passive motion.

Passive-dynamic walkers. Some useful yet simple models for studying bipedal walking are unactuated rigid-body models, first studied quantitatively by Tad McGeer [34]. Garcia et al. found that some designs can work on arbitrarily small slopes and that, for these slopes, the power(P) used scales as $P \propto v^4$ where, v is the average forward velocity down a ramp [22, 21]. Thus these machines can have an arbitrarily small specific cost of transport, c_t = energy cost per unit distance traveled per unit weight, but only with the forward speed simultaneously also going to zero. Chatterjee et al. proved that it is not possible for a McGeer-type passive dynamic walker with no upper body to walk with a non-zero speed at a zero slope angle (i.e. across horizontal ground) [10].

Singular-limit of Passive Walking. The essential key to vanishing c_t is vanishing step length. Finite-speed energy-cost-tending-to-zero walking machines can be built by adding an interleg spring with stiffness tending to infinity and thus with step frequency tending to ∞ while step length goes to zero. This does not satisfy our goal, since we seek a model with exactly (rather than in-the-limit) zero

---

[1]The author thanks Dmitry A. Fedin and Dmitriy Leykekhman for their help in translating many sections of this book
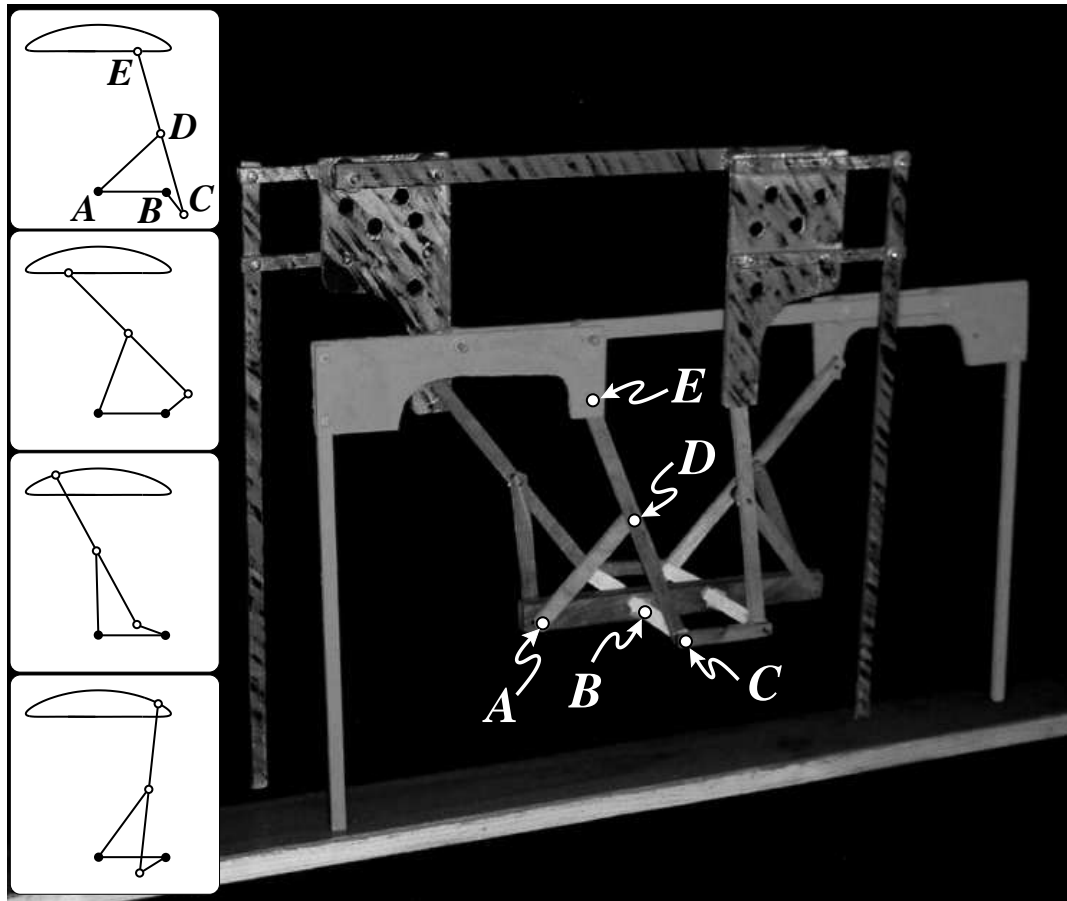
Figure 5.1: Our mockup of the 15-link Chebyshev mechanism of [12]. It is a 4-bar mechanism copied four times. The body or carriage is fixed to AB. One pair of feet is fixed to E. One or the other pair of feet is moving on a nearly-level approximately straight line relative to the body at all times. Chebyshev built a "wheel"-barrow using this mechanism.

energy cost for finite speed walking.

The model. Chatterjee et al. conjectured that a more general passive device could be capable of walking with a non-infinitesimal speed on level ground [10]. Here we verify their prediction by finding solutions for their proposed model which does in fact walk across level ground without collisions and thus with no energy loss.

5.3   Model

The model we use is depicted in Fig. 5.2 [10]. It has two identical leg links and a body link connected to each other via a common hinge joint. Each leg is also connected to the torso by a torsional spring which is relaxed when the machine stands fully upright. Thus, if both legs are at rest and touching the ground (at any angle ϕ), the upper body has an equilibrium position (stable or not stable, depending on parameter values) in the "inverted" vertical position. We assume that our model has perfectly rigid bodies, motion restricted to two dimensions, frictionless hinges, no air resistance, inelastic ground collisions, and infinite friction at ground contacts. An interleg spring could be added to the model, but we did not need that generality to find the desired solutions. Given the above model we, as opposed to all other passive dynamic walking research to date (e.g., [1, 29, 69, 34, 22, 62]), seek walking motions on *level* ground.

The equations of motion for this system consist of three second order, non-linear, coupled, ordinary differential equations. When a foot strikes the ground, angular momentum conservation determines the magnitudes of the discontinuities in each link's angular velocity. To obtain the equations of motion, we use angular momentum balance of: the free leg about the hip, the torso about the hip, and the whole system about the ground contact point (see Fig. 5.2). These are equivalent to writing Lagrange equations using θ_1, θ_2, and θ_3 as generalized coordinates.

The equations of motion can be rearranged in the form: $[M]\ddot{\boldsymbol{\theta}} = \boldsymbol{v}$, where $[M]$ is a 3x3 matrix that depends on the state, $\ddot{\boldsymbol{\theta}}$ is a vector of angular accelerations, $\boldsymbol{v}$ is a vector with gravity terms and terms quadratic in the angular rates. These equations are then formed and integrated numerically. Normally, we would also need to precisely detect the time of impacts between the swing foot and the ground to calculate the links' angular velocities after the collision. However, we do not need to form the collision transition equations explicitly since we are looking for motions which avoid these collisions entirely by having the foot touch the ground at zero velocity.

In previous passive dynamic studies [34, 35, 33, 36, 61, 10, 22, 62], there is not an extended double stance, that is, no non-infinitesimal period of time when both feet of the walker are touching the ground. Although our model is capable of motions with extended double stance, we only looked for solutions where the previous stance leg immediately lifts off of the ground when the swing leg touches the ground. See the appendix for further discussion of this issue.
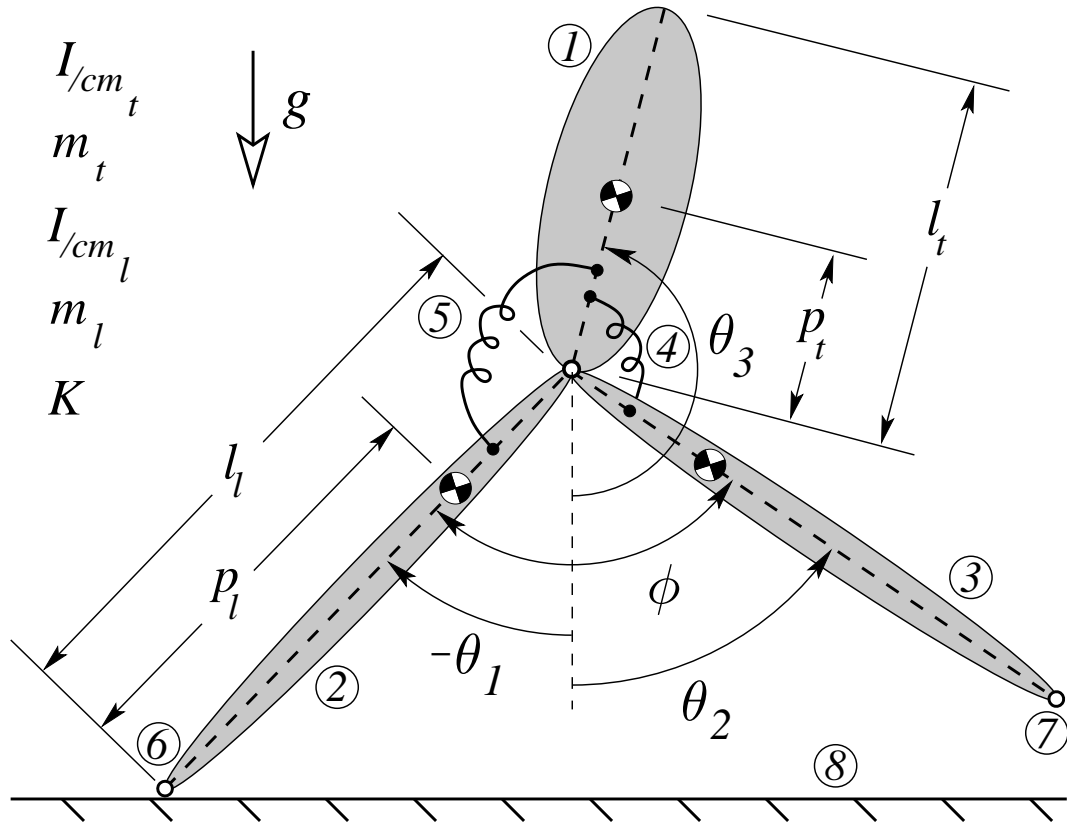
Figure 5.2: Three link walking model with hip springs. Modified from [10] ①torso, ②stance leg, ③swing leg, ④swing leg hip spring, ⑤stance leg hip spring, ⑥stance foot, ⑦swing foot, ⑧ground. Non-geometric parameters are: $I_{/cm_t}$=moment of Inertia of the torso about its center of mass, m_t=mass of the torso, $I_{/cm_l}$=moment of Inertia of the leg about its center of mass, m_l=mass of each leg, K= torsional spring constant. Modified from [10].

5.4 Counting/Symmetry Arguments

Taking the equations of motion and collision-transition equations as defining a map, a periodic motion is equivalent to finding fixed points of that map. We seek motions of the model on level ground which are periodic and thus (by energy balance) collisionless; the swing foot must touch the ground with zero velocity, like the hopping motions in [8]. Are there continuous families of solutions or do we need to modify some of the walker's mass or geometric parameters to find a single solution? To answer this question, we begin by refining, in four steps, a counting argument based on a Poincaré section.

We define our section to be the point in the walking cycle just after the swing leg strikes the ground. The input variables of the map are then, ϕ, θ_3, $\dot\theta_1$, $\dot\theta_2$, and $\dot\theta_3$ at that time. We ignore foot scuffing in the middle of the stride, as in [34, 22], (see appendix for discussion). When both feet are on the ground again, after we do the collision transition, we can describe the state of the system with five numbers, three angular velocities of each link, and two angular positions. In this case our map is $\mathbb{R}^5 \to \mathbb{R}^5$. Because the number of equations equals the number of unknowns, it would not be degenerate to find isolated periodic solutions.

However, since we desire periodic motions that are *collisionless*, our counting argument changes. We must end in a collisionless state, which requires that $\dot\theta_1 = \dot\theta_2 = 0$ (ignoring the singular configuration of "splits" $\phi = 180°$). Our motion must be periodic, so if we end the step with both legs at rest, we must also begin with both legs stationary. The input to our map is now ϕ, θ_3, and $\dot\theta_3$. Since we have no collision at the end of the step we require that the following conditions be met to attain our goal: $\phi^f = \phi^i, \theta_3^f = \theta_3^i, \dot\theta_1^f = 0, \dot\theta_2^f = 0, \dot\theta_3^f = \dot\theta_3^i$, Where the superscript ^{i} refers to the input (initial) value to the map and ^{f} to the output (final) value from the map. So our map is $\mathbb{R}^3 \to \mathbb{R}^5$. All five conditions might only be met by altering not only the three initial conditions, but at least two additional model parameters. For any fixed parameters, a solution is extremely unlikely to exist.

Our system has a time reversal mirror image symmetry which alters the above counting arguments. If we now seek solutions which share this symmetry, our goal changes to become a task of finding an initial condition which results in all three links lining up vertically as shown in Fig. 5.3a. Our map now takes us from the initial state with both legs at rest touching ground (input:ϕ, θ_3, and $\dot\theta_3$) to the point where the stance leg is perpendicular to the ground (condition:$\theta_1 = 0$) (output:θ_2 and θ_3). Thus our new mapping is $\mathbb{R}^3 \to \mathbb{R}^2$ so we should expect a one parameter family of solutions. Fig. 5.3 shows how this modified goal relates to the original goal of finding collisionless periodic motions. Fig. 5.3a show a possible solution to our modified goal. Fig. 5.3b shows the spatially reflected time reversed solution of Fig. 5.3a. Fig. 5.3b will automatically satisfy the equations of motion. The ending state (positions and velocities) of the model in Fig. 5.3a is the starting state of the motion in Fig. 5.3b. Thus we could seamlessly paste together the motions in Fig. 5.3a,b to obtain a collisionless motion which obeys the laws of physics. However, this pasted together solution although collisionless, is not, in general, periodic since
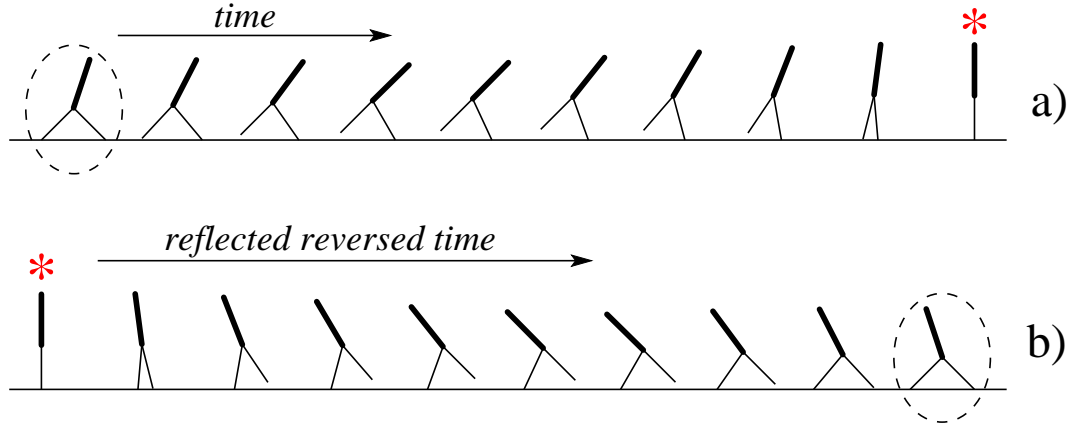
Figure 5.3: Solution for one step that is symmetric about midstance "*" and collisionless but does not extend to a periodic orbit because initial and final conditions are different. a) First half of the motion from double stance to mid-stance. b) Second half of the motion which is a spatial reflection and temporal reversal of (a).

the torso's angular position at the end of the step is not the same as it was in the beginning of the solution.

Finally, we restrict ourselves to sets of initial conditions with the torso perpendicular to the ground. Now our map input is $(\phi, \dot{\theta}_3)$ and the output when $\theta_1 = 0$ is (θ_2, θ_3). The map is $\mathbb{R}^2 \to \mathbb{R}^2$ and it would be non-degenerate to find isolated solutions for a fixed set of walker parameters. To find such solutions, we use a multidimensional numerical root finding algorithm, Newton's method, on this two dimensional map.

5.5   Results/Discussion

Fig. 5.4 shows a periodic collisionless motion. As conjectured from the argument given above, we found this motion by only varying initial conditions and not model parameters. See the appendix for a discussion of foot clearance issues at the beginning of a step.

An unexpected aspect of the solution in Fig. 5.4 is the large number of upper body oscillations per step. We searched for collisionless motions with fewer upper body oscillations, but found that they all violated our restriction that the swing foot should not immediately pass through the ground when weight shift occurs. We found that if the angular velocity of the upper body was larger at weight shift, then the swing foot would lift off the ground. The increased velocity of the upper body, given the parameters that we were using, necessitated that the upper body oscillate with a higher frequency.

Although the motions we found are symmetric, we cannot rule out that pairs of non-symmetric motions may exist for this model. In addition, periodic collisionless
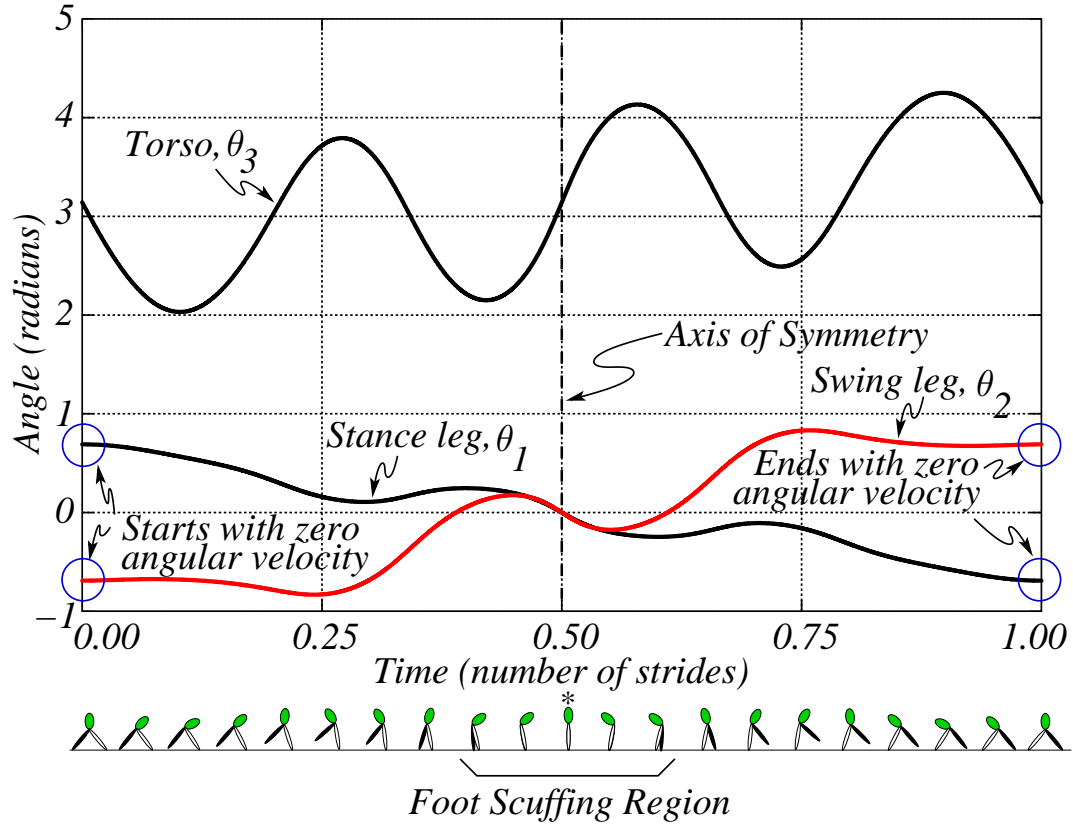
Figure 5.4: A periodic collisionless walking motion using the parameters and initial conditions listed below. The snapshots shown in this figure are spaced evenly in time. The "*" label denotes the mid stride point in the motion about which the whole stride is symmetric. This solution uses in mks units: $l_l = 0.5, m_l = 0.2, p_l = l_l/2 = 0.25, I_{/cm_l} = m_l l_l^2/12 = 0.004166\bar{6}, l_t = 0.3, m_t = 0.14, p_t = l_t/2 = 0.15, I_{/cm_t} = m_t l_t^2/12 = 0.00105, K = 1.5$, and with the initial conditions, the result of the numerical search (after convergence tests), $\phi = 1.380366043$ and $\dot{\theta}_3 = -31.37031936$. The near-coincidence of $\dot{\theta}_1$ and $\dot{\theta}_2$ at the configuration symmetry point ($t = 0.5$) is just, they are not equal.

motions which have a period of extended double stance also seem possible.

Maloiy et al. conjecture that some African women might have developed a technique to achieve a higher than normal efficiency in walking when carrying a load [31]. Perhaps these women coordinate the motions of their load to reduce their collision losses with the ground, thereby reducing their metabolic effort. We have demonstrated the possibility of using internal oscillations as a means of reducing collisional dissipation in forward walking, which can aid in future bipedal robot design and may explain aspects of animal and human coordination patterns while walking.

5.6 Ground Contact Issues

5.6.1 Double Stance.

An obvious parameter to separate double stance from single stance is the vertical component of ground reaction force(R_y) on the stance foot. Generally, the horizontal component of the ground reaction force will not be zero at the same moment that the vertical component is zero. Like McGeer in [37], we found that removing the ground constraint for the stance leg when $R_y = 0$, resulted in the foot accelerating down through the floor, rather than up. This non-intuitive result occurs because for a point on a mechanism, as opposed to an isolated point mass, jumps in force are not generally parallel to the jump in acceleration at the point of force application (in effect the foot has an anisotropic mass e.g. [11]). Our mapping starts as the foot begins its separation from the ground, so an algebraic calculation of the acceleration of the foot can determine if it immediately passes through the floor. We excluded such ground-penetrating-at-lift-off solutions.

5.6.2 Scuffing.

Straight legged walkers in 2D will scuff their feet when walking. "Scuffing" refers to the swing foot passing through the ground when the relative angle between the legs is small. In other passive dynamics research scuffing is ignored, by viewing it as a different decoupled problem (solved by various means: walking on spaced tiles, retracting ankles, or bending knees which minorly affect the leg-swing dynamics).

5.7 Chebyshev Mechanism Details

The walking mechanism that Chebyshev designed is a single degree of freedom device, with a rather complicated kinematic description. The device is a conglomeration of four sets of the simpler four bar-linkage shown (in various positions) in the insets of Figure 5.1. Chebyshev determined values for two link lengths, in the isolated four bar mechanism, that would minimize vertical deviations in the end

point trajectory for a portion of its path. After coupling four of these linkages together to obtain the walking device, the kinematics of the end point relative to the ground have changed since the base point is now moving relative to the ground. This device has many symmetries, one of which is that the two sets of linkage systems (one for each leg-pair) move 180 degrees out of phase with each other. One might think that this symmetry alone would cause the foot to contact the ground with zero velocity, since in the linkage, it appears that the start and finish of the straight line portion of the path is also 180 degrees out of phase. Figure 5.6 shows the position of the end point of the moving foot (with the other leg-pair motionless) for a complete 2π rotation of the central crank (i.e. two consecutive steps). Note that although the foot would go through the ground, we can examine its approach to the floor and see that there is a slight collision when the moving foot makes contact with the ground. This can be seen in the slightly non-zero slope of the vertical position plot when it crosses zero. This small collision would occur if we assume that the central crank arms are moving at a constant angular velocity. If we exercise control over the angular velocity, we could make contact with the floor at zero velocity. This would require that the controller bring the angular velocity of the crank arm to zero at the moment that contact is made (i.e. if $dy/d\theta \neq 0$ but $d\theta/dt = 0$ then $dy/d\theta \cdot d\theta/dt = 0$). I am not sure if it would be possible to choose a suitable set of initial conditions and/or mass and inertia parameters to obtain zero angular velocity of the crankarm when contact is made between the swing foot and the ground.

If the lengths of the links were slightly modified to eliminate this small collision, then this device, once set in motion, would continue to walk without dissipation. This would be true, for any mass distribution of the links and regardless of the initial conditions used.
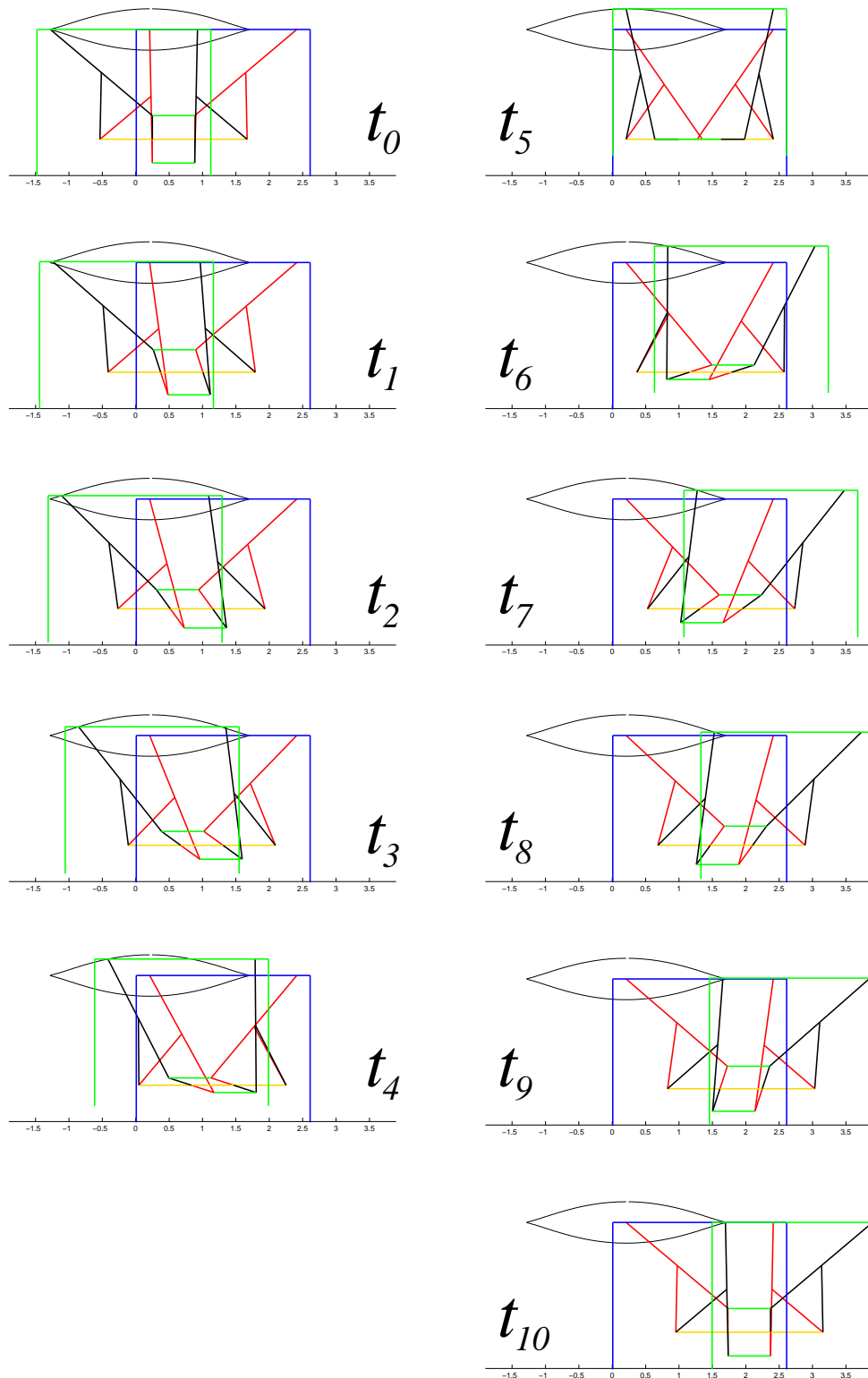
Figure 5.5: Configuration of the Chebyshev walking mechanism where the crank angle is incremented by the same amount in each snapshot. One pair of legs maintains ground contact and the other pair lifts off the ground, moves forward, and contacts the ground again.
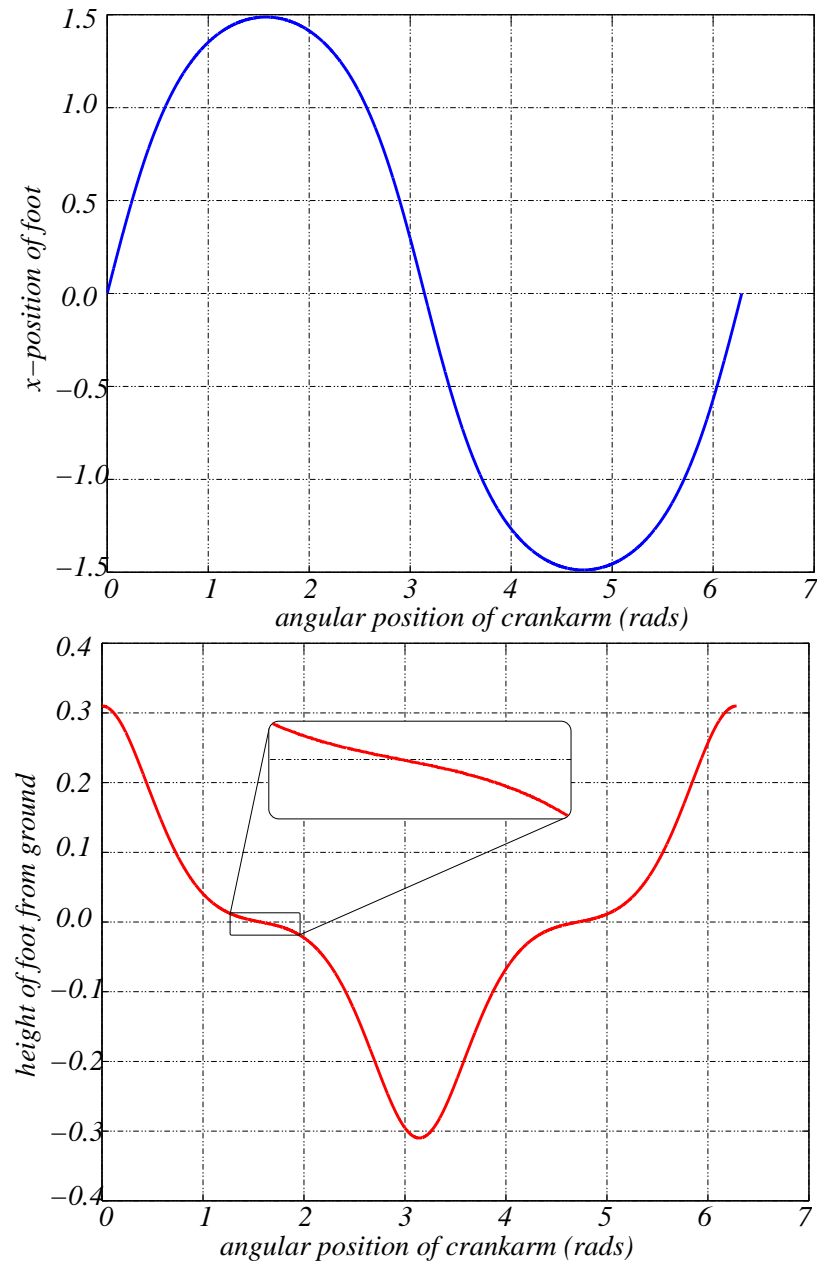
Figure 5.6: Horizontal and vertical position of the moving foot relative to the stance foot for a complete 2π rotation of the central crank arm.

Chapter 6

Continuation Methods

6.1 Introduction

Finding periodic motions in dynamical systems is a common problem whose solution becomes more difficult as the system's degrees of freedom increase. Numerically finding periodic motions in these systems is usually done using an iterative solution algorithm. The search for periodic motions can be transformed into a root finding problem using a map, first done for passive walking models by Hurmuzlu [26]. Most often, the iterative algorithm used to solve the root finding problem is some variant of Newton's method. For convergence to occur quickly or even at all, these methods depend upon having a "reasonable" initial guess that is "close" to an actual root. Some methods for obtaining a "reasonable" guess are: intuition, brute force, and continuation. Familiarity with the system my allow one to make very good guesses, guided by experience and/or intuition, for the locations of the desired roots. Intuition is wonderful, but it can also be unreliable and may fail for many reasons. Intuition is also not suited for comprehensively finding all the roots that exist in a given problem formulation, or perhaps more importantly, the unexpected roots.

Thoroughness is the major advantage of brute force methods. These approaches begin with a gridded portion of the input variable space. Those grid points are then starting guesses for the root-finding algorithm. One can also use a geometrical approach to bound solutions between surfaces [4], but this approach mixes together true roots with surface discontinuities which straddle the zero function value hypersurface. The spacing of the grid is important. A too coarse spacing may result in missed solutions. Of course, a too dense spacing may result in prohibitively long program execution times. As the dimension of the input variable space increases, the number of calculations for a given grid spacing increases as the power of the number of dimensions. Thus as the number of dimensions in the problem increases one must search smaller and smaller regions of input space, or use a coarser and coarser grid spacing to maintain reasonable computing times.

Continuation methods are also used for finding periodic solutions to differential equations [55]. The advantage of continuation methods lies in their ability to

transform a difficult problem into a more tractable one. Starting with the solution to the easier problem, this solution is then followed into the original more difficult problem by changing the continuation parameter. How one chooses to introduce this continuation parameter is often where one's skill in using continuation methods becomes critical. By design, a continuation is done in one-dimension, *i.e.* the object of interest (in this case periodic motions) is tracked as we change a single parameter. However, the number of additional degrees of freedom linked to that one parameter can be greater than or equal to one. One can start with a system that is so simple, that the periodic motion can be found by inspection. Almost any amount of complexity can be introduced by a single continuation parameter. Alternatively, one can concatenate several different continuations beginning the subsequent continuation step with the final system obtained by the previous continuation step. The brachiation models used just such a series of continuations to work toward the final five link brachiation model via a series of continuation steps.

Once a beginning system and ending system has been determined, there are an infinite number of ways to introduce the continuation parameter allowing one to move from one system to the other [55, 73]. Adding the parameter in a fairly random manner to the equations of motion can be done as long as a solution can be found for the starting value of the parameter, and we end up with the desired system at the ending value of the parameter. However, this method can easily introduce difficulties since one does not know if the modified equations admit periodic solutions for all intermediate values of the parameter, especially if there are other conditions to be met (*i.e.* maybe the equations may need to be conservative for a solution to exist). Also, when the differential equations are relatively simple, then one can try many different ways of introducing the continuation parameter at the equation level. Unfortunately, the equations of motion for linked systems of several links are too complex to write down explicitly, even with the use of computer algebra packages[1]. With these complex systems, parameter introduction at the equation level becomes prohibitively difficult and the parameter must be added at the model level. We will examine four different ways to introduce a continuation parameter to an existing model which are all constructed using traditional parts from a mechanic's toolbox (masses, springs, dashpots). Of course, one does not need to use linear elements. One could easily substitute a non-linear spring for a linear one with no extra work in forming the model. This choice will most likely affect the paths connecting desired motions between the two models. The question still remains as to how one can design a coupling element which will lead from the existing solutions that one has for a simpler model to the desired motions in the more complex model. At this point, we are not even sure if a path exists from the simple to the complex model, much less how to have it end at the right point in the complex model. The work in the chapter is limited to examining the use of simple coupling elements to introduce the continuation parameter.

---

[1] *e.g.* Macsyma (Maxima), Maple, Mathematica, . . .

6.2   Periodic orbit existence

We will not discuss existence of periodic orbits in the systems that we will examine in this chapter, but instead will assume that periodic orbits do exist. Instead, the focus for this chapter on the paths which do or do not connect periodic motions in two different but related systems. However, we can be reassured, at least for the linear systems that we examine in this section, that periodic solutions do exist. This is due to the purely imaginary roots of the characteristic equations resulting in all solutions being linear combinations of the normal mode solutions. For more complicated non-linear systems, it is sometimes possible to use either the implicit function theorem or the Brouwer fixed point theorem to show that periodic solutions exist. But, we will simply assume that periodic solutions exist and then try to find them; focusing on the nature of the paths connecting those solutions.

6.3   Path existence

Introducing a continuation parameter to move from one system to another can be done for almost any system. However, one is not guaranteed that a path exists moving from a given periodic motion in one system to a periodic motion in the other system. The proof that the path does not end abruptly, bifurcate, infinitely spiral to a point, or consist of just isolated points involves the implicit function theorem. The basic outline of the path existence theorem requires that one have an implicit formulation for the roots, $H(\boldsymbol{x}, \alpha) = \boldsymbol{0}$. Here $H : \mathbb{R}^{n+1} \to \mathbb{R}^n$ denotes the root finding function as formulated in the appendix, with α denoting the continuation parameter, and x the initial conditions which result in a periodic motion. Using the implicit function theorem, one can state that a single differentiable path will exist if H is continuously differentiable and the Jacobian $H'(y)$ is full rank for every $y \in H^{-1}$. For the linked dynamical systems that are of interest in this research, we cannot write down the solutions to the differential equations, so we have no hope of forming $H(\boldsymbol{x}, \alpha) = \boldsymbol{0}$ much less determining if it's Jacobian is continuously differentiable. We could form it numerically as we follow a path to find bifurcation points or ending points. However, for this research we will end our discussion of path existence and simply assume that a path exists.

Knowing that a path exists is one thing, but determining where it will lead to is another. To guarantee that a path will go from one model to another there are some other arguments that must be made beyond showing that the path does not simple end somewhere in the middle. A well-behaved path could still double back on itself and connect to a different periodic motion in the beginning model. Another problem could be that the path blows up ($x \to \infty$) before reaching the ending model at $\alpha = 1$. These two problems are sketched schematically in Figure 6.1. If only a single periodic orbit exists for $\alpha = 0$, then the path cannot double back and connect to a second periodic orbit in the original model since only one
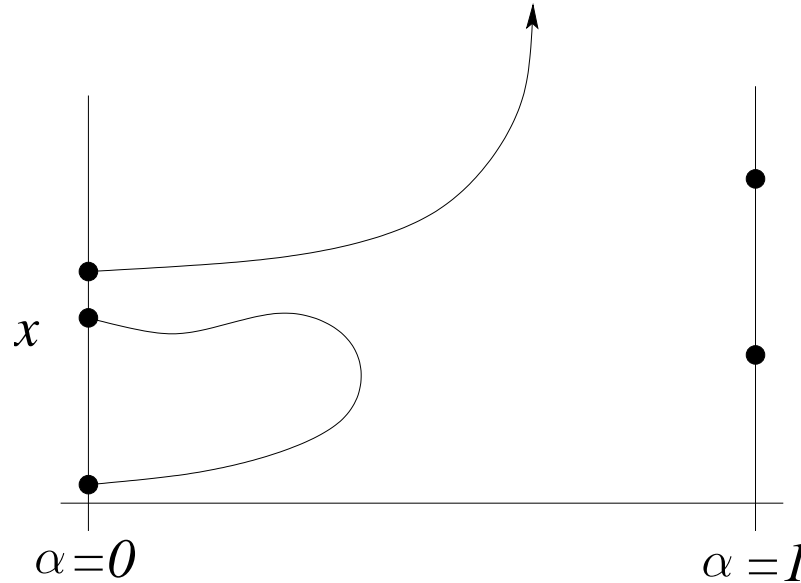
Figure 6.1: Problems that can occur even with the existence of only continuously differentiable path in the continuation. The single continuation parameter is α and x is a variable which represents the periodic motions. The dots at $\alpha = 0$ and $\alpha = 1$ respectively correspond to periodic motions in the simpler and complex model.

exists there and connecting back to the same periodic orbit would violate our earlier determination that the path was continuously differentiable. To guard against a solution blowing up, one must show that solutions to $H(\boldsymbol{x}, \alpha) = \boldsymbol{0}$ are bounded for $0 \leq \alpha \leq 1$. Although we have now defined the major problems that can occur when using a continuation method, we will not attempt to use the criteria given to show the existence of any of these problems in our models. Instead will keep the criteria in mind when we explain the numeric results when we apply our continuation methods to our models.

Having outlined what is involved in determining if a path exists connecting a periodic motion from a simple model to a periodic motion in the more complex model, we can see how these criteria would be applied to the specific cases of interest, linked rigid-body models. Since our differential equations can be very complicated (*i.e.* too lengthy to even write down explicitly) and are non-linear, it is impossible to find an analytic solution to them. This is the largest difficulty posed by the problem when taking a analytic approach to solving it. If we ignore that difficulty and assume that for a given problem we have an explicit solution $(\boldsymbol{x}(t))$ to the differential equations, we would then need to proceed in the following manner. First, we would need to form our requirements for a periodic collisionless motion for a given Poincaré section (in this work we chose to find a symmetric motion which, by construction, would be a periodic collisionless motion). For example, for the two link brachia-tor's continuous contact motions (see chapter

2 starting each motion with $\theta_1 = \theta_2 = 0$, we required two conditions to be met when $\dot{\theta}_1(t^*) = 0$ (our Poincaré section) (1) $\dot{\theta}_2(t^*) = 0$ and (2) $y_{\text{hand}}(t^*) = 0$. Note that the equation determining the Poincaré section ($\dot{\theta}_1(t^*) = 0$) also requires and additional integer value to be assigned (the number of times we cross the surface of intersection before we evaluate the map, *i.e.* we want our two conditions to be met when $\dot{\theta}_1 = 0$ for the second time since the starting state). Using the conditions for periodic motions, the analytic solution to the ODEs, and the equation defining the Poincaré map, we would then solve that set of nonlinear equations for the periodic solutions, which in our example would be, $\dot{\theta}_1(0)$, $\dot{\theta}_2(0)$, and t^*(the time when we evaluate our map). It is apparent that even if one has an explicit expression for the solution to the non-linear ODEs, determining the initial conditions which result in a periodic motion is still non-trivial. Since we do not have the solutions to the ODEs we carry out each of the above steps using numerical approximations.

There are several way to execute a continuation numerically. One aspect has to do with numerically approximating the solution to the set of ODEs. Since the the results of the approximate solution for the base upon which the continuation is done, the numerical issues involved it the approximation do play a role in the results given by the continuation method. However, for the sake of clarity, we will view the whole numerical integration procedure as a black box in order to briefly explain the numerical continuation procedures.

6.4   Adding degrees of freedom

The continuation methods in this chapter are all designed to add degrees of freedom to an existing simpler model. Adding degrees of freedom (DOF's) to a rigid-body model is usually considered a discrete processes, but by using a specially designed continuation method, we have made it a smooth process. The four methods presented in this chapter allow one or more degrees of freedom to be added to a model in a continuous manner. These four methods divide naturally into two categories, those which tend to initially couple the dynamics of the additional degree(s) of freedom to the existing model (spring, damper, and inertia/mass coupling), and those whose additional degree(s)-of-freedom dynamics are initially uncoupled from the existing model (connection of a new link at its center of mass).

The coupling methods all share the common idea of viewing kinematic constraint as the limiting case of a coupling parameter going to a zero or infinite value. The methods then relax the rotational constraint of welded joints, becoming hinge joints in a continuous constraint-dissolving process. Spring and damper coupling, although intuitive, lead to stiff differential equations and their associated numerical accuracy problems which we will discuss in more detail in section 6.6.5.

A simple two-link continuous-contact brachiation model is used to demonstrate each the coupling methods. This example also demonstrates that using damping coupling for conservative systems will not result in periodic solutions for the intermediate values of the continuation parameter. Lastly, we demonstrate the in-

ertia/mass coupling method for a more complicated 5 link brachiation model and show the resulting periodic motion. The last example shows that one's definition of a surface of section used in the model can cause the continuation path to end prematurely.

Since we are usually not interested in the solutions for intermediate values of the continuation parameter, these methods fall into the general category of homotopy. We will discuss when the methods that we examine can be used to obtain periodic solutions for intermediate values of the continuation parameter, and when they can not for our sample brachiation model as well as for a general passive linked model.

6.5   Previous Work

Using continuation methods to find periodic motions is common practice [55, 73]. But usually this is done within a given fixed dimension of state space for all values of the continuation parameter. One good example of this is given by Rand and Ramani [49] where a nonholonomic constraint by fins on a submerged supercavitating underwater projectile is gradually enforced via a scaled constraint force which ranges from 0 (no constraint) to 1 (pure no-slip nonholonomic constraint). The class of continuation methods that we present here are unique in that they are designed to increase the order of the differential equations that are being solved, taking us from a passive linked system with fewer links into one with more links. The idea of using continuation to move from a lower dimensional system to a higher dimensional one is also not new. Meyer [39] used a continuation method to move from the restricted three-body problem to the reduced three-body problem.

The idea of continuously relaxing a constraint to move smoothly from one system to another is not a new idea. One example of this comes from classical beam theory, where one can move from a beam supported by built-in supports to pin supports [63]. In this example, the built-in support is modeled as a leaf spring of very high stiffness and this spring constant is smoothly decreased down to zero stiffness, resulting in a pin joint support. Although, this particular examples does not increase the dimension of the system being examined, it is a very good example of the spring coupling examined in section 6.6.1. The use of stiff springs as a proxy for a rigid constraint is not new, but we believe that the idea of using damping and mass/inertia coupling are new. Borzova and Hurmuzlu [6] have, independently, used the uncoupled method presented here, to add a torso to a passive walking model.

6.6   Method descriptions and possible problems

Here, we describe each previously mentioned continuation method in more detail and discuss the existence of singularities in a simple representative example using a rigid body pendulum. The existence of singularities for certain values of the

continuation parameter may invalidate the use of that method to track periodic motions depending on where those singularities are located. For the simple examples presented in this section, we start with a single rigid body pendulum and transform it into a double pendulum using the continuation method being examined. The non-linear equations of motion are then linearized about the straight down equilibrium point $(\theta_1 = \theta_2 = \dot{\theta}_1 = \dot{\theta}_2 = 0)$. The linear equations are then examined for singularities. Each link in the double pendulum is a homogeneous line with mass=m, length=l, center of mass location at l/2 from either end, moment of inertia about the center of mass $(I_{cm}) = (1/12)ml^2$, and spring constant $= (1/\epsilon)mgl$. We use m, l, and $\sqrt{(l/g)}$ to non-dimensionalize the equations.

6.6.1 Spring Coupling

This method uses a stiff spring as a proxy for a welded joint. To add a degree of freedom to an existing model: break a link in the existing system into two pieces, join those two pieces at the break with a frictionless hinge, place a torsional spring of infinite stiffness at the joint where the ends of the spring are connected to each link, and then relax the stiffness of that spring while tracking the original periodic motion. If the torsional spring has infinite stiffness, the two links are then as rigidly connected as two halves of a single rigid link. If the torsional spring stiffness drops to zero then the two links are free to rotate relative to each other and are only constrained in their relative position by the pin joint.

As an example system to explore singularities in this method, we take a rigid body pendulum and transform it into a double pendulum. This system, after the break, is depicted in Figure 6.2. We obtain the equivalent single rigid body system when $k = \infty$. Our desired system is obtained when $k = 0$. This system is conservative for all values of ϵ which is a necessary requirement for the existence of periodic solutions. The linearized non-dimensional equations of motion are:

$$\begin{pmatrix} \theta_1'' \\ \theta_2'' \end{pmatrix} = \frac{1}{7\epsilon} \begin{bmatrix} -18\epsilon - 30 & 9\epsilon + 30 \\ 27\epsilon + 66 & -24\epsilon - 66 \end{bmatrix} \begin{pmatrix} \theta_1 \\ \theta_2 \end{pmatrix} \tag{6.1}$$

The frequencies of oscillation for the two normal modes of this system are:

$$-\omega_1^2 = -\frac{6\sqrt{(7\epsilon^2 + 42\epsilon + 64)} + 21\epsilon + 48}{7\epsilon} \tag{6.2}$$

$$-\omega_2^2 = \frac{6\sqrt{(7\epsilon^2 + 42\epsilon + 64)} - 21\epsilon - 48}{7\epsilon} \tag{6.3}$$

$$\tag{6.4}$$

The frequencies of oscillation as the spring stiffness approaches infinity or as $\epsilon \to 0$ are: $\omega_1 = \infty$ and $\omega_2 = \sqrt{(3/4)}$. As we expect, the frequencies of the two linear normal modes as the stiffness approaches zero or $\epsilon \to \infty$ are $lim_{\epsilon \to \infty} - \omega_1^2 = (-6\sqrt{7} - 21)/7$ and $lim_{\epsilon \to \infty} - \omega_2^2 = (6\sqrt{7} - 21)/7$. We have found the main problem with this method. As soon as the spring constant drops from
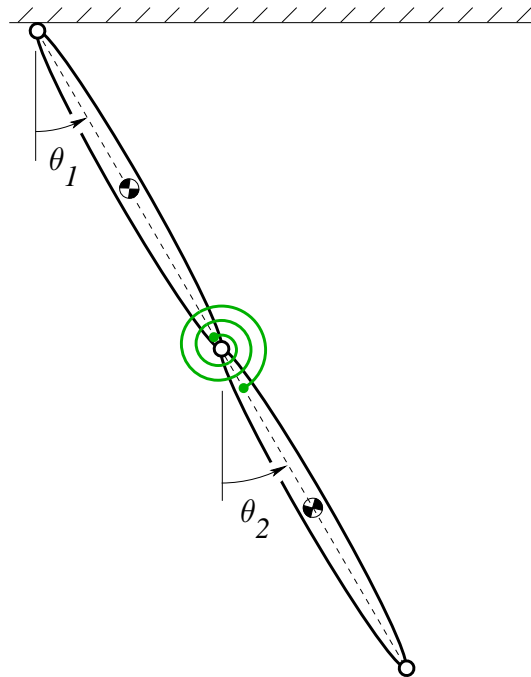
Figure 6.2: Rigid body pendulum split into two separate bodies and connected via a hinge and a torsional spring. This is the intermediate system for the *spring coupling* method of adding a degree of freedom.

infinity to a large finite value, the equations of motion for the system become stiff and it becomes difficult to obtain a reasonably accurate numerical approximation to their solution. However, implicit integration routines such as the Backwards differentiation formulas of 6th order and less can give very good results for stiff equations. These results of this class of integration routines for these problems will be discuss in section 6.6.5.

6.6.2   Damper Coupling

When breaking a link in two one could also couple the two links via a dashpot with a large damping coefficient. The dashpot would provide a torque, resisting relative motion, on each link in proportion to the links' relative angular velocity. Also, the dashpot would, like the spring, tend to move the two links together as one for large values of the damping coefficient. This method is advantageous because we do not have the problem of very high frequency oscillations that the stiff spring has. However, a dashpot will dissipate energy, so energy must be injected into the system in order for periodic orbits to exist. For energy conservative motions like the collisionless motions found in the brachiation and walking models discussed in chapters 2 and 5 respectively, this method will not result in periodic motions for intermediate values of the continuation parameter. For extreme values of the damping coefficient (0 and ∞) the system will conserve energy. It might be possible to modify the system to couple some sort or energy injection system to the value of the continuation parameter (i.e. letting it move down a ramp). Although, this approach may work, it seems unnecessarily cumbersome for the goal that it achieves (periodic motions for all intermediate values of ϵ). The coupling of the continuation parameter with an energy injection system is not required for a system which is already dissipative and has energy injection, such as passive walkers walking down a ramp.

However, if we disregard our wish for periodic motions as solutions to the map equations for intermediate values of the continuation parameter, we can use this method as a homotopy. In this way, we accept that solutions to the map equations will not, in general, be symmetric or periodic except for extreme values of the continuation parameter. Note that all solutions will still satisfy our homotopy function.

For very large values of the damping coefficient, we again have a time scale issue in our solutions. Because of the large damping coefficient relative motion between the two bodies will damp out extremely fast, but the whole system's motion (connected to the support) has no damping and will tend to move at a slower time scale. As we shall see in section 6.6.5, having two widely varying time scales in our solutions is normally a symptom of a set of stiff differential equations. In this case, we shall see that large damping coefficients do not cause us the normal difficulties normally encountered when dealing with stiff ODEs.
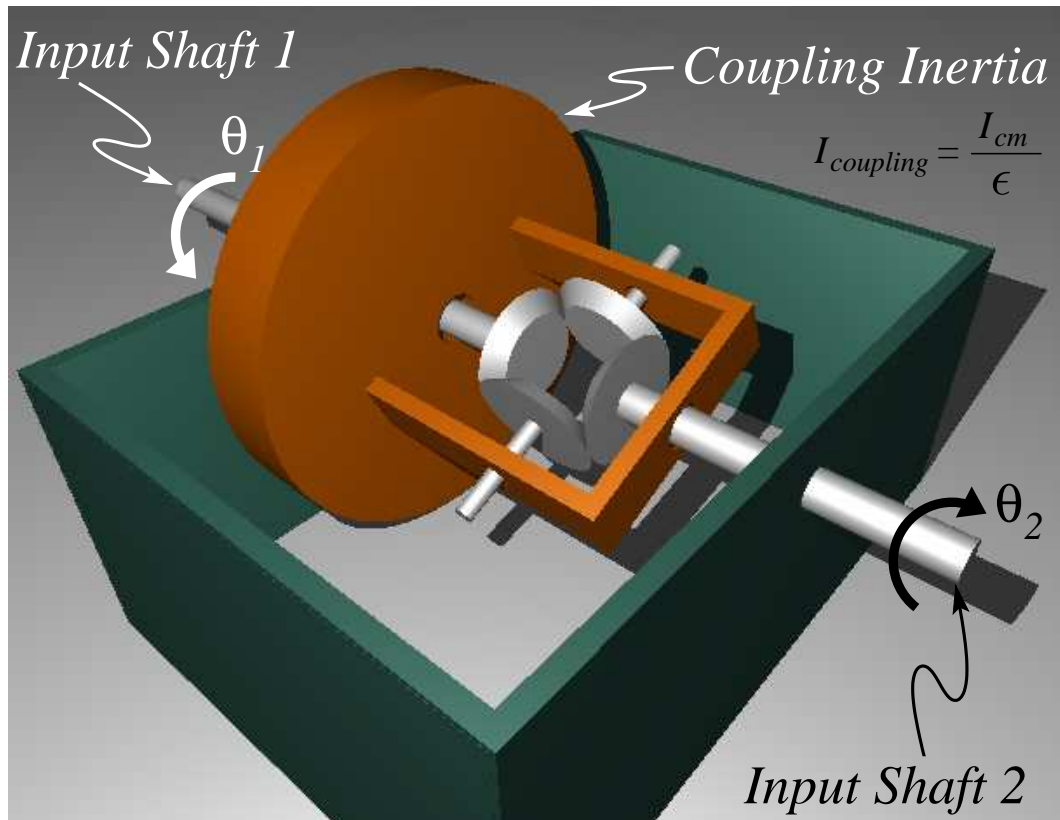
Figure 6.3: Mechanical differential used to couple the motion of the two link segments via a large rotary inertia. The large wheel is the *coupling inertia* and the two input shafts are connected to the two links via some rotational connection (e.g. speedometer cables, pulleys leading to a mutual axis, ...). The inertia is kinematically coupled to the motion of the two links. If $\dot{\theta}_1 = \dot{\theta}_2$ then the differential mechanism causes the inertia to be stationary.

6.6.3 Inertial Coupling

Here, we examine a method for coupling the motion of the two split links with an inertia that tends to resist relative motion of the two links. A mechanical differential is the physical interpretation of such a term in the equations of motion. The coupling inertia is attached to what would normally be the "input" shaft of the automobile differential and the two "output" shafts which would normally go to the tires, are now attached to each of the two half links. Figure 6.3 depicts the the basic parts of a differential with labels as to which shafts are connected to which half links.

If the inertia which couples the two half links is large then the amount of relative motion between the two links will tend to persist. If the relative motion is zero then the inertia will tend to cause the two links to move as a single link.

The mass of the coupling inertia can be made arbitrarily low by use of a transmission or large radius. If the mechanism needs to be place on the moving device, the center of mass of the large inertia can be placed at the center of mass of a link, uncoupling the large inertia's dynamics from the rest of the system. The mass of the large inertia can be made arbitrarily small by the use of a transmission or large radius. In some cases the mechanism can be stationary by using speedometer cables to couple the the rotary motion of the links to the input shafts, or by using pulleys to bring the motion of the links to a common non-translating shaft.

Unlike spring coupling, this method does not introduce high frequency oscillations when the continuation parameter is slightly perturbed from its initial value (∞). The differential mechanism applies a torque on each link that is equal and in opposite directions. The magnitude of the torque applied is equal to $I_{coupling}(\ddot{\theta}_2 - \ddot{\theta}_1)/4$, where $I_{coupling}$ is the moment of inertia of the coupling inertia about its center of mass in the direction of its axis of rotation, where $I_{coupling} = I_{cm}/\epsilon$. The non-dimensional linearized equations of motion are:

$$\begin{pmatrix} \theta_1'' \\ \theta_2'' \end{pmatrix} = \frac{1}{56\epsilon + 16} \begin{bmatrix} -144\epsilon - 9 & 72\epsilon - 3 \\ 216\epsilon - 9 & -192\epsilon - 3 \end{bmatrix} \begin{pmatrix} \theta_1 \\ \theta_2 \end{pmatrix} \tag{6.5}$$

The frequencies of oscillation for the two normal modes of this system are:

$$-\omega_1^2 = -\frac{3\sqrt{(448\epsilon^2 - 40\epsilon + 1)} + 84\epsilon + 3}{28\epsilon + 8} \tag{6.6}$$

$$-\omega_2^2 = \frac{3\sqrt{(448\epsilon^2 - 40\epsilon + 1)} - 84\epsilon - 3}{28\epsilon + 8} \tag{6.7}$$

$$\tag{6.8}$$

As can be seen from the above equations, the frequencies of the two normal modes remain bounded as the moment of inertia of the rotary inertia approaches infinity (as $\epsilon \to 0$). Specifically $lim_{\epsilon \to 0}\omega_1 = \sqrt{3/4}$ and $lim_{\epsilon \to 0}\omega_2 = 0$. Again, this method is useful since the perturbation does not introduce high frequency oscillations. Note that the frequencies of oscillation for $\epsilon \to 0$ should not be the same as for the previous system with $\epsilon = 0$ since the two systems are different.

As we expect, the frequencies of the two linear normal modes as the rotary inertia approaches zero inertia or $\epsilon \to \infty$ are the same as in the previous method we reached the end of the continuation procedure with $\epsilon = 1/2$. The two frequencies for this system at the end of the procedure are: $lim_{\epsilon \to \infty} - \omega_1^2 = (-6\sqrt{7} - 21)/7$ and $lim_{\epsilon \to \infty} - \omega_2^2 = (6\sqrt{7} - 21)/7$.

If for a given motion, the integral of the torque on the inertia is not zero then the two links which originally started at zero relative velocity will end up with a nonzero relative angular velocity. This will not result in a periodic motion. However, in general this will not be the case unless there is a periodic motion which has a particular torque history on the link for half the motion and the exact same torque history of opposite sign on the inertia for the other half of the motion. But the collisionless periodic motions have exactly this symmetry, so the method
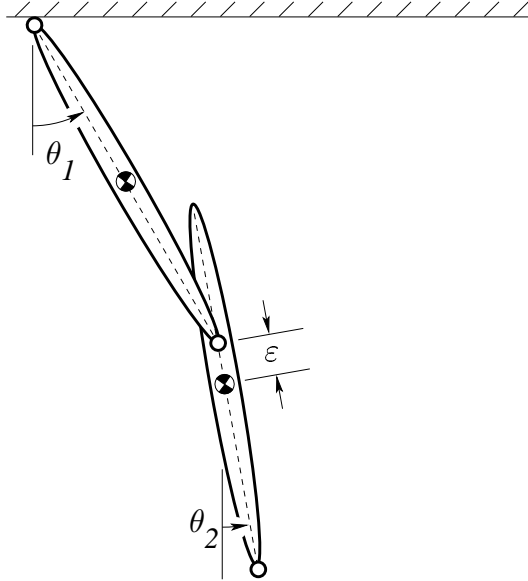
Figure 6.4: Rigid body pendulum with additional link added at it's center of mass.

should work perfectly, and it does. This method could be modified to work for systems which do not have this symmetry. The hinge point could be moved to a point where the integral of the torque on the rotary inertia is zero. Although, one does not know a priori where that point will be, it could be found as part of the numerical root finding procedure.

For realistic values of the continuation parameter (*i.e.* positive values of coupling inertia) the differential equations will not be stiff and we do not have to concern ourselves with special methods for integrating them with high (near ∞) or low (near 0) values of coupling inertia. Note that for negative values of coupling inertia, we will have stiff equations for some intermediate values. Again, implicit integration routines will help in these cases, please see the section on stiffness in this chapter for a further discussion (section 6.6.5).

6.6.4 Adding a link at its center of mass

We now examine a method for adding a link without affecting the solutions and without introducing high frequency oscillations when the parameter is varied.

As an example system to apply this method, let's take a rigid body pendulum and add to it a link at the end of the first link. This system, after the addition, is depicted in Figure 6.4.

We obtain the equivalent single rigid body system when $\epsilon = 0$. Our desired system is obtained when $\epsilon = 1/2$. This system is conservative for any value of ϵ, which is a necessary requirement for the existence of periodic solutions as Lets now examine what happens as we change ϵ. We again linearize the equations
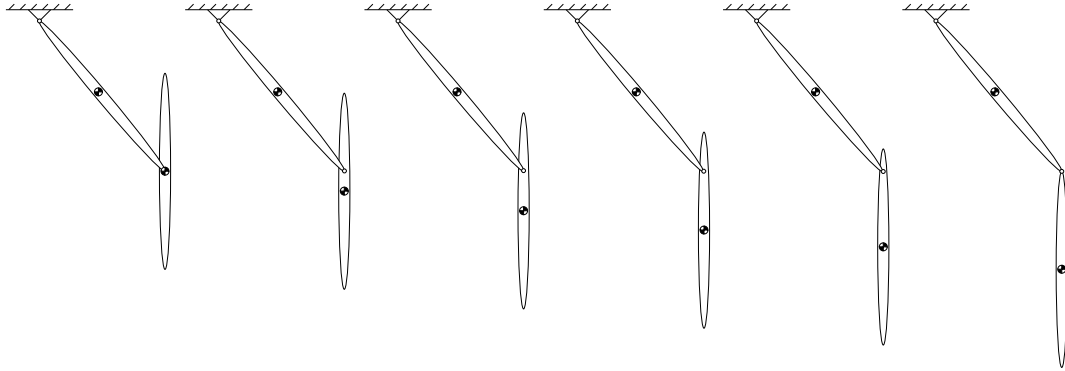
Figure 6.5: Diagram showing the procedure for moving the pivot point from the center of mass of the added link to the desired location.

of motion about the straight down equilibrium point ($\theta_1 = \theta_2 = \dot{\theta}_1 = \dot{\theta}_2 = 0$). In this example, each link has mass=m, length=l, and moment of inertia about the center of mass $= 1/12ml^2$. The equations are non-dimensionalized, where ($'$) denotes differentiation with respect to non-dimensional time ($\tau = t\sqrt{g/l}$). Note that Borzova and Hurmuzlu [6], independent of this work, found periodic motions of a walking mechanism by adding a torso using a similar procedure as described in the section.

$$\begin{pmatrix} \theta_1'' \\ \theta_2'' \end{pmatrix} = \frac{1}{3\epsilon^2 + 1} \begin{bmatrix} (108\epsilon^2 - 9)/8 & 9\epsilon^2 \\ 27\epsilon/2 & -12\epsilon \end{bmatrix} \begin{pmatrix} \theta_1 \\ \theta_2 \end{pmatrix} \tag{6.9}$$

The eigenvalues of the above matrix are both negative for the range of ϵ that we are interested in. Thus the frequencies of oscillation for the two normal modes of this system are:

$$-\omega_1^2 = -\frac{3\sqrt{(1296\epsilon^4 + 1152\epsilon^3 + 1240\epsilon^2 - 192\epsilon + 9)} + 108\epsilon^2 + 96\epsilon + 9}{48\epsilon^2 + 16} \tag{6.10}$$

$$-\omega_2^2 = \frac{3\sqrt{(1296\epsilon^4 + 1152\epsilon^3 + 1240\epsilon^2 - 192\epsilon + 9)} - 108\epsilon^2 - 96\epsilon - 9}{48\epsilon^2 + 16} \tag{6.11}$$

As can be seen from the above equations, the frequencies of the two normal modes remain bounded at $\epsilon = 0$. Specifically $\omega_1 = 3/\sqrt{8}$ and $\omega_2 = 0$. This is the result that we desire. This perturbation to the equations of motion do not introduce high frequency oscillations.

As we expect, the frequencies of the two linear normal modes at $\epsilon = 1/2$ and we have the double pendulum system, we have. $-\omega_1^2 = (-6\sqrt{7} - 21)/7$ and $-\omega_2^2 = (6\sqrt{7} - 21)/7$.

6.6.5 Stiffness

Some values of the continuation parameter will result in *stiff* equations. In differential equations, stiffness is an imprecise term. Cleve Moler, chairman and co-founder

of MathWorks[2] gave the following description: "A stiff problem is not unstable, or ill-conditioned, or even difficult to solve; it justs takes classic Runge-Kutta or Adams methods an impossibly long time to achieve reasonable accuracy"[40]. Trefethen, in [64], gives some general criteria that one can use to determine of a set of differential equations are stiff or not. A strict mathematical definition of stiffness does not yet exist. Trefethen in [64] states that a stiff ODE usually exhibits the following three symptoms:

> 1) The problem contains widely varying time scales.
> 2) Stability is more of a constraint on [step size] than accuracy.
> 3) Explicit methods don't work.

In 1952, Curtiss and Hirschfelder [16] first identified and named the concept of stiff equations and also gave a method for solving them (backwards euler, a first order implicit backwards-differentiation method). The behavior of implicit integration routines is quite surprising to someone who has only experimented with integration routines with bounded stability regions. Sand and Østerby have compiled stability region plots for many integration methods of varying order in [52]. Not all implicit methods have unbounded stability regions. For example, the implicit linear multistep methods of Adams-Moulton (3rd order and above) have bounded stability regions. The family of implicit Backward Differentiation Formula methods of 6th order and less have unbounded stability regions, making them very useful for the numerical integration of stiff equations. Methods which have stability regions which include the entire left half plane are known as A-stable methods [64]. All A-stable methods must be implicit but not all implicit methods are A-stable [59].

As with bounded-stability methods, a method with an unbounded-stability region generally converges to the actual solution with decreasing stepsize. However, since no integration method has a stability region which covers the entire complex plane, there are usually some step-size values which will result in unbounded solutions.

Figures 6.7 and 6.8 show the results of the simplest explicit[3] and implicit[4] methods applied to the simple linear two mass, two spring model depicted in Figure 6.6.

When the stiffness is infinite, and we obtain the simpler reduced degree of freedom model, we begin with a low frequency motion. This low frequency motion is what we'd like to find when we change the coupling spring stiffness to a finite but very large value, which gives a set of very stiff differential equations). If, in the physical system, our state is not exactly on this slowly oscillating motion, we will excite very high frequency oscillations around that slowing varying solution.

---

[2] publisher of the popular commercial software MATLAB
[3] Euler's method
[4] Backward Euler's method
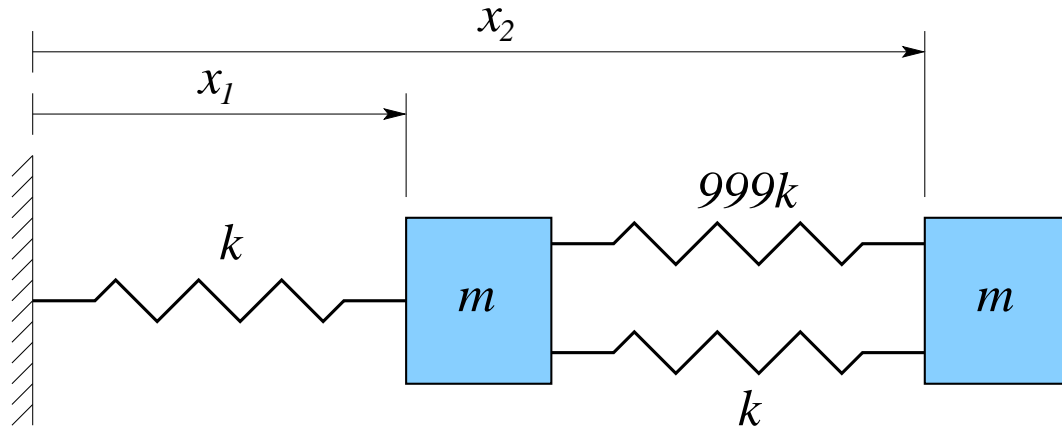
Figure 6.6: Simple two mass, two spring linear model with m=1 and k=1. Approximate numeric solutions for $X_1(t)$, with step sizes that have been chosen to be too large so as to give very non-accurate solutions, are given in figures 6.7 and 6.8 for the following initial conditions: $X_1(0) = 0.9, X_2(0) = 1.1, \dot{X}_1 = 0, \dot{X}_2 = 0$. The reason for giving highly non-accurate solutions is discussed in the text.

As the equations increase in stiffness, approaching the starting system which has a system of ODEs with "infinite" stiffness, the integration step size required to get an accurate solution must continually decrease and the time needed to form an accurate approximate solution must increase. There is a limit to the accuracy that can be obtained using numerical integration. One cannot continually obtain more and more accuracy using smaller and smaller step sizes. At some point, no matter what the order of the integration routine one is using, cumulative numerical roundoff error begins to dominate, and the amount of error will begin to rise again for smaller step sizes. Non-accurate, unstable, explicit methods are not helpful in finding the solutions that we seek. Note that this is true regardless of the stiffness of the differential equations that one in integrating. However, this problem become very noticeable for stiff equations since one must use very small step sizes to obtain a reasonable, if not accurate, solution. If the true mathematical solution which satisfies both the differential equations and initial conditions has high frequency oscillations, then an integration step-size that is smaller than the scale of those oscillations is required for an accurate solution. It might be possible that, for the same differential equations, there may exist a set of initial conditions whose resulting motion does not have these high frequency motions. The small amount of error which will exist for any numerical approximation, will excite those oscillations if one is using a explicit method. Implicit methods will not excite those oscillations, and this is the main advantage of these methods. To examine the behavior of these two types of methods on a concrete example, we apply the simplest explicit and implicit methods to a simple two mass-spring system and discuss their results.
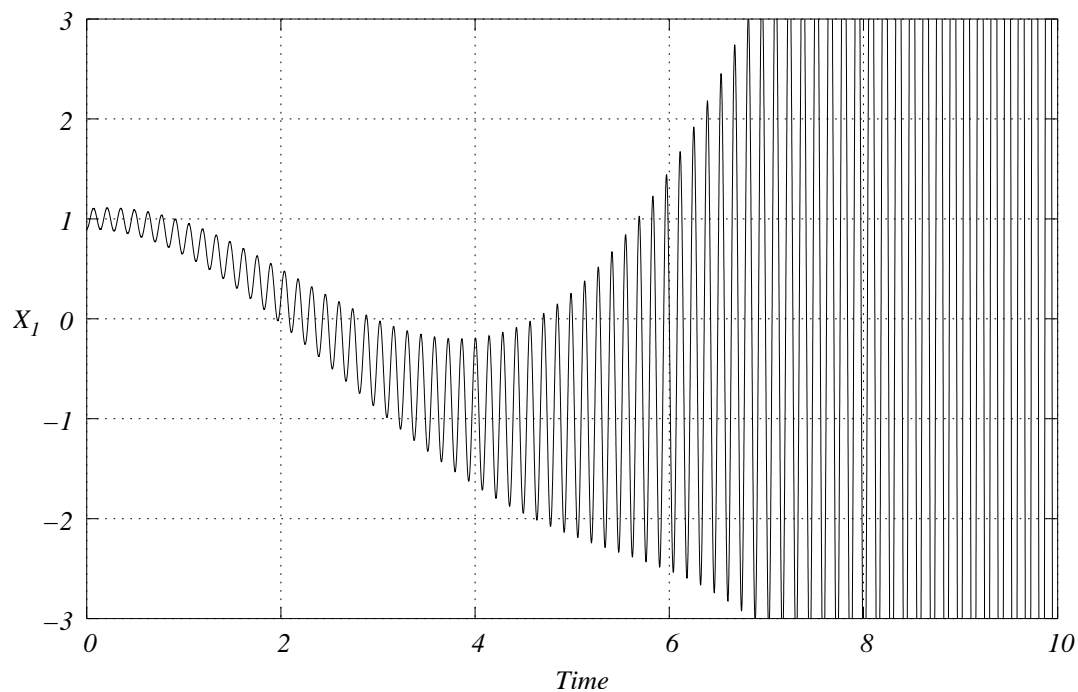
Figure 6.7: An inaccurate numerical solution of the linear two mass-spring system with stiff coupling spring, as shown in Figure 6.6. The "solution" was obtained by numerically integrating using the explicit Euler's method with a constant integration step size of 0.0005. Smaller step sizes delay the growth of the large amplitude, high frequency oscillations and give a more accurate solution for the given initial conditions. Since the eigenvalues of the matrix defining the ODEs are purely imaginary and the stability region for Euler's method does not include any portion of the imaginary axis, no step step size exists for this method which will result in a bounded numerical solution.
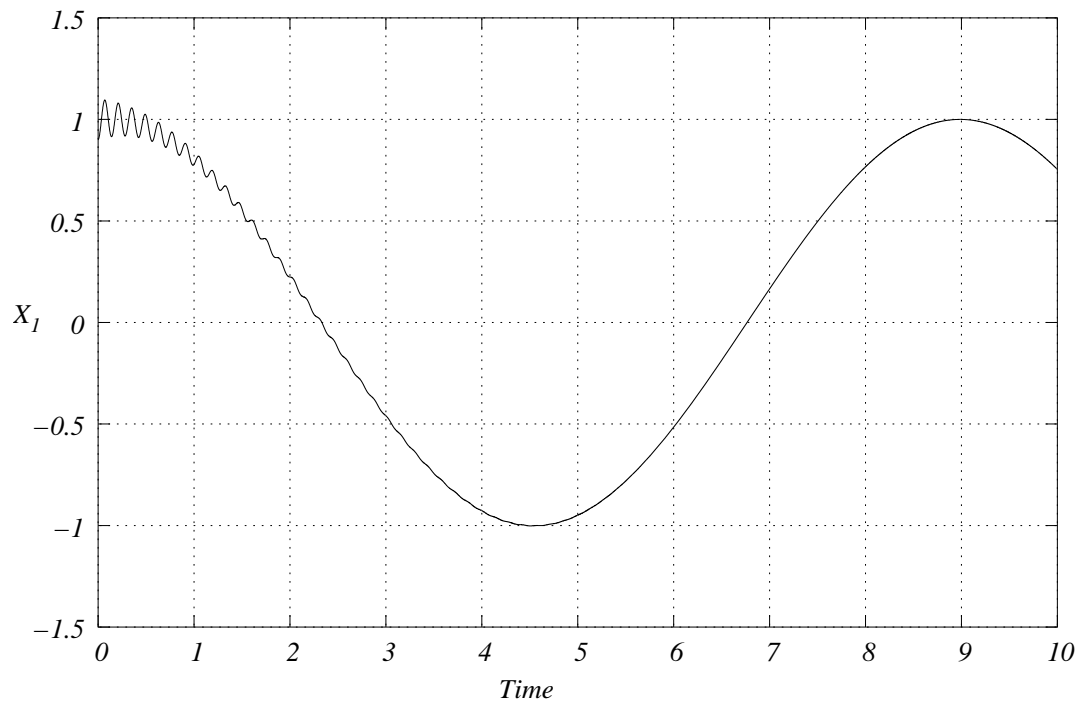
Figure 6.8: Inaccurate numerical solution for the two mass model with stiff coupling spring shown in Figure 6.6. This "solution" was obtained by numerical integration using the implicit backward Euler's method with a constant integration step size of 0.001. Smaller step sizes will increase the duration of the initial oscillations, converging closer and closer to the real solution. Since the eigenvalues of the matrix defining the ODEs are purely imaginary and the stability region for Euler's method includes the entire imaginary axis, the numeric solution will remain bounded for any choice step-size no matter how large.

For both of the numerical experiments, we begin with initial conditions which are not on the desired periodic motion. If we started with initial conditions which were exactly on the desired periodic motion, the errors which are inherent in numerical integration would cause the state of the system to be slightly off in the next time step. Thus we will always have to deal with some numerical error in the current state. Unstable methods will cause this error to grow. An argument can be made to reduce this error by simply decreasing the integration step size for the integration process, or to use a higher order integration method. This will work, but only to a point. As the coupling spring gets stiffer and stiffer (and the ODEs get stiffer and stiffer) the stability problems will get worse and worse no matter what step size or order we use for the explicit method.

The implicit methods reduce the magnitude of the high frequency motion and find the slowly moving solution that exists in the system. As the equations get stiffer and stiffer, the rate at which the implicit methods squash the high frequency motion increase. This behavior is what makes the implicit integration methods so ideally suited for finding the low frequency periodic motions in stiff sets of differential equations. Thus, implicit integration routines with unbounded stability regions (such as backwards euler or the family of backward differentiation formula of order 6 or less) or implicit Runge-Kutta methods are very appropriate for use for the region of parameter values where the equations are stiff [64, 56, 57].

Having now discussed stiff ODEs and how to effectively deal with them, we can discuss whether large values of the damper coupling result in stiff ODEs. The eigenvalues for the linear two mass/spring/dashpot system are all complex with negative real parts. This means that any oscillation will eventually decay to the equilibrium position (zero). For large positive values of the damping coefficient, the eigenvalues of the solutions will remain in the left half plane. Thus, any explicit integration routine whose stability region includes the left half plane can be used and will give stable results. Larger and larger damping coefficients will push the eigenvalues further away from the origin, so even routines like fourth order Runge-Kutta, which includes a small portion of the left half plane near the origin, can be used without stability problems.

Although stiff equations which may arise for some values of the continuation parameters pose difficulties with accurate numerical integration, implicit integration routines can be used to circumvent these problems. The implicit routines are ideally suited for our searches since they pick out the slowly varying solutions that we seek in the set of stiff ODEs.

6.7   Linear Analogues

It is interesting to modify the procedures given above to a linear, instead of rotational, system. Again, we focus solely on a representative two degree-of-freedom linear system. The stiff spring and highly damped damper methods readily suggest a linear analogue consisting of two masses connected to each other with a stiff
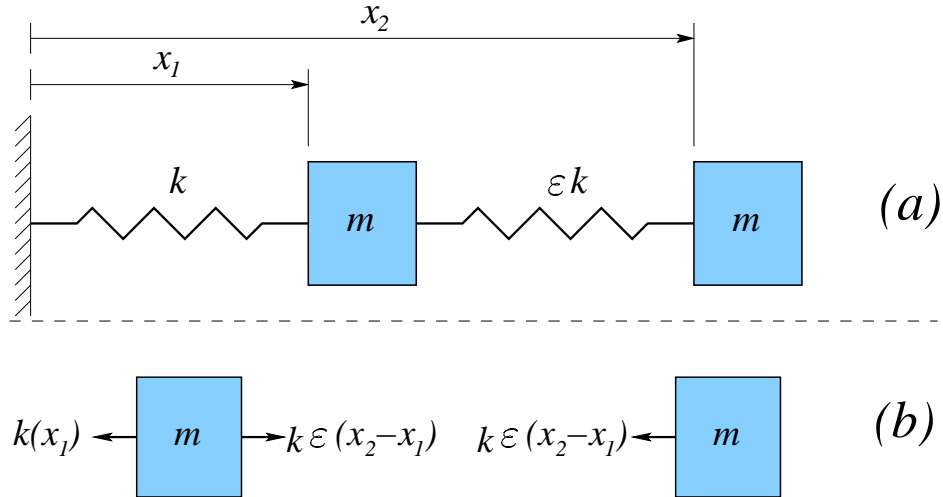
Figure 6.9: (a) Diagram of a system that is a linear analogue of the procedure given in section 6.6.4, where a degree of freedom is added whose motion is initially uncoupled from the initial system.

spring or highly damped damper and one of the masses connected to the support via a spring of nominal stiffness.

The procedure discussed in section 6.6.4, where we add a new degree of freedom whose motion is initially uncoupled from the dynamics of the rest of the system, has a linear analogue which is depicted in Figure 6.9.

The procedure discussed in section 6.6.3, where the two split links are coupled via an inertia, has a linear analogue which is depicted in Figure 6.10.

It should be noted that the equations of motion for these linear analogue systems are not the same as the equations of motion for the linearized two link system. In some cases a mass spring system can be constructed where the two masses and three springs have non-negative values. In other cases this is not possible with modifications to the linear analog.

6.8   Simple Non-linear Numerical Examples

Here, we describe the results we obtained by applying the inertia and damping coupling methods to a simple brachiation model. We only examined continuous contact brachiation with this model. We began with a very simple single link with "hands" on either end which are capable of grabbing onto and releasing handholds on the ceiling. We then found a continuous contact brachiation motion for this model which is collisionless and periodic. For this simple one link model, it is immediately obvious that if one begins the model at rest with both hands on the ceiling, then releasing one hand will result in the desired motion. Using this model and motion, we then split this single link into two separate links(arms) and coupled them via an inertia or dashpot. With a starting value of ∞ for the coupling inertia

$$x_2$$

$$x_1$$

$$k$$

$$k$$

$$m$$

$$m$$

(a)

$$m/\varepsilon$$

$$\frac{x_2-x_1}{2}$$

$$kx_1$$

$$k(x_2-x_1)$$

$$k(x_2-x_1)$$

$$m$$

$$f$$

$$m$$

$$f$$

(b)

$$2f$$

$$m/\varepsilon$$

$$f = \frac{m}{\varepsilon}\frac{(\ddot{x}_2-\ddot{x}_1)}{4}$$
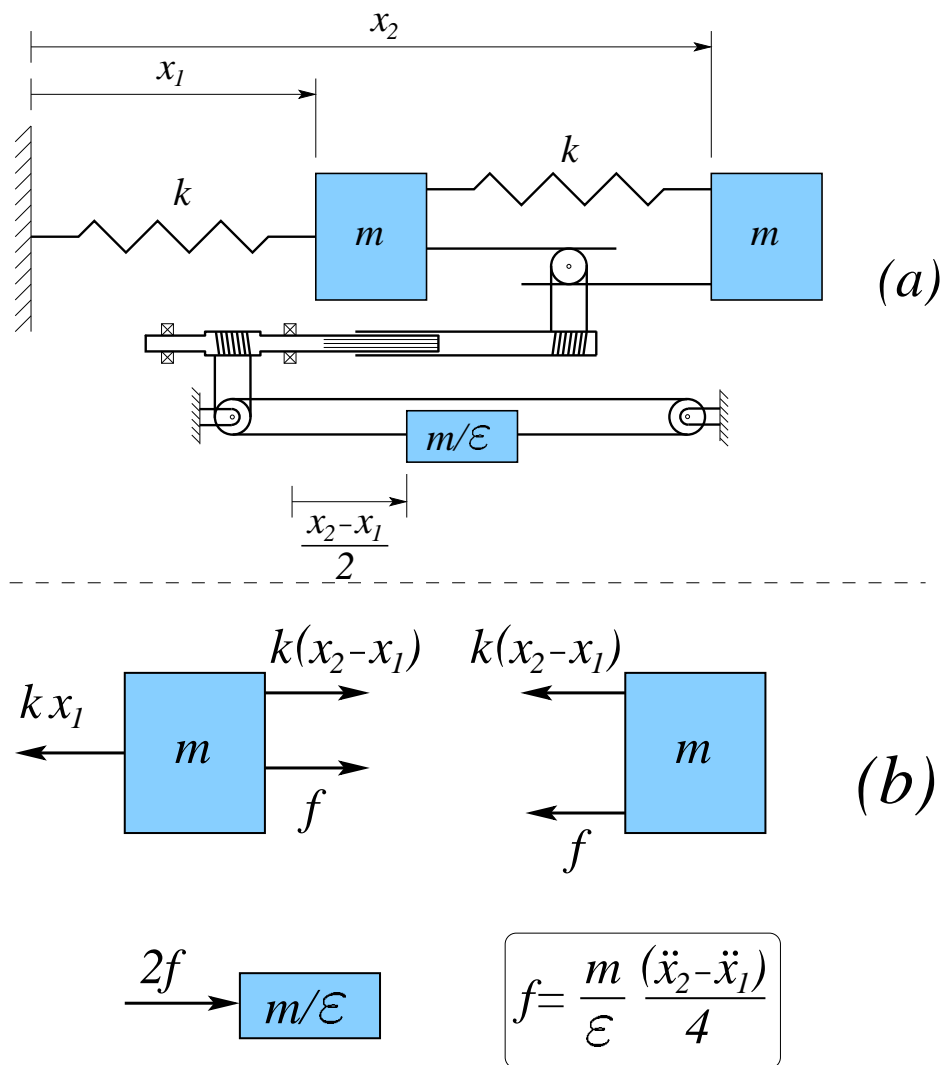
Figure 6.10: Diagram of a system that is a linear analog of the procedure given in section 6.6.3 where an inertia is used to add a degree of freedom.
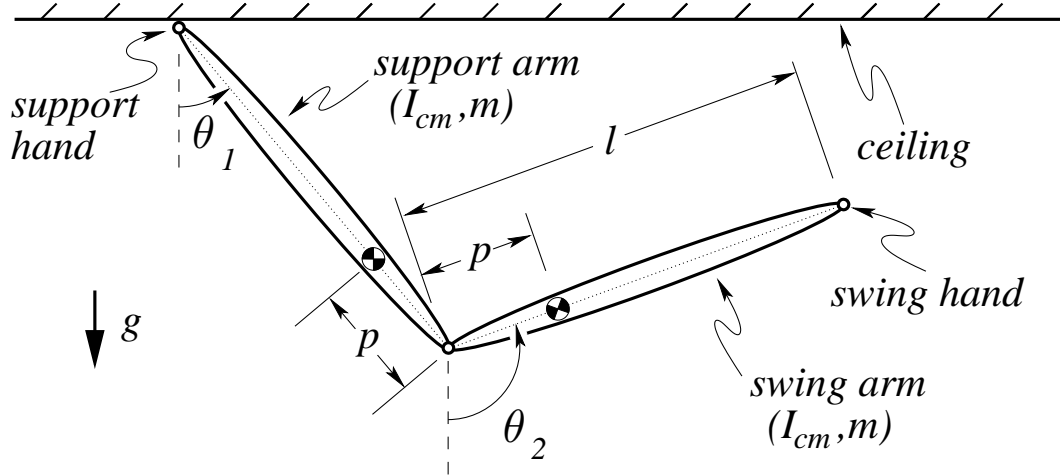
Figure 6.11: The two link model for which we would like to obtain periodic collisionless motions. The dimensional parameters for the two links are the rounded numeric values for the two-link brachiator discussed in chapter 2: $l = 0.61$m, $p = 0.0638$m, $m = 3.083$kg, $I_{cm} = 0.0539$kg $\cdot$ m^2, $g = 9.81$m/s^2

or damping coefficient, the system is equivalent to the single link before splitting the link. The collisionless periodic motion for infinite coupling, has a relative angle between the two links, ϕ, is equal to π throughout the whole motion. For all of the coupling methods applied to the two link brachiating system, numerical integration along with a brute force algorithm was used to create the continuation diagrams. This is, of course, impractical or impossible for systems with many degrees of freedom. However, for this simple case, having the complete diagram allows one to see paths being created, disappearing, etc.

6.8.1 Positive Inertial Coupling

We define the coupling inertia as follows:

$$I_{\text{coupling}} = I_{\text{arm}}(1 - \varepsilon)/\varepsilon$$

We begin with an infinite value of the coupling inertia, $\varepsilon = 0$, which effectively locks the two links together. We then find the special value of ϕ in the starting position (with both hands on the ceiling, and both links at rest) which results in a collisionless periodic motion. We track the special value of ϕ as we increase ε until the coupling inertia is zero, $\varepsilon = 1$.

Since it is impossible to execute these numeric calculations with an infinite value of I_{coupling}, we begin our continuation with a very large but finite value of I_{coupling}. The periodic motion of the system with this non-infinite coupling value will be similar to the motion with the infinite value of I_{coupling}, since there is no
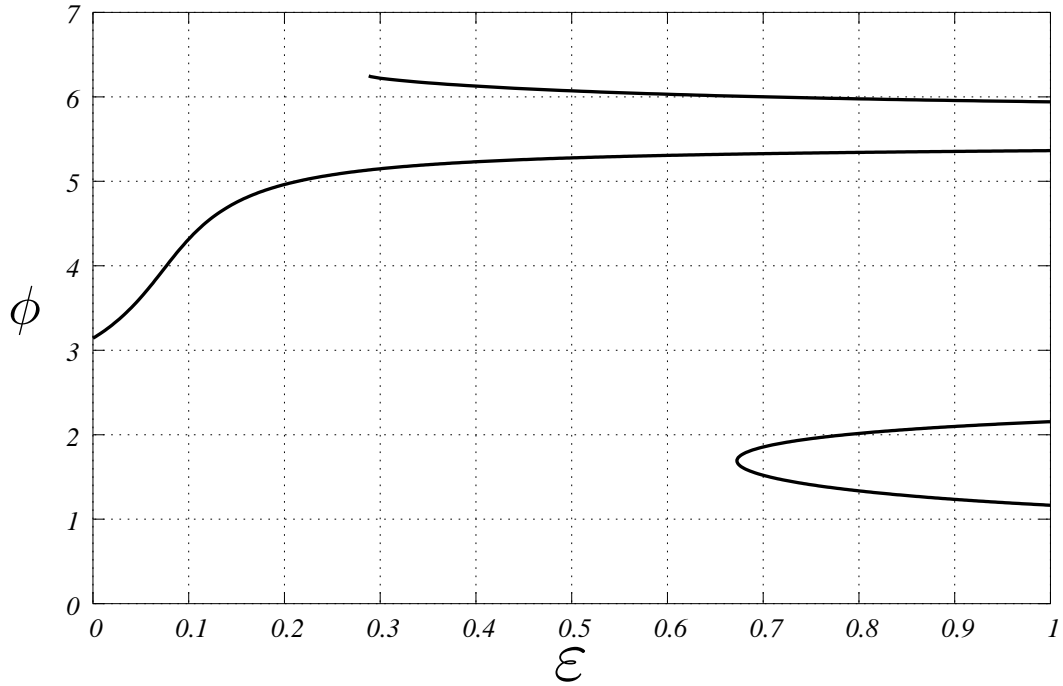
Figure 6.12: Continuation from one link to two link brachiator using a positive value for the coupling inertia. Note that there is a direct connection between the collisionless motion of the single link and a collisionless motion of the frictionless-central-joint two-link system. The other two curves were obtained from by having previously done a brute force search for this system. All points on these curves represent collisionless periodic motions which have no reversals in sign of $\dot{\theta}_1$ for a half cycle of motion.

singularity at that point, as evidenced by the analytical frequency calculations shown in section 6.6.3.

Figure 6.12 shows that one can track the single link periodic motion to the two link system. However, this motion of the two-link system has an initial value of $\phi > \pi$, which means that the central hinge begins the collisionless periodic motion above the ceiling. Although, this is not the motion that we had hoped for, since it is not very ape-like, it is nonetheless a motion which meets our non-collision and periodicity requirements.

The other lower curve on this plot shows that there are two motions for the non-coupled two link system which start with the central hinge below the ceiling. Using this method of inertia coupling, we have shown that they are connected to each other via a continuous path. One might conjecture that we were lucky in the first case, that the single link motion was connected to an uncoupled two-link motion and did not turn back on itself and connect to another single link motion. For a generic system with more than one satisfactory single link motion, this could

well have been the case. However, for this system, there is only one value of ϕ in $0 \le \phi \le 2\pi$ which meets our non-collision and periodicity requirements. Since there is only one point on the graph in Figure 6.12 for $\varepsilon = 0$ there is nothing else for the curve emanating from that point to connect to on that side of the graph, so it cannot double back.

That curve could have just ended, like the top curve shown in Figure 6.12. The reason for the abrupt ending of this curve has to do with the system reaching the maximum energy level for periodic collisionless motions with both hands on the ceiling at the beginning and ending of the motion. The domain of ϕ is $0 < \phi < 2\pi$. $\phi = 0$ corresponds to the minimum possible energy level of the two link system with both hands simultaneously in contact with the ceiling. $\phi = 2\pi$ corresponds to the maximum possible energy level of the two link system with both hands simultaneously in contact with the ceiling. Both of the extreme energy levels are equilibrium positions for this system.

6.8.2 Negative Inertial Coupling

In this section, we give the results for a brute force search using a negative inertia to couple the two links of the brachiation model. As was expected, and shown in Figure 6.13, we find that for some values of ε ($\sim 0.15 < \varepsilon < \sim 0.2$) the approximate solution of the the two link coupled brachiator become so error ridden that any spurious root-finding results cannot be trusted. This makes the negative-inertia method useless for continuously tracking collisionless periodic motions to higher degree of freedom models.

6.8.3 Damper Coupling

In the previous section we show the results of using damping to couple the two links to each other. A rotary damper is placed at the central hinge of the two link brachiation model. The damping coefficient is defined as:

$$b = 1.0(1 - \varepsilon)/\varepsilon$$

The torque acting on the second link from the first link via the rotary damper is:

$$\tau = -b(\dot{\theta}_2 - \dot{\theta}_1)$$

Unlike the inertia method, for which there is a fully periodic collisionless motion for each intermediate value of ε, this method only has periodic motions at the extreme values of $\varepsilon = 1, 0$. The inertia method, can store energy in the rotary inertia on one half of the swing and then return it to the two link system during the second half of the swing. The damping method dissipates energy and thus cannot result in periodic motions except at the extreme values of the damping coefficient. Since, we are only interested in solutions at the extreme values of the homotopy variable, damping can be used to continuously add a degree of freedom.
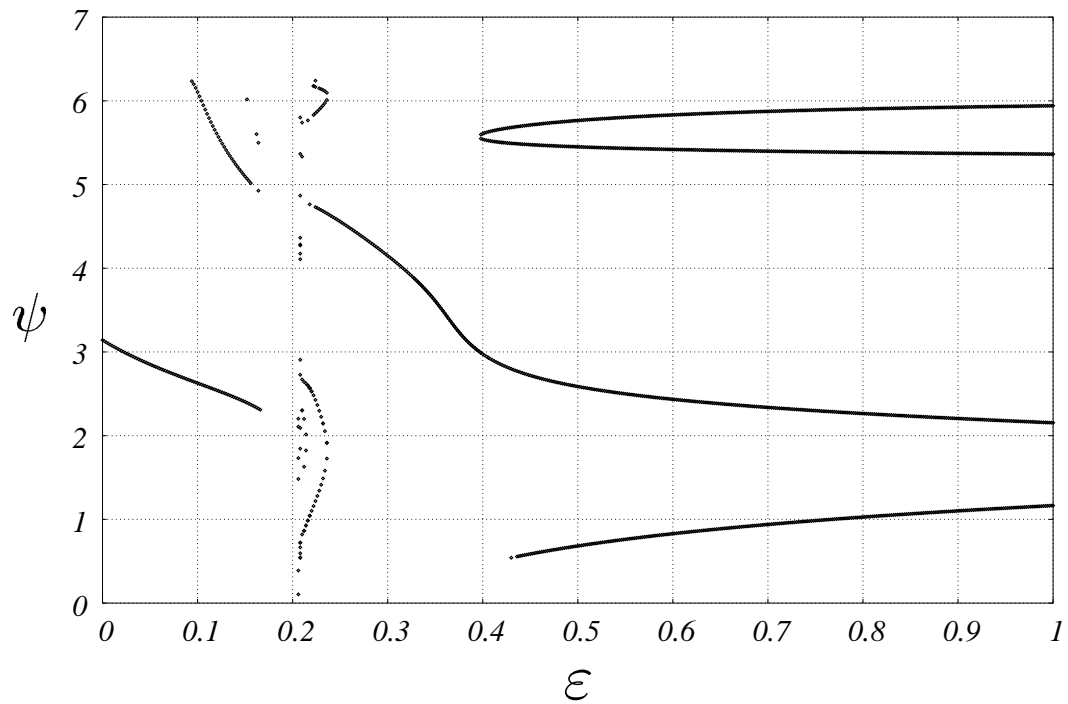
Figure 6.13: Continuation plot using a negative value of inertia for the coupling inertia. As expected from the analytical work presented earlier for negative inertial coupling, we run into numerical difficulties around a specific value of ε probably due to a singular mass matrix in the equations of motion.
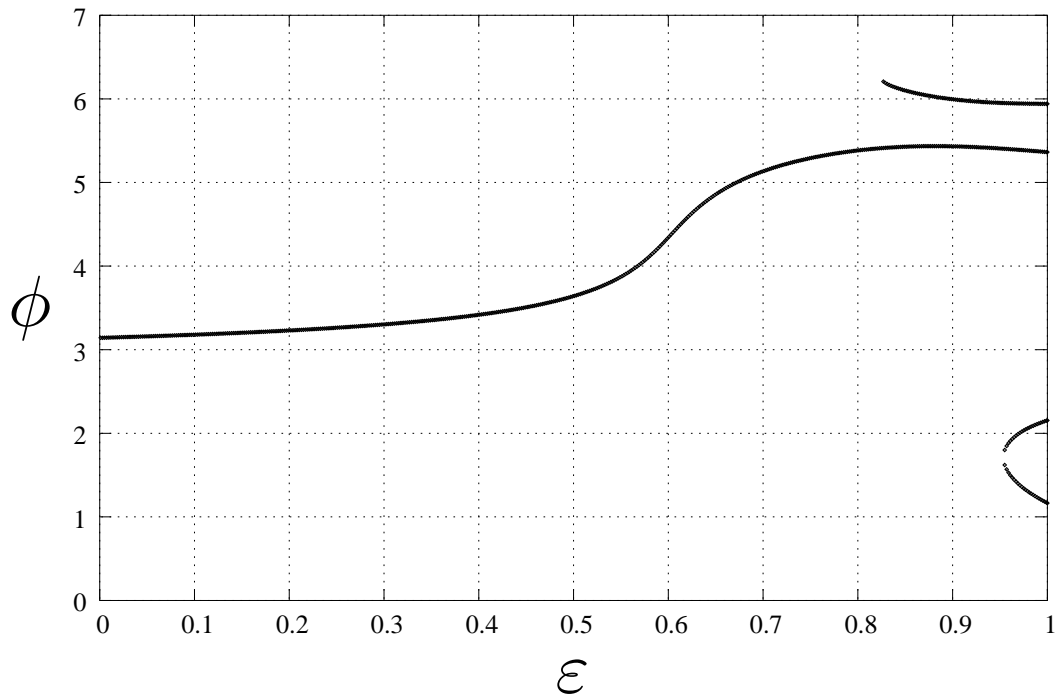
Figure 6.14: This is a plot of the symmetric motions which first cross the surface of section ($\theta_1 = 0$) using damping coupling. Note that these curves seem topologically similar to the curves obtained using inertial coupling shown in Figure 6.12.
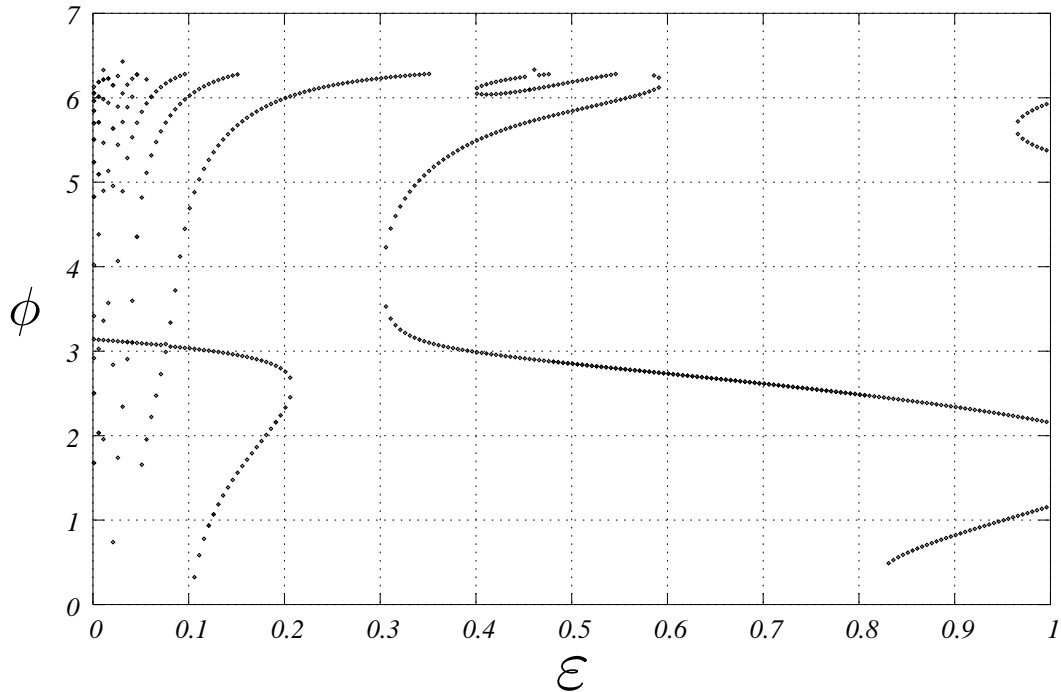
Figure 6.15: This is a plot of the symmetric motions which first cross the surface of section ($\theta_1 = 0$) using spring coupling. Note that the scattered points at small values of ε represent the explosion of periodic collisionless solutions with many fast oscillations of the relative angle between the two links during a single swing. When the coupling spring becomes stiffer, there is time to complete numerous oscillations in the relative angle between the two links in the time that it takes for both of them to swing up to the next handhold. ε.

6.8.4 Spring Coupling

Here, we explore the effects of spring coupling between the two links of the brachiation model. Note that we expect to run into numerical difficulties for a range of values around $\varepsilon = 0$. We were able to track the symmetric motion which emanates from the single rigid body model with no explosion of numerical error, but the other points scattered above and below $\phi = \pi$ which are shown for $0 < \varepsilon <\sim 0.4$ are a result of numerical error.

One thing to note about the solution curves shown in Figure 6.15 are that there are many curves which appear for large values of the coupling spring constant ($\varepsilon \approx 0$). These solutions represent periodic solutions with large numbers of small oscillations around a larger slow oscillation. As the coupling stiffness increases, one can pack more and more of these fast oscillations into one periodic motion. However, at infinite coupling stiffness, all of the motions with fast oscillations

disappear and we are left with the single motion which only had the simple slowly oscillating solution.

6.8.5 2$^{\text{nd}}$ Surface of Section

Inertial coupling and damping coupling both cause the two links to move together for $\varepsilon = 0$. Therefor, one might think that the positive inertia coupling and the damping coupling methods will result in topologically similar continuation plots. Although this is true for the first crossing of the surface of section, it is not true in general. This can be seen in Figure 6.16 showing a particular curve for two different coupling methods which end in the same point.

6.9 More Complicated Numerical Example

In this section, we show the results of using one of the methods described in a previous section on a system with more complexity than the two link models previously described. Both the model and gait are different than in the above models. We begin with a three link model and wish to add elbows to each arm which will result in a five link model. We are concerned with ricochetal, instead of continuous contact, gaits for this 3-5 link model. We define a ricochetal gait as a gait with a ballistic flight phase with no contact being made between the model and the support [23].

We start with a symmetric motion for the three link model. Then we track that motion as we change the coupling inertia from $\varepsilon = 0$ to $\varepsilon = 1$. A zero coupling inertia ($\varepsilon = 1$) is equivalent to frictionless pin joints at the elbows. We use the parameters for the 5 link brachiation model shown in chapter 2. We have defined our initial configuration as the minimum potential energy position of all the links with the supporting hand grasping the ceiling ($\theta_1 = \theta_2 = \theta_3 = \theta_4 = \theta_5 = 0$). Thus we only need five initial angular velocities to define a complete initial state of the system. Figure 6.18 gives the initial angular velocities which result in a symmetric, and thus collisionless and periodic, motion. Although there are probably multiple ricochetal gaits for the 3 link model with this release angle, the path does not double back on itself and connect to one of them. Instead the path connects to the 5 link model.

Because of the way in which we have limited our search space (no sign reversals in $\dot{\theta}_1$ for a half cycle), it is very possible that the curves could simply end, like the curves shown in Figure 6.20 The limitation criteria involves the definition of the map section. In our case, our function begins with all links in the minimum potential energy configuration. We then change the equations of motion (release of the ceiling) at the first event (when the supporting forearm reaches a defined angle ($\theta_1 = 22.3°$). We then integrate the new equations of motion until the vertical component of the shoulder's velocity drops to zero (the second event).

If either event-function (ceiling release or map evaluation output) can have
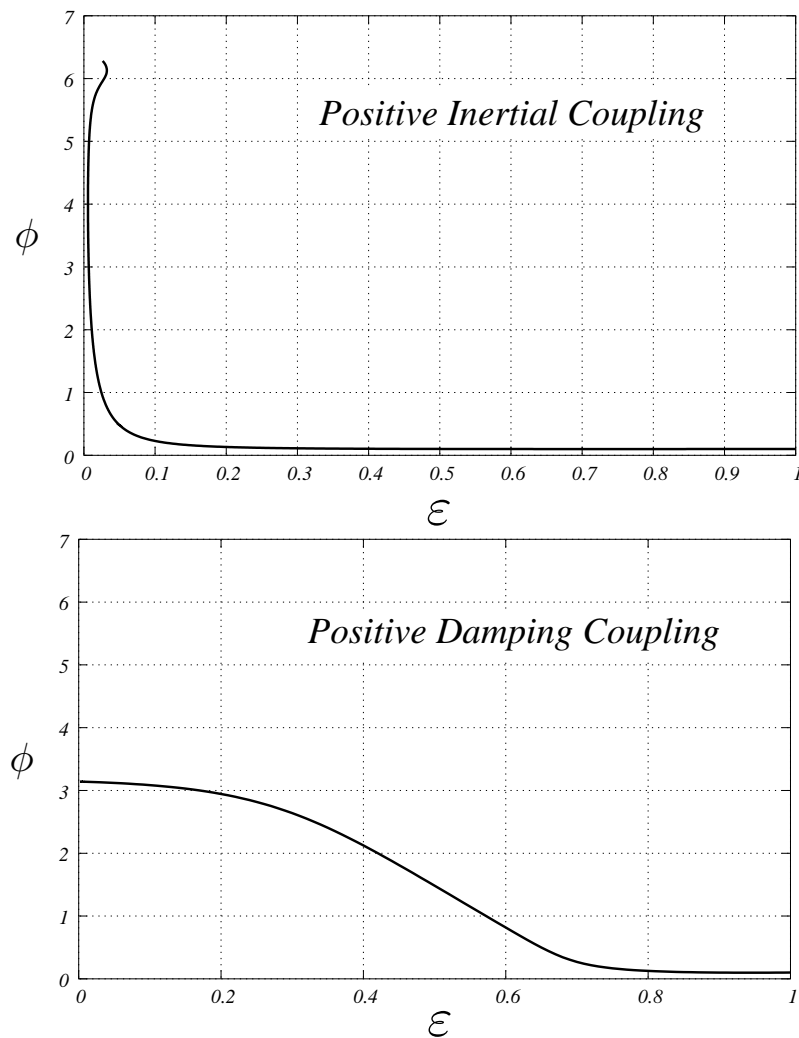
Figure 6.16: This is a plot of some of the values of phi which result in $\theta_2 = 0$ at the second crossing of the surface of section $\theta_1 = 0$ using two different continuation parameters. Although figures 6.12 and 6.14 are topologically equivalent, this figure shows that the two methods do not result in topologically equivalent homotopies when using a larger number of swings. The plot on top uses positive inertial coupling and the plot on the bottom uses positive damping coupling. Although both curves end at the same motion for the uncoupled two link system, the curves themselves are very different.
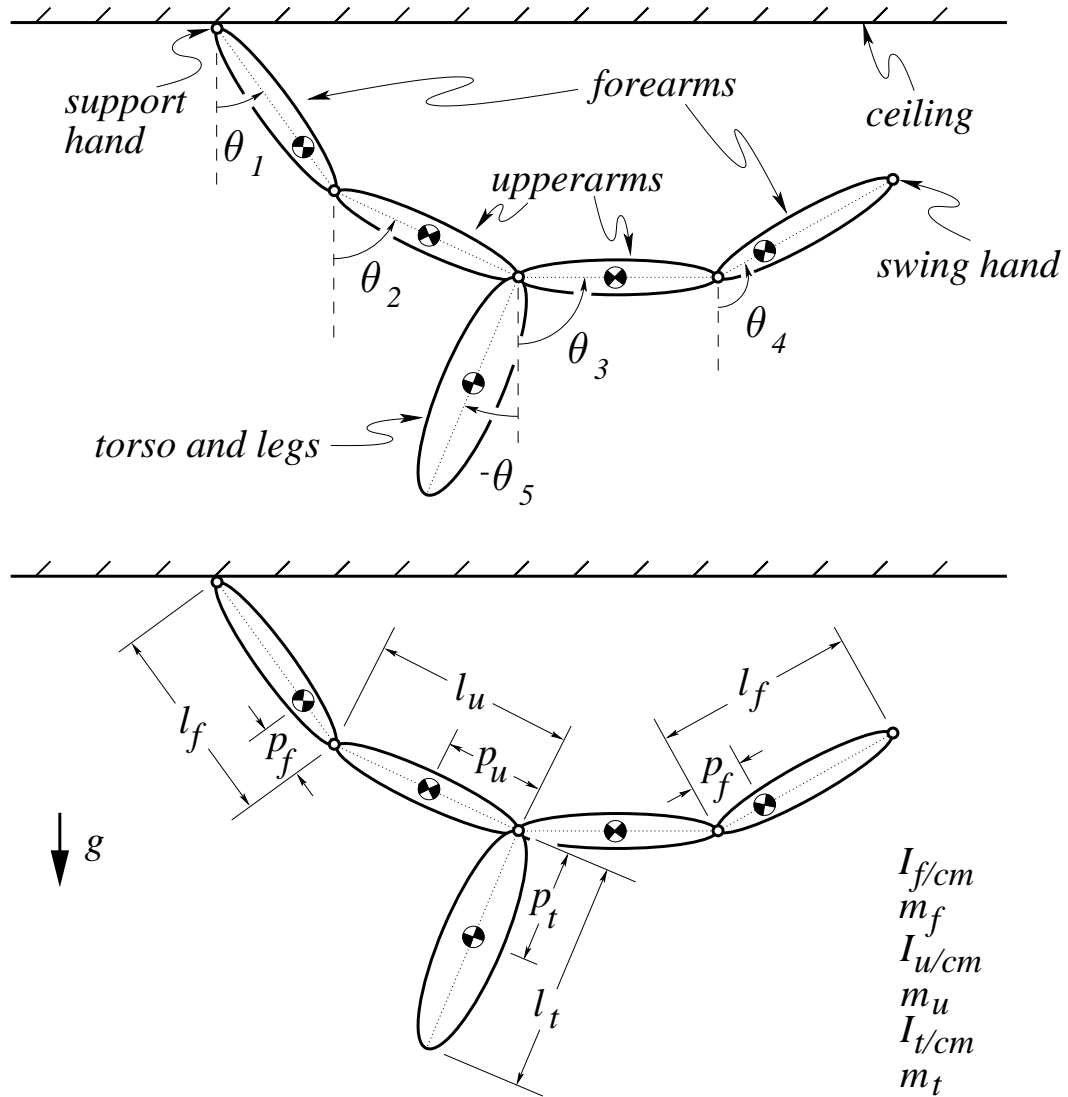
Figure 6.17: Five link brachiation model. We conduct our continuation method with a positive inertial coupling at each elbow connecting the forearms with their corresponding upperarms.
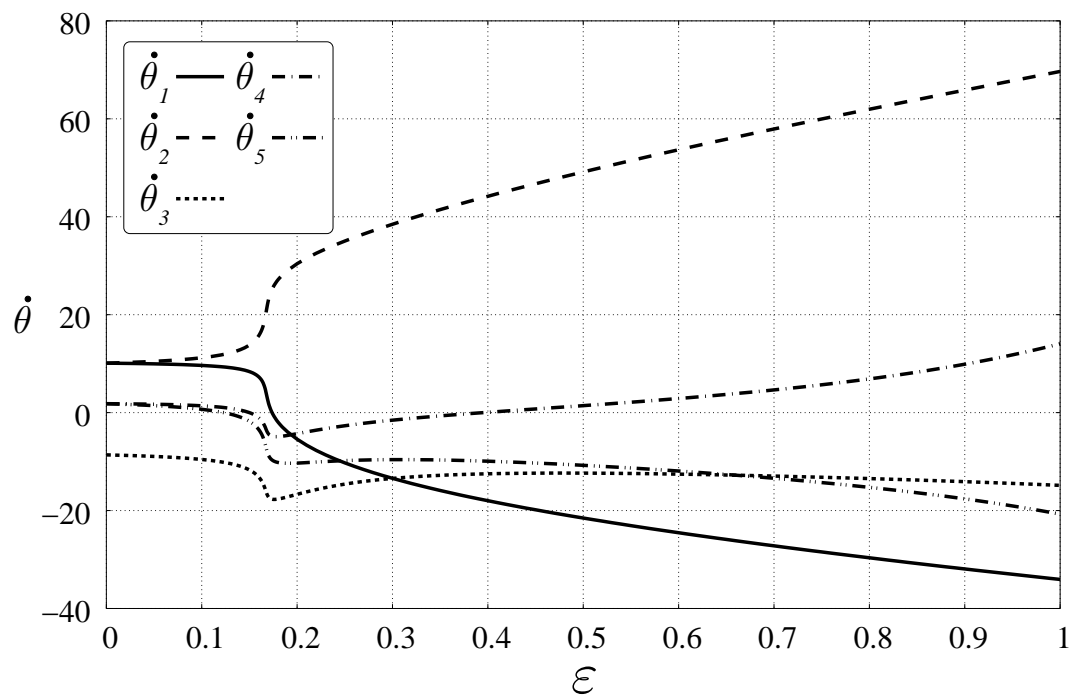
Figure 6.18: A set of points on each of the 5 curves, for a given value of ε, are the initial conditions for a periodic collisionless motion. Note that there is a connection via the inertial coupling from the 3 link ricochetal gait to the 5 link ricochetal gait. The motions of the two different models are depicted in Figure 6.19.
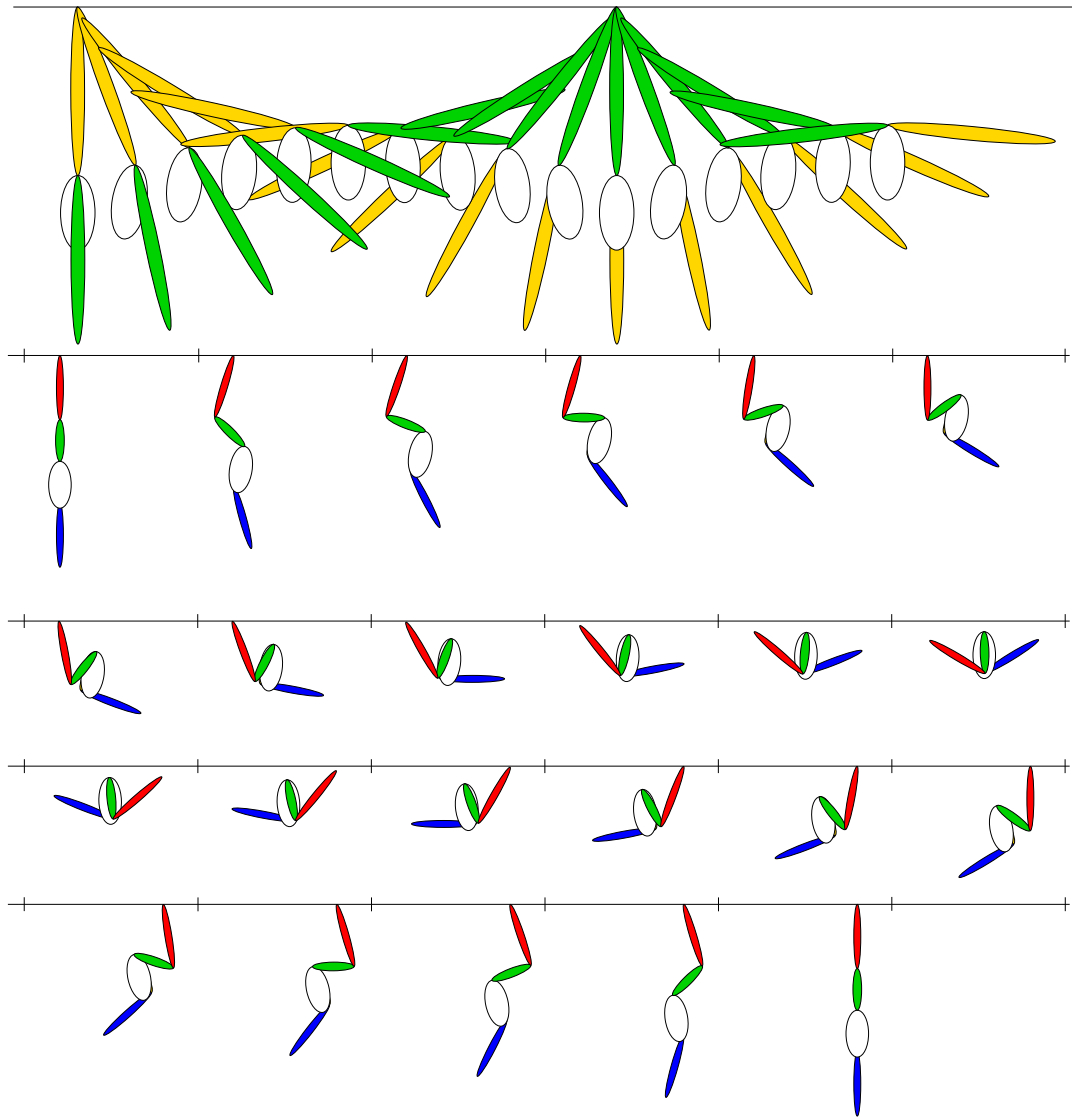
Figure 6.19: Symmetric (periodic and collisionless) motions for both the 3 link and 5 link ricochetal brachiation models. Note the parameters of the two models are consistent with one another, and the release angle is the same for both models 22.3°.
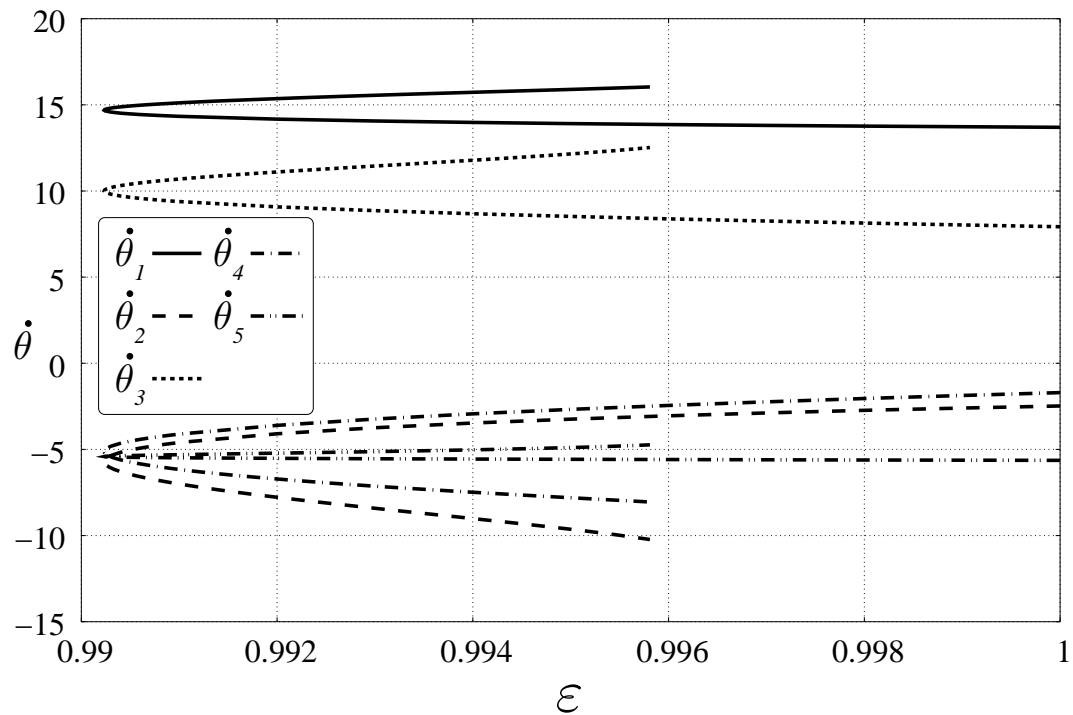
Figure 6.20: Periodic Collisionless motions emanating from the "gibbon-like" motion of the 5 link model given in chapter 2. Note that as we track this motion, the path simply ends. This is due to the non-monotonic nature of the first event criteria (the ceiling release criteria).

multiple crossings of the surface of section, then a decision must be made as to how many crossings we will allow before evaluating the function. For Figure 6.18 & 6.20, we chose to evaluate the function on the first crossing of our surface of section to obtain fairly simple symmetric motions, but we could just have well chosen a larger number of crossings. The problem with defining the surface of section via a possibly non-monotonic function (i.e. a state variable θ_1) is that as we change the continuation parameter, the motion that we track can begin to just barely cross the surface of section, and then eventually completely miss the surface of section where it used to cross. This results in a discontinuity in the map function. Since we are searching for symmetric motions, we cannot modify the surface of section for the second event so that it does not depend on state variables and we are thus stuck with the possibility of abruptly ending curves in our continuation plots. However, for the first event, the ceiling release criteria, we can arbitrarily choose the event function so that it does not depend on a non-monotonic function. We modified the event function to be simply dependent on time (a monotonically increasing function) and redrew the continuation plot corresponding to Figure 6.20 and found that there was no abrupt end in the path.

Figure 6.21 shows shows one of the curves given in Figure 6.20 and labels the first point at which the path was lost, which was recovered, and then the point where the path was lost a second time and from which it is impossible to recover. The curve below the first transition event corresponds to the first crossing of the surface of section (see the (a&b) cartoons of θ_1 in Figure 6.23). Then the motion that we were tracking ceases to correspond to the first crossing of the surface of section and instead corresponds to the third crossing (see cartoon (c) in Figure 6.23). We then continue tracking the motion using the third crossing of the first event function. However, eventually, the motion that we are tracking ceases to cross the surface of section anymore (see cartoon (d) in Figure 6.23).

6.10   Conclusions

We have shown that one does not need to depend on intuition or brute force methods in order to find periodic motion in higher degree of freedom models. Instead, one use a series of models which increase in complexity to to add degrees of freedom to a model in a continuous manner. This can be done in several ways. The choice of the method will have an impact on the motion that one will end up with. Different choices will, in general, connect different motions to each other. There are no guarantees that these methods will result in a higher degree of freedom device since it is possible that the paths might curve around to a different motion with $\varepsilon = 0$ again. It is also possible that the curve might end with $0 < \varepsilon < 1$ due to many reasons, two of which are described in the paper.

Two of the coupling methods (inertia, and spring) result in motions which are conservative for intermediate values of ε. However, the spring coupling has the difficulty of resulting in stiff equations for small values of ε. Damper coupling is not
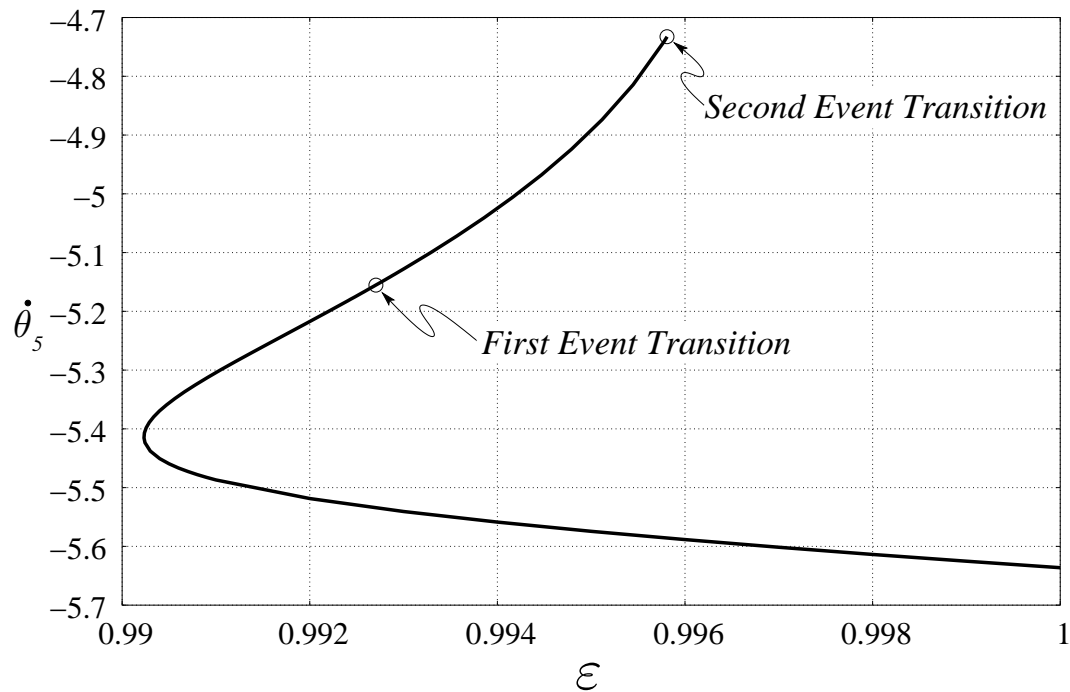
Figure 6.21: Periodic Collisionless motions as we change the coupling inertia from ∞ to zero.

conservative for intermediate values of ε, but is useful nonetheless as a homotopy method where one is only concerned with the motions at $\varepsilon = 0$ and $\varepsilon = 1$.

It is hoped that these methods may prove useful to others who wish to find periodic motions in systems with many degrees of freedom.
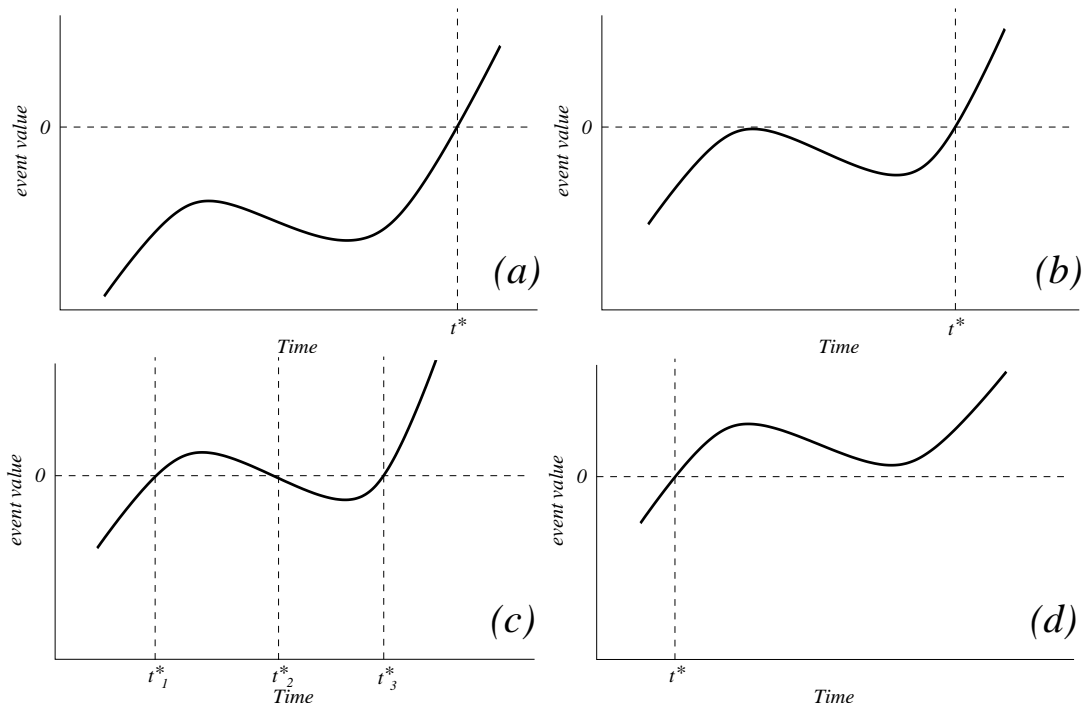
Figure 6.22: Schematic drawings of the first event function as we change the continuation parameter. These drawings show the underlying mechanism as to why the continuation path simply ends in Figure 6.20.
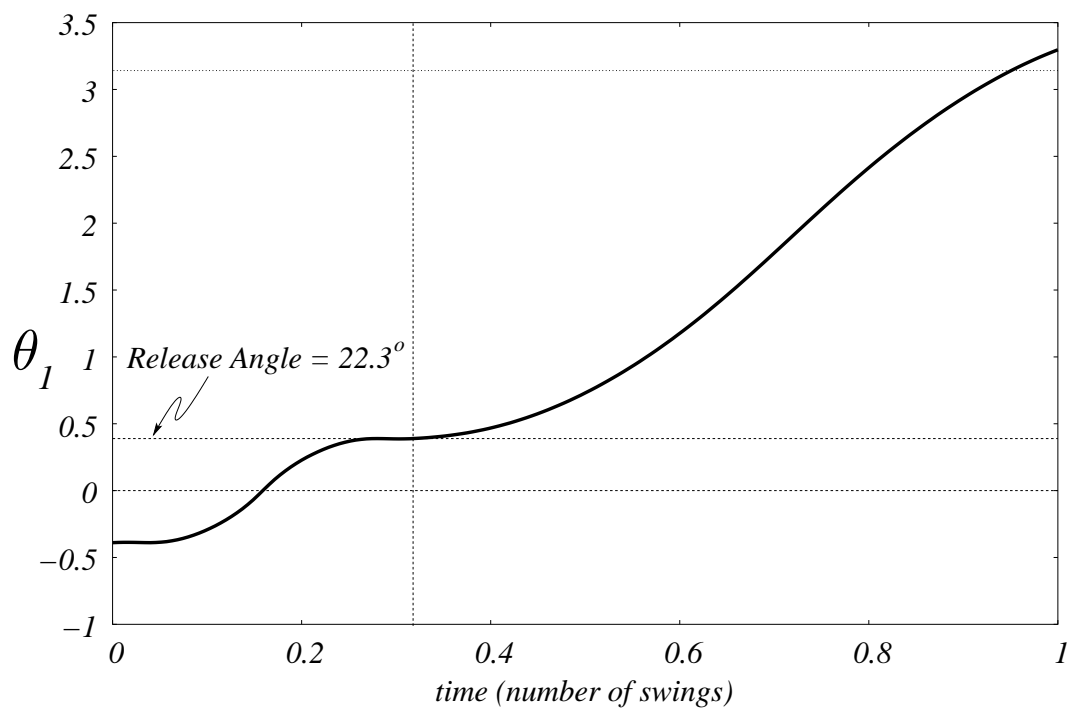
Figure 6.23: Plot of θ_1 vs. time for the five link system just before the first event transition labeled in Figure 6.21. This plot shows that there is a very flat portion of the curve very near the event point with two slight humps in flat portion. This section is exaggerated in the schematic drawings shown in Figure 6.22.

Appendix A

Simulation Details

When simulating the models which appear in this thesis some care must be taken when formulating the equations of motion and also in numerically approximating their solutions. The equations of motion for the system must first be determined. Explicitly writing the equations of motion using computer algebra packages is prohibitively difficult in all but the relatively simple models (ones with less than three serially connected links). In the algebraic derivation of equations of motion, one can stop right before the last step and obtain a simpler form of the equations of motion. To make the above description more concrete, consider the two dimensional rigid body system depicted in Figure 2.8. We then isolate each body and draw a free body diagram for each link. Writing linear and angular momentum balance for each link give us equations A.1 and A.2.

$$\sum_{i=1}^{m} \boldsymbol{f} = m\ddot{\boldsymbol{a}}_{cm_i} \tag{A.1}$$

$$\sum_{i=1}^{n} \boldsymbol{\tau}_{/cm_i} = \dot{\boldsymbol{H}}_{/cm_i} \tag{A.2}$$

Since the Linear Momentum Balance equations are linear in the forces one can isolate the constraint forces from everything else. Setting up the system to solve for the unknown constraint forces gives

$$[M(\theta_{1...n})]\,\boldsymbol{f}_{constraint} = \boldsymbol{g}(f_{applied}, \theta_{1...n}, \dot{\theta}_{1...n}, \ddot{\theta}_{1...n}) \tag{A.3}$$

If $[M(\theta_{1...n})]$ is nonsingular, which it will be for correctly written equations of motion, the constraint forces can be solved for. Solving for the unknown constraint forces, assuming the $\ddot{\theta}_{1...n}$ are known in the linear momentum balance equation, gives

$$\boldsymbol{f}_{constraints} = f_1(\theta_{1...n}, \dot{\theta}_{1...n}, \ddot{\theta}_{1...n}, \boldsymbol{f}_{applied}) \tag{A.4}$$

If one now plugs the expressions that we have for the constraint forces into the angular momentum balance equations A.2 we get

$$\boldsymbol{f}_2(\theta_{1...n}, f_{constraints}, f_{applied}) = \boldsymbol{f}_3(\theta_{1...n}, \dot{\theta}_{1...n}, \ddot{\theta}_{1...n}) \tag{A.5}$$

The equations of motion for a rigid body system are also linear in the angular accelerations of the bodies. Setting up those equations so that we can solve for the unknown angular accelerations gives

$$\left[M(\theta_{1...n}, \dot{\theta}_{1...n}) \right] \ddot{\boldsymbol{\theta}} = \boldsymbol{f}_4(\theta_{1...n}, \dot{\theta}_{1...n}, f_{applied}) \tag{A.6}$$

If $\left[M(\theta_{1...n}, \dot{\theta}_{1...n}) \right]$ is nonsingular, which it will be for correctly written equations of motion, the angular accelerations of the bodies can be solved for, giving the equations of motion for the system.

In practice explicitly solving for the equations of motion involves a lot of algebra. The involved algebra is primarily from the expressions of the accelerations of the center of mass of each link. As we add more links to the end of a chain of links the expressions for the positions of the center of mass of the last link in the chain depends trigonometrically on the angular position of each of the preceeding links. This position expression is then differentiated twice to obtain the absolute acceleration of the center of mass. It is this twice differentiated expression whose number of terms explodes exponentially in the number of links. Using computer algebra packages such as Macsyma, Mathematica, or Maple, help in reducing the number of mistakes that one would make by hand. However, since the number of terms in the equations explode so quickly as we add more links to the end of the chain the computer algebra packages become unable to cope with the problem and a more practical method is required.

One stop-gap measure which can help in reducing the size of the expressions is to stop the analytic work just before the last stage when we explicitly solved for the equations of motion. This helps in that we don't have to invert a low dimensional nxn matrix analytically which has rather large expressions for each entry in the matrix. Instead, at each step in the the numerical integration when we need the value for the angular accelerations, we calculate a numerical value for each entry in the nxn matrix using our expressions for the entries. We also calculate the right hand side of equation A.6, an n-dimensional column vector. Solving this system numerically each time the equations of motion are needed is a way to circumvent the prohibitive analytical inversion of the matrix. This method will work for slightly more complicated systems than the previous method would allow. However, as more links are added to the system, even the size of the entries in the matrix become too large for the computer algebra packages to handle.

If we were to continue this conversion from analytic to numeric we could go to the extreme case where we form all of the primary vectors numerically and then form the equations of motion from those numeric vectors. If we do this we run into the problem of how to isolate the unknown constraint forces and the unknown angular accelerations. To isolate the unknowns numerically we form the equations of motion by forming a function and calling it multiple times. The function's input arguments that we form consist of the state vector, the unknown angular accelerations, and the unknown constraint forces. Writing this function in matrix

144

vector form gives

$$
\begin{bmatrix} fcn_1 \\ \vdots \\ fcn_m \\ fcn_{m+1} \\ \vdots \\ fcn_{m+n} \end{bmatrix} = \begin{bmatrix} \boldsymbol{M}_1 \\ \vdots \\ \boldsymbol{M}_m \\ \boldsymbol{M}_{m+1} \\ \vdots \\ \boldsymbol{M}_{m+n} \end{bmatrix} \begin{bmatrix} f_{1_{constraint}} \\ \vdots \\ f_{m_{constraint}} \\ \ddot{\theta}_1 \\ \vdots \\ \ddot{\theta}_n \end{bmatrix} + \begin{bmatrix} f_1(\boldsymbol{\theta}, \dot{\boldsymbol{\theta}}, f_{applied}) \\ \vdots \\ f_m(\boldsymbol{\theta}, \dot{\boldsymbol{\theta}}, f_{applied}) \\ f_{m+1}(\boldsymbol{\theta}, \dot{\boldsymbol{\theta}}, f_{applied}) \\ \vdots \\ f_{m+n}(\boldsymbol{\theta}, \dot{\boldsymbol{\theta}}, f_{applied}) \end{bmatrix} \tag{A.7}
$$

Rewriting and compressing the matrix vector form now gives

$$
\boldsymbol{f}cn = [M]\,\boldsymbol{u} + \boldsymbol{f} \tag{A.8}
$$

We then form the equations of motion by first calling this function with the current state vector and zeros for the unknown values of the angular accelerations and constraint forces. This would give the values for $\boldsymbol{f}$ To form the unknown $[M]$ matrix, the function can be called $m + n$ times with the current state vector and with one of the unknown contraint forces, or unknown angular accelerations equal to one and the rest of those unknown equal to zero. For instance to get the first row of $[M]$, $\boldsymbol{M}_1$ we call the function with

$$
\boldsymbol{u} = \begin{bmatrix} 1 \\ 0 \\ 0 \\ \vdots \\ 0 \end{bmatrix} \tag{A.9}
$$

$\boldsymbol{M}_1$ can then be obtained using

$$
\boldsymbol{M}_1 = \boldsymbol{f}cn - \boldsymbol{f} \tag{A.10}
$$

This process can then be repeated to obtain all of the numeric entries of $[M]$. Once all of the entries in in $[M]$ have been obtained we can solve the following system for the vector of unknown constraint forces and angular accelerations,$\boldsymbol{u}$ at this time step.

$$
[M]\,\boldsymbol{u} = -\boldsymbol{f} \tag{A.11}
$$

This gives the angular acclerations that are required to integrate the equations of motion forward to the next time step. This is then repeated at each time step. In this manner, the addition of links does not exponentially increase the size of the analytic expressions that we need to form in order to integrate the equations of motion. This is the method that was used to simulate the systems with more than 3 degrees of freedom in this thesis.

Bibliography

[1] Jesper Adolfsson, Harry Dankowicz, and Arne Nordmark. 3d passive walkers: Finding periodic gaits in the presence of discontinuities. *Nonlinear Dynamics*, 24:205–229, 2001.

[2] R. McN. Alexander. Modelling approaches in biomechanics. *Philosophical Transactions of the Royal Society of London B*, 358:1429–1435, 2003.

[3] R. McNeill Alexander. Design by numbers. *Nature*, 412:591, Aug. 2001.

[4] Eugene Allgower and Kurt Georg. Simplicial and continuation methods for approximating fixed points and solutions to systems of equations. *SIAM Review*, 22(1):28–86, January 1980.

[5] J. E. A. Bertram, Andy Ruina, C. E. Cannon, Young Hui Chang, and Michael J. Coleman. A point-mass model of gibbon locomotion. *Journal of Experimental Biology*, 202:2609–2617, 1999.

[6] Elena Borzova and Yildirim Hurmuzlu. Passively walking five-link robot. *Automatica*, 40:621–629, 2004.

[7] S. Brody. *Bioenergetics and Growth*. Reinhold Publishing Corporation, Baltimore, 1945.

[8] A. Chatterjee, R. Pratap, C.K. Reddy, and A. Ruina. Persistent passive hopping and juggling is possible even with plastic collisions. *The International Journal of Robotics Research*, 21(7):621–634, July 2002.

[9] A. Chatterjee and Andy Ruina. Two interpretations of rigidity in rigid body collisions. *Journal of Applied Mechanics*, 65(4):894–900, Dec 1998.

[10] Anindya Chatterjee and Mariano Garcia. Small slope implies low speed for mcgeer's passive walking machines. *Dynamics and Stability of Systems*, 15(2):139–157, June 2000.

[11] Anindya Chatterjee and Andy Ruina. Realizability of arbitrary local mass matricies in single-point rigid body collisions. *Proceedings of the International Symposium on Impact and Friction of Solids*, pages 1–4, June 1998.

[12] Chebyshev. *The Scientific Legacy of Cheybshev*. Publishing House of Academy of Sciences of USSR;Moscow, Leningrad, 1945.

[13] E.J. Cheng, I.E. Brown, and G.E. Loeb. Virtual muscle: a computational approach to understanding the effects of muscle properties on motor control. *Journal of Neuroscience Methods*, 101(2):117–130, September 2000.

[14] Michael Jon Coleman. *A Stability Study of a Three-Dimensional Passive-Dynamic Model of Human Gait*. PhD thesis, Cornell University, Department of Theoretical and Applied Mechanics, Februrary 1998.

[15] S.H. Collins, M. Wisse, and A. Ruina. A 3-d passive-dynamics walking robot with 2 legs and knees. *International Journal of Robotics Research*, 20(7):607–615, July 2001.

[16] C. F. Curtiss and J.O. Hirschfelder. Integration of stiff equations. *Proceedings of the National Academy of Sciences of the United States of America*, 38(3):235–243, March 15 1952.

[17] M.H. Dickinson, F.O. Lehmann, and et al. Wing rotation and the aerodynamic basis of insect flight. *Science*, 284:1954–1960, 1999.

[18] G.E. Erikson. Brachiation in new world monkeys and in anthropoid apes. *Zoological Society of London*, ?(10):135–164, 1962.

[19] John Fleagle. Dynamics of a brachiating siamang. *Nature*, 248:259–260, 1974.

[20] Toshio Fukuda, Hidemi Hosokai, and Fumihito Arai. A study on the brachiation type of mobile robot: Heuristic creation of driving input and control using cmac. *IEEE/RSJ International Workship on Intelligent Robots and Systems, IROS '91*, ?:478–483, Nov. 1991.

[21] Mariano Garcia, Anindya Chatterjee, and Andy Ruina. Efficiency, speed, and scaling of two-dimensional passive-dynamic walking. *Dynamics and Stability of Systems*, 15(2):75–99, 2000.

[22] Mariano Garcia, Anindya Chatterjee, Andy Ruina, and Michael Coleman. The simpliest walking model: Stability, complexity, and scaling. *Journal of Biomedical Engineering*, 120:281–288, April 1998.

[23] Mario W. Gomes and Andy L. Ruina. A five-link 2d brachiating ape model with life-like motions and no energy cost. *Journal of Theoretical Biology*, ?(?):In Process, 2004.

[24] H. Hatze. A mathematical model for the computational determination of parameter values of anthropomorphic segments. *Journal of Biomechanics*, 13:833–843, 1980.

[25] A. V. Hill. The heat of shortening and the dynamic constants of muscle. *Proceedings of the Royal Society of London, Series B, Biological Sciences*, 126:136–195, October 1938.

[26] Y. Hurmuzlu and G.D. Moskowitz. The role of impact in the stability of bipedal locomotion. *International Journal of Dynamics and Stability of Systems*, 1(3):217–234, 1986.

[27] A. F. Huxley. Muscle structure and theories of contraction. *Prog. Biophysics and Biophysical Chemistry*, 7:255–318, 1957.

[28] Hikeki Kajima, Yasuhisa Hasegawa, and Toshio Fukuda. Learning algorithm for a brachiating robot. *Applied Bionics and Biomechanics*, 1(1):57–66, 2003.

[29] Arthur D. Kuo. A simple model of bipedal walking predicts the preferred speed-step length relationship. *Journal of Biomechanical Engineering*, 123:264–269, 2001.

[30] N. Lifson, G. B. Gordon, and R. McClintock. Measurement of total carbon dioxide production by means of D_2O^{18}. *Journal of Applied Physiology*, 7:704–710, 1955.

[31] G. M. O. Maloiy, N. C. Heglund, L. M. Prager, G. A. Cavagna, and C. R. Taylor. Energetic cost of carrying loads: have african women discovered and economic way? *Nature*, 319:668–669, Feb. 1986.

[32] Rodolfo Margaria. *Biomechanics and Energetics of Muscular Excercise.* Clarendon Press, Oxford, 1976.

[33] Tad McGeer. Passive bipedal running. *Proceedings of the Royal Society of London B*, 240:107–134, 1990.

[34] Tad McGeer. Passive dynamic walking. *The International Journal of Robotics Research*, 9(2):62–82, 1990.

[35] Tad McGeer. Passive walking with knees. *Proceedings of 1990 IEEE Internation Conference on Robotics and Automation*, pages 1640–1645, 1990.

[36] Tad McGeer. Passive dynamic biped catalog. *Proceedings of Experimental Robotics II: The International Symposium*, pages 465–490, 1992.

[37] Tad McGeer and Leigh Hunt Palmer. Wobbling, toppling, and forces of contact. *American Association of Physics Teachers*, 57(12):1089–1098, December 1989.

[38] Brian Keith McNab. *The Physiological Ecology of Vertebrates: A View From Energetics.* Comstock Publishing Associates, 2002.

[39] Kenneth R. Meyer. Continuation of periodic solutions in three dimensions. *Physica D*, 112:310–318, 1998.

[40] Cleve Moler. Golden ode's, new ordinary differential equation solvers for matlab and simulink. *Cleve's corner, in Mathworks online publication*, Summer 1996.

[41] Jun Nakanishi, Toshio Fukuda, and Daniel E. Koditschek. A brachiating robot controller. *IEEE Transactions on Robotics and Automation*, 16(2):109–123, 2000.

[42] J. R. Napier and P. H. Napier. *A Handbook of Living Primates*. Academic Press Inc. (London) Ltd., 1967.

[43] Hidekazu Nishimura and Koji Funaki. Motion control of brachiation robot by using final-state control for parameter-varying systems. *Proceedings of the 35th Conference on Decision and Control*, pages 2474–2475, Dec. 1996.

[44] Hidekazu Nishimura and Koji Funaki. Motion control of three-link brachiation robot by using final-state control with error learning. *IEEE/ASME Transactions on Mechatronics*, 3(2):120–128, 1998.

[45] Hiroshi Odagaki, Anotonio Moran, and Minoru Hayase. Analysis of the dynamics and nonlinear control of under-actuated brachiation robots. *Proceedings of the 35th SICE Annual Conference*, ?:2137–1142, July 1997.

[46] Claude A. Piantadosi. *The Biology of Human Survival: Life and Death in Extreme Environments*. Oxford University Press, 2003.

[47] H. Preuschoft and B. Demes. *Biomechanics of Brachiation*, pages 96–118. Edinburgh University Press, 1984.

[48] Holger Preuschoft and Brigitte Demes. *Influence of Size and Proportions on the Biomechanics of Brachiation*, pages 383–399. Plenum Press, 1985.

[49] Richard Rand and Deepak Ramani. Relaxing nonholonomic constraints. In *Proceedings of the First International Symposium on Impact and Friction of Solids, Structures, and Intelligent Machines*, pages 113–116. Ottawa, Canada, June 27-30 2000.

[50] R. M. Rosenberg. The normal modes of nonlinear n-degree-of-freedom systems. *Journal of Applied Mechanics*, ?:7–14, Mar. 1962.

[51] Fuminori Saito and Toshio Fukuda. *A First Result of The Brachiator III–A New Brachiation Robot Modeled on a Siamang*, chapter 43, pages 354–361. MIT Press, 1997.

[52] Jørgen Sand and Ole Østerby. Regions of absolute stability. *??*, 1979.

[53] Adolph H. Schultz. Observations on the growth, classification and evolutionary specialization of gibbons and siamangs. *Human Biology*, 5(2):212–255, May 1933.

[54] Adolph H. Schultz. Observations on the growth, classification and evolutionary specialization of gibbons and siamangs (continued). *Human Biology*, 5(3):385–428, September 1933.

[55] R. Seydel. Tutorial on continuation. *International Journal of Bifurcation and Chaos*, 1(1):3–11, 1991.

[56] L. F. Shampine and C. W. Gear. A user's view of solving stiff ordinary differential equations. *SIAM Review*, 21(1):1–17, January 1979.

[57] Larry F. Shampine. *Stiff Computation*, chapter Introduction to Stiffness. Oxford University Press, New York, 1985.

[58] Mark W. Spong. Swing up control of the acrobat. *Proceedings IEEE International Conference on Robotics and Automation*, ?:2356–2361, 1994.

[59] Gilbert Strang. *Introduction to Applied Mathematics*. Wellsley-Cambridge Press, 1986.

[60] Sharon M. Swartz. Pendular mechanics and the kinematics and energetics of brachiating locomotion. *International Journal of Primatology*, 10(5):387–418, 1989.

[61] Clay M. Thompson and Marc H. Raibert. *Passive Dynamic Running*, pages 135–146. Technical Report 1179 LL-6, 1989.

[62] Benoit Thuillot, A. Goswami, and B. Espiau. Bifurcation and chaos in a simple passive bipedal gait. *Proceedings of 1997 IEEE International Conference on Robotics and Automation*, 1:792–798, April 20-25, 1997.

[63] Stephen P. Timoshenko. *Theory of Elastic Stability*. McGraw-Hill book company, inc., New York, 4th edition, 1936.

[64] Lloyd N. Trefethen. *Finite Difference and Spectral Methods for Ordinary and Partial Differential Equations*. 1996. Unpublished text available at http://web.comlab.ox.ac.uk/oucl/work/nick.trefethen/pdetext.html.

[65] Warwick Tucker. *The Lorentz Attractor Exists*. PhD thesis, Uppsala University, S-751 06, September 1998.

[66] R. H. Tuttle. Does the gibbon swing like a pendulum? *American Journal of Physical Anthropologists*, 29:132, 1968.

[67] James R. Usherwood and John E. Bertram. Understanding brachiation: insight from a collisional perspective. *The Journal of Experimental Biology*, 206:1631–1642, 2003.

[68] Jack H. Wilmore and David L. Costill. *Physiology of Sport and Exercise*, pages 92–121. Human Kinetics, 1994.

[69] M. Wisse, A. L. Schwab, and R. Q. vd. Linde. A 3d passive dynamic biped with yaw and roll compensation. *Robotica*, pages 1–12, May 2000.

[70] N. Yamazaki. The effects of gravity on the interrelationship between body proportions and brachiation in the gibbon. *Human Evolution*, 5(6):543–558, 1990.

[71] George I. Zahalak and Shi-Ping Ma. Muscle acitvation and contraction: Constitutive relations based directly on cross-bridge kinetics. *Journal of Biomechanical Engineering*, 112:52–62, February 1990.

[72] Felix E. Zajac. Muscle coordination of movement: A perspective. *Journal of Biomechanics*, 26 Supplement 1:109–124, 1993.

[73] W. I. Zangwill and C. B. Garcia. *Pathways to Solutions, Fixed Points, and Equilibria*. Prentice-Hall Inc., 1981. Prentice-Hall Series in Computational Mathematics.

[74] Vladimir M. Zatsiorsky and Robert J. Gregor. Mechanical power and work in human movement. In W. A. Sparrow, editor, *Energetics of Human Activity*, chapter 7, pages 195–227. Human Kinetics, 2000.